MASTER THESIS

Title:	Delivered:
Prediction of ice loads of an Arctic SPAR	May 30, 2011
	Availability: Restricted
Student: Heidi Fjellvang	**Number of pages:** Report: 77

Abstract:

A substantial amount of the world's hydrocarbon deposits is assumed to be found in the Arctic. The Arctic region differs from other regions mainly due to the climate and presence of sea ice features. In order to minimize the ice loads from the drifting ice, structures with sloping waterline geometry have been introduced to the marked. The breaking angle in the waterline allows the ice to fail in a flexural mode, and to further transport the broken ice pieces around the hull.

A numerical model for estimation of the level ice loads acting on a sloping structure in the time-domain has been developed based on the existing methodology given in the new ISO 19906 standard on Arctic Offshore Structures. The numerical model has been corrected based on actually measured time series and videos recorded from an ice test campaign performed in the Aker Arctic Technologies ice model tank.

Keywords:

Level ice
Ice action
Ice model test

Supervisor:

Jørgen Amdahl

Adress:
NTNU
Department of Marine Technology
N-7491 Trondheim

Location
Marinteknisk Senter
O. Nielsens vei 10

Telephone..... +47 73 55 01
Fax.....+47 73 59 56 97

PROBLEM TEXT

MASTER THESIS, SPRING 2011
for
Stud. Techn. Heidi Fjellvang,
Marine Hydrodynamics

Prediction of ice loads of an Arctic SPAR
Beregning av islaster for en arktisk SPAR

Field developments in the Arctic require specially designed offshore structures to facilitate drilling and production. In geographical areas where the occurrence of drifting ice coexists with a large water depth at the fields location, a robust floating structure, which can cope with both open water and ice loading, must be developed. This calls for research and development on different existing offshore structure concepts. This study will focus on the applicability of an Arctic SPAR in the above-mentioned conditions.

The determination of the global ice load and responses of the structure is a complex process which often includes many assumptions and uncertainties in the methods applied. Depending on the applied method and person performing the evaluations, different results will be obtained, often with large deviation between estimates.

As the ice conditions for structures located in Arctic regions most likely will govern the design conditions it is extremely important to be able to estimate the design load induced by these conditions in order to develop a safe and cost efficient platform concept for the field development.

Presently there exist many methods to determine ice induced response on a floater for different structure geometries proposed for areas with drift ice; analytical load models, ice basin model testing, numerical analysis tool using analytical models as input and use of previous full scale measurements performed (scaling).

A. OBJECTIVE

The problem text is defined by Aker Solutions and provided the students 27 January, 2011. (Notice that the text given in *italic* is not to be answered in this master thesis, see Preface.)

The main objectives, among others, with the thesis proposal are to:

- Give the students an introduction to ice as a material.
- Increase the students understanding of ice-structure interaction processes and which ice and structure factors that governs the processes.
- Give the students an introduction to ISO 19906 and the load methodologies by Croasdale and Ralston for estimation of level ice loads on structures with a conical surface in the waterline. In addition a review of the recommended load model for level ice loads on vertical structures shall be performed.
- Give the students an introduction to ice basin model testing.
- Develop a MATLAB-script for ice-structure interaction for fixed structures.

B. THESIS BUILD UP

The thesis is divided into two phases. The first phase emphasizes on the understanding of the ice load algorithms recommended in ISO 19906 and how to apply these for structures with a sloping surface in the waterline and a vertical phase in the waterline. In addition a model test analysis of structures tested in fixed mode is included in the scope of work.

The scope for Phase II will be clarified as soon as Phase I is finished.

In the Phase I of the thesis the three models given in Figure A.42, Figure A.43 and Figure A.44 in Appendix A shall be considered. The following division is performed for the tasks to be performed:

- Model A to be considered by student Fredrik R. Larsen for the tasks proposed in the various sections including the ice model test analysis.
- Model B to be considered by student Heidi Fjellvang for the tasks proposed in the various sections including the ice model test analysis.
- Model C shall only be considered in section C. 5.

An exception is made in section C. 4 where the students shall consider both structure A and B.

The models described can for simplicity be considered as the upper part of moored deep draft buoys.

C. PHASE I

C.1 LITERATURE STUDY ON EXISTING EXPERIENCE FROM MOORED FLOATERS IN ICE

Perform a literature study on the previous experience from using moored floating structures in Arctic waters (with drift ice present). The following items shall be discussed:

- *What are the reference projects for moored floating structures operating in the Arctic?*
  - *Describe the used structures including mooring system, and areas for operation*
- *In which ice conditions was the operations performed?*
- *What are the experience from the operations and learnings?*
- *Any effect of ice management (if used)?*

Option: A short presentation and description of gravity based structures applied in Arctic waters can be performed.

C.2 LITERATURE STUDY ON ICE PROPERTIES

The students shall perform a literature study and describe the properties (physical and mechanical), and their variability depending on time of the year) of first-year and multi-year level ice, ice ridges, rubble fields, hummocks and ice bergs.

A discussion shall be performed on geographical variability of the ice properties and the presence of the different ice features for different geographical areas of the world.

C.3 LITERATURE STUDY ON ISO 19906

The ISO 19906 code should be reviewed based on existing methodology for estimation of level ice loads on structures with a sloping surface in the waterline. The two methodologies shall be assessed:

- Ralston's methodology
- Croasdale's methodology

The methodologies shall be described and compared for the following items, with respect to the model geometry to be studied by the students, see Section C.4, with emphasis on the following items:

- *Description and discussion of each term in the algorithms with respect to physics and trigonometry behind the term and where and how the load resultant from the term will act on the considered structure during the ice structure interaction (variation in the time-domain during the stages of interaction between the structure and the ice)*
- *Discussion on simultaneously appearance of the terms during ice structure interaction*
  - *Will all the terms in the algorithm act simultaneously on the structure or will they act at different time during the ice-structure interaction?*
  - *Will each term load vary in angle and location on the structure during the interaction?*

In addition a review shall be performed on the method recommended for estimation of the global ice load on vertical structures.

C.4 DEVELOP MATLAB-SCRIPT FOR STATIC AND TIME-DOMAIN ANALYSIS OF ICE-STRUCTURE INTERACTION

For the relevant structure considered by the student a MATLAB-script for time-domain analysis of ice-structure interaction (using Croasdale's methodology) shall be developed. The script shall reflect the work performed in Section C.3 with emphasis on:

- Ice breaking period
- Rubble accumulation period before failure and ice transported around the structure
- Are the two above events occurring simultaneously (reference to other terms in the load methodology)?

OPTION: Based on the script developed an additional script can be developed describing how the total ice load resultant (sum of the resultant from all the different terms in Croasdale's methodology) varies during the ice-structure interaction (variation in angle and size of ice load resultant during the ice-structure interaction).

For both the static and time-domain MATLAB-script the following shall be assumed by the student:

- A ride up/down height of the broken ice
- An angle of the repose of the ice accumulated in front of the structure

C.5 VERTICAL VS. SLOPING GEOMETRY IN THE WATERLINE DISCUSSION

A comparison of the horizontal and vertical loads on sloping structures shall be performed for the respective sloping structures considered by the student.

- A static load estimate for the ice condition given in Table A.34 shall be performed comparing the sloping structure A and B (for both students) with the vertical structure C, see Appendix A.
  - Using both Croasdale's and Ralston's methodology

The three structures reflect the upper part of either a gravity based structure or a floating structure. A discussion and documentation shall be performed on:

- The potential benefit of using a sloping geometry in the waterline, compared to vertical, for floating structures.
- If sloping geometry in the waterline is applied for gravity based structures, which (upward or downward breaking) would be beneficial?

The discussion shall be supported by numerical calculations.

C.6 PRE-SIMULATION OF ICE MODEL TEST

Based on the work performed in section C.3 and section C.4 a pre-simulation of an ice model test campaign, see section C.7, shall be performed using the ice data in Table A.35, see Appendix A. The following shall be assumed by the students:

- Ride down/ride up height (depending on structure considered) of ice rubble.
- Ice breaking/failure period shall be estimated based on theory (ISO 19906).
- Angle of load resultant and vertical variation of resultant over the failure area.
- Other parameters shall be assumed based on relevant references identified by students.

C.7 ICE MODEL TEST ANALYSIS

When sections prior to section C.7 are completed data (report, videos and time series) from a performed ice model test with fixed structures having sloping geometry in the waterline (similar to model A and B and test matrix as given in Table A.35 and Table A.36, see Appendix A) will be delivered the students. The following tasks shall be performed in the analysis of the ice model test data (the students shall only analyse results from their respective models):

Set-up and measurement analysis:

- A description and discussion of the model test set-up (set-up including instrumentation of the model) and ice preparation and ice measurement methods shall be performed including a discussion on:
  - Are all relevant ice properties measured, ref section C.2?
  - Variation in level ice properties from target to actually achieved
    - A comparison shall be performed
  - Spatial distribution of level ice properties in the prepared ice sheets

- Discussion of using results from model testing of structures in fixed mode vs. model testing of structures in moored mode (what are the main advantages with the fixed set-up vs. a moored set- up and visa versa)

Analysis of test results:

For the ice model tests performed the following work is proposed:

- Comparison of results (plot in MATLAB) obtained for the sensitivities performed on:
  - Velocity
  - Ice thickness
- Use basic statistical measures to describe the measured ice load time series for the tests and compare these results for the sensitivities performed on velocity and ice thickness and comment on differences in results:
  - Including identification and comparison of ice breaking period for the tests, including average ice breaking length, and compare ice rubble accumulation failure period for the tests
    - Comment on potential simultaneously occurrence with ice breaking failure
- Describe, quantify and compare the following items for the tests performed:
  - Describe geometry of ice rubble accumulation and ice transport for the tests and how this varies in the time-domain during the tests
  - Any specific events identified in the time load series shall be explained (peak loads, load build up etc)

If large deviation in ice properties between the tests are identified this shall be commented on and discussed with respect to its possible influence on the ice-structure interaction.

C.8 COMPARISON WITH DEVELOPED MATLAB-SCRIPT AND CORRECTION OF IT

Based on the activities performed in section C.6 and section C.7 the results obtained with the MATLAB-script, for the tests analysed, shall be compared with the measured ice load time series for the relevant tests with the following use/input of the developed MATLAB-script:

- Use of MATLAB-script with target ice properties and assumed ice transport and accumulations scenario
- Use of MATLAB-script with actually obtained ice properties and identified average breaking period of the ice, and assumed ice transport and accumulations scenario
- Use of MATLAB-script corrected for actual measured ice properties, identified average breaking periods of the ice and geometry of ice accumulation and transport on the structure

The comparison shall be performed for all relevant tests. A discussion, including possible reasons, for differences obtained between estimated load time series and measured shall be performed for the three above items.

As a final activity the following shall be performed:

- Use of MATLAB-script with target ice mechanical properties and, identified average breaking periods of the ice and geometry of ice transport on the structure.

  - The results from this exercise shall be compared with:
    * Estimation performed with target ice properties and assumed ice transport and accumulation scenario
    * Measured time series

A discussion on the validity of performing numerical simulations compared to performing ice model testing shall be performed based on the above comparison.

C.9 PHASE II

- Analysis of ice ridge test
- Analysis of model test with moored set-up

(Phase II has been left out of the scope of work in agreement with Professor Amdahl due to time limitations)

D. OTHER

- All assumptions done by the student shall be clearly stated in the report
- References shall be clearly stated

THESIS FORMAT

The thesis should be organized in a rational manner to give a clear exposition of results, assessments and conclusions. The text should be brief and to the point, with a clear language. Telegraphic language should be avoided.

The thesis shall contain the following elements: A text defining the scope, preface, list of contents, summary, main body of thesis, conclusions with recommendations for further work, list of symbols and acronyms, references and (optional) appendices. All figures, tables and equations shall be numerated.

The report shall be submitted in two copies:

- Signed by the candidate
- The text defining the scope included
- In bound volume(s)
- Drawings and/or computer prints which cannot be bound should be organized in a separate folder

OWNERSHIP AND CONFIDENTIALITY

Reference is to confidentiality agreement between Aker Solutions and Heidi Fjellvang/Fredrik Røssel Larsen/Jørgen Amdahl dated 22.03.2011.

The model test results presented in the thesis are the property of Aker Solutions and therefore this thesis shall be kept confidential for a period of 5-years.

THESIS SUPERVISOR

Prof. Jørgen Amdahl Dept. of Marine technology

Deadline: June 14, 2011

Trondheim, February 06, 2011

Jørgen Amdahl

PREFACE

This report is the result of my master thesis work at the Department of Marine Technology at the Norwegian University of Science and Technology (NTNU). The master thesis counts for 30 credits in the tenth semester of the Master of Science in Marine Technology education.

The purpose for this work has been to develop numerical model for estimation of the level ice loads acting on a structure with a conical surface in the waterline in the time-domain.

Parts of the problem text are answered by the master thesis candidate Fredrik R. Larsen and will therefore not be covered in this report. These parts are written in *italic* in the problem text given on page II under section C.1 and C.3.

I have found it both challenging and time consuming to work with the time series and model test videos provided by Aker Solutions due to limited background knowledge on this area. To overcome the challenges met I have had weekly discussions with Larsen which has been very valuable.

The working load of the first intended scope presented in the problem text turned out to be too extensive to cover within the period of work. It was therefore decided in agreement with Per Kristian Bruun and Professor Jørgen Amdahl to leave Phase II out of the thesis work, see C.9 in problem text.

First of all I would like to thank Per Kristian Bruun in Aker Solutions for very helpful guidance during the whole semester. He has shown enthusiasm and interest for my work which has been very inspiring. I also want to thank my supervisor, Professor Jørgen Amdahl, for the valuable discussions we have had during the period of work.

My gratitude goes to DSc. Professor Kaj Riska and Professor Sveinung Løset for proving articles that have been helpful for my work.

Trondheim May 30, 2011

Heidi Fjellvang

EXECUTIVE SUMMARY

A literature study on the physical and mechanical properties of sea ice has been performed in Chapter 2. A brief introduction to the most common failure modes involved in an ice-structure interaction is also given.

The new ISO 19906 standard on Arctic Offshore Structures has been reviewed based on existing methodology for estimation of level ice loads on structures with sloping geometry in the waterline. Two different methodologies are assessed, namely Ralston's methodology and Croasdale's methodology. Ralston's methodology is suitable for *narrow structures* where the waterline diameter is typically less than 5 m (ISO 19906, 2010) and is based on theory of plasticity. Croasdale's methodology is more appropriate for *wide structures* with waterline diameter $>>$ 5 m. In the latter methodology, the ice sheet is considered as an elastic beam resting on an elastic foundation. The presence of rubble on the face of the structure is only included in Croasdale's methodology. In addition, a third methodology for estimation of level ice loads acting on vertical structures is described. The purpose for the review has been to get a deep understanding of the ice-structure interaction processes and which ice and structure factors that governs the processes.

Based on the review of the ISO 19906, a static load estimate of ice loads acting on an upward breaking, a downward breaking and a vertical structure is given in Chapter 4. All structures have a waterline diameter of 30 m. The main findings from the analysis are;

- The two methodologies, namely Ralston's methodology and Croasdale's methodology, assessed for the calculation of ice loads acting on sloping structures give different results for the upward breaking structure.
- Upward breaking results in higher ice loads compared to downward breaking for a structure of same waterline diameter and inclination angle between the structure's sloping plane and waterline.
- A vertical structure is subjected to larger loads than a structure with sloping waterline geometry. The static analysis shows that the loads are more than 10 times higher than for both the upward and the downward breaking structure.

A numerical model has been developed based on Croasdale's methodology for estimation of ice loads on an upward breaking structure in the time-domain. The ice transport around the structure as well as the rubble accumulation scenario were assumed based on the best available material which was readily available at the time. A pre-simulation of an ice model test campaign has been performed where the numerical model was utilized. The campaign contains four different ice model tests, all with an unique combination of ice thickness and drift velocity (see table below). The calculated horizontal loads are ranging from 4.0 MN to 5.5 MN while the vertical loads are in the range of 2.9 MN to 4.1 MN.

Ice test no.	**Velocity [m/s]**	**Ice thickness [m]**
1	0.5	1
2	1	1
3	0.5	1.5
4	1	1.5

Aker Solutions has performed an ice model test campaign with similar target ice conditions and structure geometry as the four tests presented in the table above. The ice thickness, flexural strength, compressive strength, Young's modules and the ice density were measured either before or after the ice model tests were performed. All properties showed small variations from

the target properties both within the prepared ice sheet and from one day to another. Important ice properties for the calculation of the ice-structure interaction that were not measured are; the tensile strength, ice salinity, poissons ratio, ice-to-ice friction, cohesion, friction angle of the ice rubble and porosity. Time series and videos recorded during the tests have been provided the student. The measured horizontal loads are ranging from 4.5 MN to 5.7 MN while the vertical loads are in the range of 6.9 MN to 9.0 MN, hence larger than first estimated in the pre-simulation.

The table below summarizes both the first assumed rubble geometry and ice transport scenario used in the pre-simulation in addition to what has been identified from the model test videos. The assumed parameters differ from the observed ones, in particular the average breaking period, load build-up period and the rubble failure period.

Parameter		**Ice model test no.**			
		1	**2**	**3**	**4**
Rubble height [m]	Identified	6	7	6	7
	Assumed	5	5	5	5
Average breaking period [sec]	Identified	6	2	7.5	6
	Assumed	25.8	12.9	34.8	17.4
Average load build-up period [sec]	Identified	280	93	175	66
	Assumed	50	50	50	50
Average rubble failure period [sec]	Identified	61	33	130	84
	Assumed	0	0	0	0
Rubble angle with horizontal [deg]	Identified	30	35	31	33
	Assumed	35	35	35	35

A sensitivity test on ice thickness (thick vs. thin) and drift velocity (high vs. low) has been performed based on the measured time series from the ice test campaign performed by Aker Solutions. The main findings from the study are;

- Both an increase in ice thickness and in velocity leads to higher ice loads. However, the ice loads are more sensitive to an increase in velocity than in ice thickness, ref. table below.
- The load build-up period is shorter for the high-velocity ice and for the thick ice, compared to the low-velocity ice and the thin ice.
- A larger standard deviation in measured loads is registered for the thick ice and low-velocity ice compared to thin ice and high-velocity ice.

The table below summarizes how the mean resultant forces are affected by increasing the ice thickness from 1 m to 1.5 m (see II and III) and the velocity from 0.5 m/s to 1 m/s (see I and IV).

Sensitivity test no.	**Description of tests**	**$F_{RESULTANT}$ (Mean)**
I	h = 1 m v increases from 0.5 m/s to 1 m/s	+19%
II	v = 0.5 m/s h increases from 1 m to 1.5 m	+5%
III	v = 1 m/s h increases from 1 m to 1.5 m	+8%
IV	h = 1.5 m v increases from 0.5 m/s to 1 m/s	+23%

The numerical model used in the pre-simulation was later corrected stepwise in order to obtain a closer correlation with the measured loads. Notice that all cases presented below originates from the numerical model used in the pre-simulation.

- Case 1 is the first made model used in the pre-simulation. It can be seen that the time series calculated differs from the measured both visually and numerically. Hence the first-made assumptions are incorrect.
- Case 2 differs from Case 1 by including the identified ice properties and breaking period of the ice sheet in the model. Also here a deviation from the measure loads can be seen.
- Case 3.a is corrected in agreement with the identified ice properties, rubble geometry, ice transport etc. The trend in the plot is more similar to the measured time series than the first two cases. However the calculated loads are too large.
- Case 3.b differs from Case 3.a by reducing the horizontal load by a factor of 3 and the vertical load by a factor of 1.5. This has been done in order to get a closer correlation to the measured loads.

The cases are summarized below.

Case no.	Ice properties		Breaking period		Ice transport		Ice accumulation	
	Target	Measured	Assumed	Identified	Assumed	Identified	Assumed	Identified
1	x		x		x		x	
2		x		x	x		x	
3.a		x		x		x		x
3.b		x		x		x		x
4	x			x		x		x

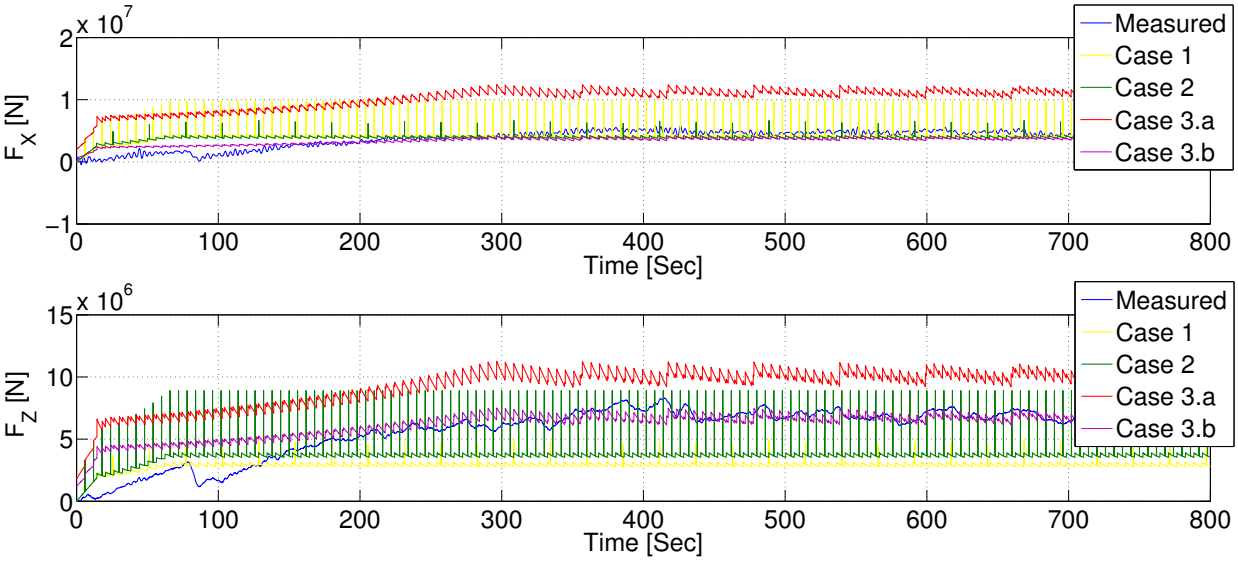

A fourth case is shown below, plotted against the measured time series. Case 4 is equal to Case 3.b except that target ice properties are used instead of the actually measured ice properties. The main differences between the measured time series and Case 4 are the following;

- The calculated and the measured time series are following more or less the same trend. However, the random behavior of the rubble failure has not been included in the numerical simulation.
- The calculated forces are more or less in the same range as the measured loads. However, it was necessary to reduce the total horizontal load by a factor of 3 and the vertical load

by a factor of 1.5 in order obtain the same range in loads.

- According to Croasdale's methodology in combination with the given structure geometry and friction coefficient between ice and structure, the vertical load is less than the horizontal load. This was not in agreement with the measured time series and had to be corrected for.

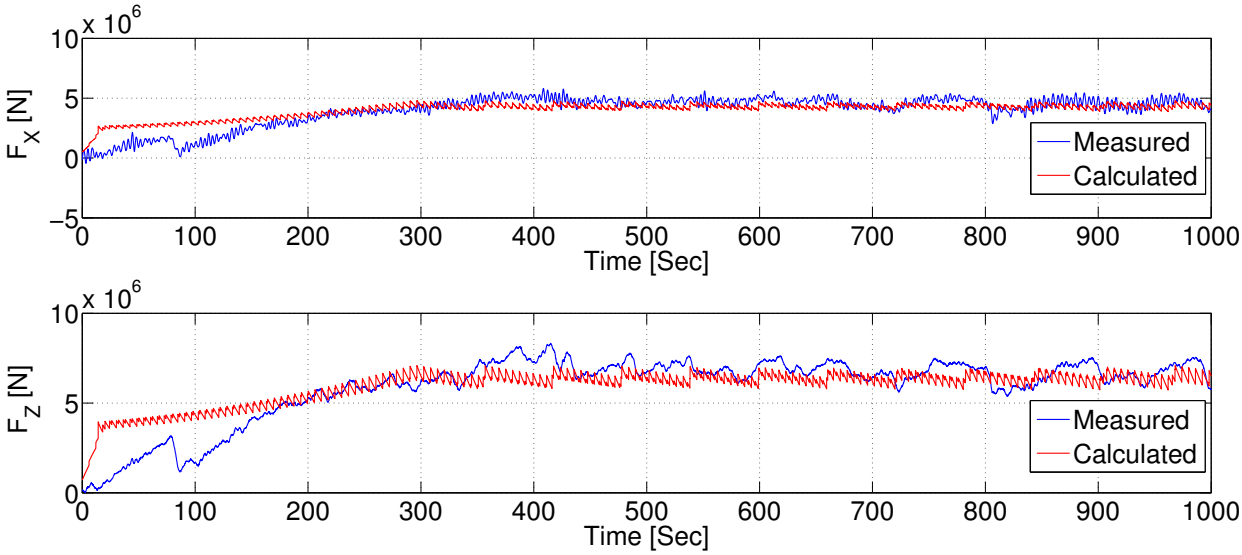

Although the loads estimated show deviations from the measured time series, it is reasonable to believe that a numerical simulation of the ice failure process against a sloping structure may give results in the same range as an ice model test. However, it is recommended that a few additional tests should be included in the tests campaign where the focus is on identifying important parameters needed in the numerical model such as breaking length of the ice sheet and rubble geometry.

TABLE OF CONTENTS

LIST OF FIGURES

LIST OF TABLES

NOMENCLATURE

All symbols, abbreviations and definitions used in the analyses are given below.

Latin symbols

A_N	Nominal contact area
c	Cohesion angle of the ice rubble
C_R	Ice strength coefficient
e	Porosity of the ice rubble
E	Elastic modulus
F	Ice action
g	Acceleration due to gravity
h	Thickness of the ice sheet
H_B	Horizontal action on the cone due to ice breaking
h_i	Ice thickness (alternative notation to h)
H_L	Load required to push the sheet ice through the ice rubble on the top of the advancing ice sheet prior to breaking it
H_P	Load required to push the sheet ice through the ice rubble
H_R	Horizontal action on the cone due to ride up
h_r	Ice ride-up thickness/rubble height
H_T	Load to turn the ice block at the top of the slope
k_i	Thermal conductivity of ice
L	Latent heat of fusion of the ice sheet
N	Component normal to the structure surface
p_G	Ice pressure averaged over the nominal area associated with the global action
SD	Standard Deviation
t	Time
T	Period of action
T_a	Temperature at the top of an ice sheet
T_b	Temperature at the bottom of an ice sheet
V_B	Vertical action on the cone due to ice breaking
V_R	Vertical action on the cone due to ride up
v_s	Sliding velocity
w	Waterline diameter of the cone or width of a sloping structure
w_T	Top diameter of the cone

Greek symbols

α	Inclination angle of the structure surface from the horizon
θ	Angle the rubble makes with the horizon
μ	Coefficient of kinetic friction between the ice and structure surface
μ_i	Ice-to-ice friction coefficient normally taken as 0.03 (kinetic friction)
ν	Poission's ratio
ρ_i	Density of ice
ρ_w	Density of water
σ_f	Flexural strength of the ice sheet
τ	Duration of loading/unloading cycle
ϕ	Friction angle of the ice rubble
ϕ_i	Heat flux from ice to air

Abbrevations

FY-ice	First year-ice
ISO	International Organization for Standardization
MY-ice	Multi year-ice
Psu	Practical salinity unit

Definitions

Action	External load applied to the structure or an imposed deformation
Brine	Water that is saturated or nearly saturated with salt
Columnar ice	Ice crystals are elongated in the vertical direction
Downward cone	A cone that breaks the oncoming ice downwards
First-year ice	Sea ice of no more than one winter growth
Grain structure	Grain arrangement in the ice
Granular ice	Ice composed of crystals with equal dimensions
Hummock ice	A form of pressure ice in which pieces of ice are piled arbitrary, one piece over another, forming an uneven surface
Iceberg	Glacial or shelf ice (greater than 5 m freeboard) that has broken (calved) away from its source
Ice feature	Level ice, rafted ice, ridge, rubble, iceberg etc.
Ice thickness	The average thickness of the ice formation without snow at the surface
Multi-year ice	Sea ice that have survived one or more summer melt season(s)
Rafted ice	Ice feature formed from the superposition of two or more ice sheet layers
Ridge	Ice formation consisting of ice blocks formed as a result of compression or shear of the ice fields
Rubble field	Region of broken ice blocks floating together as a continuous body
Sea ice	Any form of ice formed as a result of seawater freezing
Sloping Structure	A structure with inclined walls in the waterline area towards the direction of the ice action
Structure	Any man-made obstacle exposed to ice action
Upward Cone	A cone that breaks the oncoming ice upwards

1 INTRODUCTION

A substantial amount of the world's hydrocarbon deposits is assumed to be found in the Arctic. The Arctic region differs from other regions mainly due to the climate and presence of sea ice features.

In order to minimize the ice loads from drifting ice, structures with sloping waterline geometry have been introduced to the marked. The breaking angle in the waterline allows the ice to fail in a flexural mode, and to further transport the broken ice pieces around the hull.

Thesis outline

The purpose for this master thesis has been to develop a time-domain MATLAB-script in order to describe the ice action loads acting on an upward breaking structure. Firstly the ice transport and rubble accumulation scenarios were assumed based on the best available material which was readily available at the time. The script has later been corrected based on actually measured time series and videos recorded from an ice model test campaign performed by Aker Solutions.

A literature study on the mechanical and physical properties of sea ice is performed in Chapter 2. Additionally, a short introduction to the most common failure modes and load scenarios involved in an ice-structure interaction is included.

A review of the new ISO 19906 standard on Arctic Offshore Structures is given in Chapter 3 based on the existing methodology for estimation of level ice loads on structures with sloping geometry in the waterline. In addition is the method recommended for estimation of the global ice load on vertical structures reviewed.

Chapter 4 presents a comparison study between structures with sloping geometry in the waterline and vertical structures. The purpose has been to justify the use of structures with sloping waterline geometry.

A MATLAB-script has been developed in order to calculate the ice action forces acting on offshore structures in the time-domain. The script is presented in Chapter 5. All assumptions made by the student regarding ice transport and ice rubble accumulation scenarios are clearly stated.

A pre-simulation of the four model ice tests presented below is performed in Chapter 6. The numerical model developed is utilized.

Ice test no.	Velocity [m/s]	Ice thickness [m]
1	0.5	1
2	1	1
3	0.5	1.5
4	1	1.5

Chapter 7 summarizes the main findings from the ice model tests performed by Aker Solutions. Basic statistics are given for all four tests in addition to a description of actually observed ice transport and ice rubble accumulation scenario.

The results from the numerical simulation have been compared to the actually measured time series in Chapter 8. Based on the comparison, the script has been modified in order to get a close correlation to the measured time series.

Chapter 9 and Chapter 10 include conclusions and recommendations for further work.

2 LITERATURE STUDY ON ICE PROPERTIES

The global ice action between an ice feature and a structure depends on two factors, the contact area and the stresses (or nominal contact area and effective pressure). These two depend on many others such as the scenario of ice-structure interaction, the ice properties, type of ice features (e.g. level ice, ridge, rubble), the structure's geometry etc. This dependence is presented in the flowchart shown in Figure 2.1 (Løset et al., 2006). All five main categories given in Figure 2.1 are discussed in this chapter.

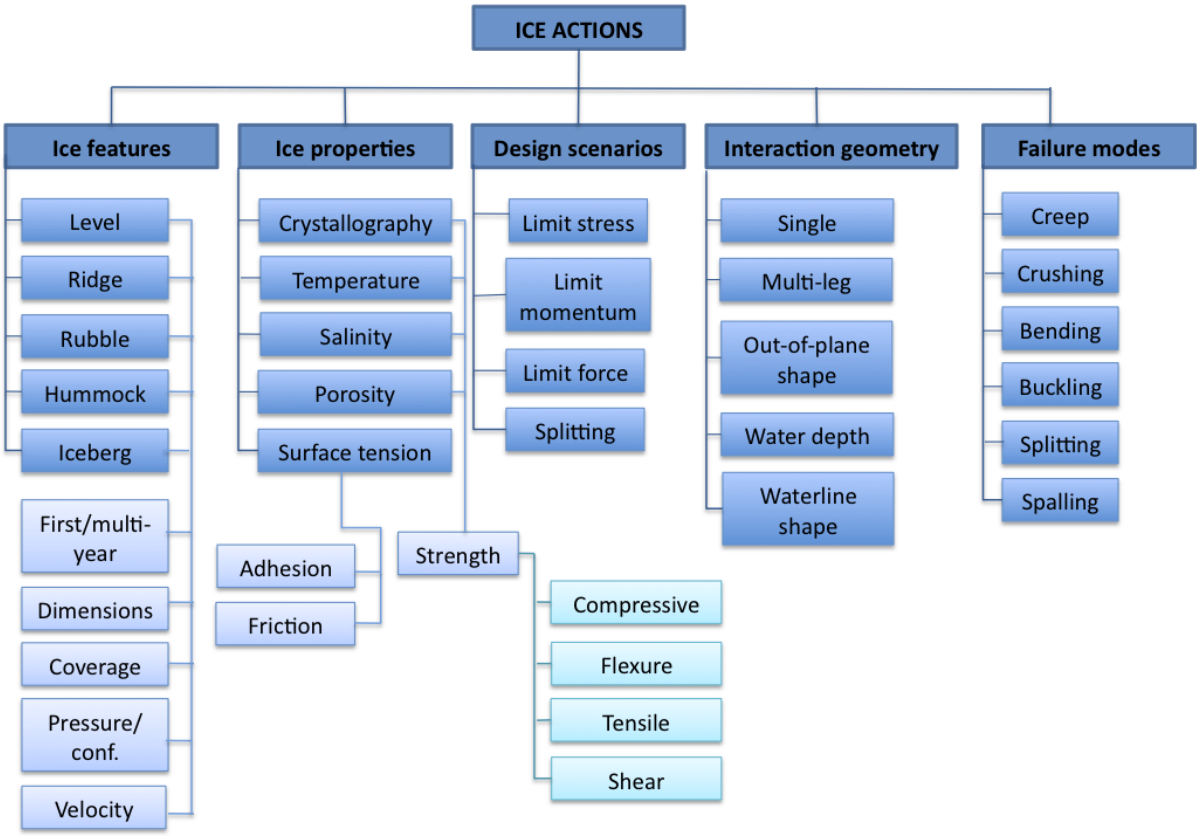

Figure 2.1: The major parameters affecting the ice action

2.1 Mechanical and physical properties of ice

The most important *physical properties* (thickness/growth, salinity, porosity and density) and *mechanical properties* (tensile, flexural, shear, uni-axial compression strength, elastic and strain modulus, and friction coefficient) of sea ice are described in this chapter. Physical and mechanical properties of the sea ice are important input in the load methodology for calculation of ice action on offshore structures.

Both first-year ice (FY-ice), multi-year ice (MY-ice), ice ridges, rubble fields, hummocks and ice bergs are outlined. *First-year ice* is sea ice of no more than one winter growth while *multi-year ice* is sea ice that has survived at least one summer melt season. An *ice ridge* is a feature which is formed under pressure or shear processes in the ice cover. A *rubble field* is a region of broken ice blocks floating together as a continuos body. *Ice bergs* are glaciers or a shelf ice (greater than 5 m freeboard) that have broken (calved) away from its source. *Hummocked ice* is a form of pressure ice in which pieces of ice are piled arbitrarily, one piece over another, forming an uneven surface.

A large amount of research has been conducted during the years especially during the boom in Canadian and American Beaufort Sea in the 1970's. When studying ice properties it is important to keep in mind that the properties are varying during the year due to changes in temperature, sunlight etc.

The majority of the results presented in this chapter originates from sites in the North Atlantic Arctic. It should be mentioned that the physical and mechanical properties of FY-ice are well understood. There is less information available regarding MY-ice and ice ridges even though the ice blocks which form the ridges are made from level ice. Consequently, FY-ice will be in focus when describing the sea ice properties.

2.1.1 Geographical variations

Ice properties and the presence of the different ice features are varying both within and outside the Arctic region. This has to be taken into account in the design of offshore structures in these areas. A brief discussion on the geographical variations within the Arctic region is given below in addition to a comparison between Arctic and Antarctic. Illustrations of FY-ice, MY-ice, an idealized pressure ridge and an iceberg are given in Figure 2.2, Figure 2.3, Figure 2.4, and Figure 2.5. Sail height and keel depth are important parameters for rubble fields and pressure ridges and described on page 7.

Variations within the Arctic region

Four different seas within the Arctic region are highlighted and compared, namely the Beaufort Sea, the Bering Sea, the Baltic Sea and the Barents Sea. If a parameter is not given in Table 2.2 it means that it is not found in that particular region. The intension for the table is not to provide design parameters, but rather to give an insight in typical values in the four different regions in the Arctic.

Table 2.1 indicates the duration of the winter and summer season for the four regions (ISO 19906, 2010).

Table 2.1: Geographical variations in winter and summer season in the Arctic

Season / Sea	Beaufort	Bering	Baltic	Barents
Winter	Sept - May	135 - 210 days/year	Nov- June	All year
Summer	June - Aug	155 - 230 days/year	Apr - Dec	None

The data presented in Table 2.2 are taken from Table B.7-3, B.9-3, B.15-3 and B.16-3 in ISO-19906 (ISO 19906, 2010). Four locations are given for both the Bearing Sea, the Baltic Sea and the Barents Sea. An average value has therefore been calculated for the different parameters.

Table 2.2: Sea ice conditions for Beaufort, Bering, Baltic and Barents Sea

		Parameter	Average annual value			
			Beaufort	**Bering**	**Baltic**	**Barents**
Sea ice	**Occurrence**	First ice	Sept	Dec	Dec	All year
		Last ice	Aug	May	April	All year
	Level Ice (FY)	LFI thickness (m)	1.8	1	0.6	1.5
		Floe thickness (m)	1.8	1	0.6	1.4
	Rubble Fields	Sail height (m)	5	3	1-2	-
		Length (m)	-	100-300	100-1000	-
	Ridges (FY)	Sail height (m)	5	3-4	2-3	4.2
		Keel depth (m)	25	1 0-15	3-25	15
	Land Fast Ice (MY)	LFI thickness (m)	0	-	-	2.5
		Floe thickness (m)	5	-	-	2.8
	Ridges (MY)	Sail height (m)	Significant	-	-	-
		Keel depth (m)	20	-	-	-
	Rubble Fields (MY)	Ave. sail height (m)	-	-	-	-
		Length (m)	-			-
Icebergs	**Size**	Mass (tonnes)	$10 \cdot 10^6$	-	-	$4 \cdot 10^6$
	Frequency	Months present	Poorly known	-	-	All year
		Number per year	Poorly known	-	-	
		Max. per month	Rare	-	-	

Arctic vs. Antarctic

To exemplify that the ice conditions in the Arctic differ from other areas in the world, a brief comparison between Arctic and Antarctic is given below (National Snow and Ice Data Center, 2009).

Arctic	**Antarctic**
∗ The Arctic is a semi-enclosed ocean almost completely surrounded by land	∗ The Antarctic is a land surrounded by ocean
∗ The sea ice in the Arctic is not freely to move which causes the ice to stay in the cold Arctic water	∗ Due to no land boundary, the forming ice is free to float into warmer waters and eventually melt
∗ Floes are prone to converge and pile up into thick ridges	∗ Ridges are much less often formed in the Antarctic
∗ Multi-year ice features can be found in different areas within the Arctic region	∗Almost all ice that forms during the winter melts during the summer season
∗ Arctic ice is typically 2 - 3 m in average	∗Antarctic ice is typically 1 - 2 m in average
∗ The maximum ice extent in the Arctic is asymmetric	∗ The pattern of maximum ice extent is almost symmetric around the pole
∗ Arctic sea ice can extend all the way to the North Pole	∗ The Antarctic sea ice does not reach the South Pole

2.1.2 Ice growth

Sea ice is composed of air, brine, solid ice and, depending on the temperature, various types of salts. Depending on the prevailing conditions, the ice growth mechanism can produce several different grain structures. All details regarding the microstructure of the ice will affect the mechanical and the physical properties of the ice.

When the surface water in the ocean reaches the freezing temperature, small needle-like crystals of pure ice are formed. A continuous accumulation of crystals will result in an oily-appearance in the water. The surrounding water will become both a little saltier and denser as a result of this freezing process. As more and more crystals are freezing together, small pockets will remain between the crystals where brine tends to get trapped. These brine pockets are the reason why seawater ice is less strong compared to freshwater ice. The volume of the brine pockets are dependent on the temperature, which causes the ice strength to increase as the temperature decreases. The brine volume fraction of sea ice can be calculated by the relationship (Frankenstein & Garner, 1967).

Where;

v_b	Brine volume fraction
S	Salinity as a fraction of the ice melt volume
T	Ice temperature (°C)

$$v_b = S\left(\frac{49.18}{|T|} + 0.53\right) \tag{2.1}$$

The brine pockets in FY-ice are shown in Figure 2.2. If the process of ice freezing is slow, less brine gets trapped in the pockets and the ice will become less salt compared to a quick ice freezing process. In general, sea ice contains much less salt than the water from which it froze because most of the water is rejected back to the ocean during the freezing process.

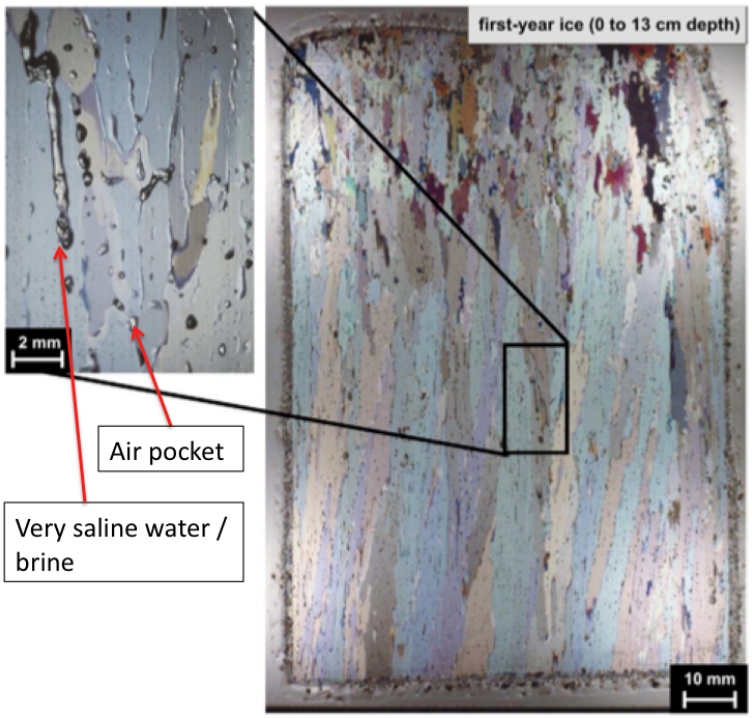

Figure 2.2: Thin section of first-year ice

FY-sea ice has typically an average salinity in the range of 4 to 6 ‰ salt. To compare, seawater has an average salinity in the range of 32 to 35 ‰ (Timco & Weeks, 2009). Unlike the FY-ice, MY-ice usually has a very low salinity because more salt has migrated through the ice and back in the seawater. As such, there is little porosity in MY- ice which is the explanation why it is stronger than younger ice. Further, due to the small amount of salt, the change in the volume

of the brine in the ice with increasing temperature is small. The ice properties of MY-ice are more similar to the properties of ice made from fresh water and glaciers than FY-ice. The oldest layer of undeformed MY- ice is on the top while the bottom layer is FY-ice. Both growth and thickness of MY- ice are results of metrological and mechanical conditions unlike the FY-ice which is only controlled by the overlying metrological conditions.

Once an ice sheet has been formed it can increase its thickness by freezing of water on its lower surface which means that heat must be removed from the water. When the air temperature is lower than the temperature of the water below the ice sheet, heat will be removed through the ice by conduction. Heat is removed from the warm body (water) to the colder body (air). The rate of heat flow is proportional to the temperature difference between the cold and warm body, and inversely proportional to the thickness of the ice sheet.

The expected thickness of a FY-ice cover can be estimated mathematically by the freezing degree method. According to the lectures given by Gunnar Furnes at NTNU in the period September-November 2010 (Furnes, 2010), the ice thickness can be calculated as given below.

The parameters used are;

ϕ_i	Heat flux from ice to air
ρ_i	Ice density
L	Latent heat of fusion of the ice
t	Time
h_i	Ice thickness

$$\phi_i dt = \rho_i L dh_i \tag{2.2}$$

A steady state condition is assumed and the heat transfer between the water and ice is negligible. The growth rate is determined by the energy balance at the ice-water interface.

Further we assume that the top ice surface temperature is the same as the air temperature, then

$$\phi_i = \frac{k_i(T_b - T_a)}{h_i} \tag{2.3}$$

Where;

T_b	Temperature at the bottom of the ice sheet
T_a	Temperature at the top of the ice sheet (equal to T_{air})
k_i	Thermal conductivity of ice

Integration of Equation 2.2 using Equation 2.3 and letting $h_i = 0$ at t = 0, gives:

$$h = \left(\frac{2k_i}{\rho_i L}\right)^{0.5} \cdot [(T_b - T_a)]^{0.5} \tag{2.4}$$

This equation is commonly referred to as the *Stefan's equation*. This is a direct approach to find the ice thickness and does not take for instance snow (which acts as an insulator) into account. Therefore it is more common to use empirical formulas to include parameters that will affect the ice thickness. Typically the FY-level ice in the Canadian and American Beaufort Sea reaches 2 m at the end of the winter (Melling et al., 2005).

MY- ice can be extremely thick and is a result of thermal growth and mechanical consolidation through pressure-ridging processes. In average, the mean thickness of a level ice MY-feature is 5.6 m (±2.2 m) (Timco & Weeks, 2009). A thin section of MY- ice is shown in Figure 2.3. The absence of salt can be observed in addition to the variation of grain structure.

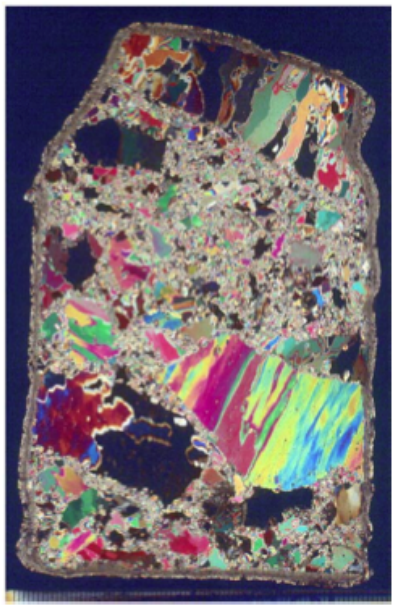

Figure 2.3: Thin section of multi-year ice

First-year ridges and hummock fields can be found anywhere FY-ice forms and is mobile enough to create them. A typical first-year ridge is shown in Figure 2.4 and is usually divided into two parts, keel and sail. The *sail* (A) is made from ice blocks above the waterline. The *keel* (C) is to be found below the waterline and consists of submerged ice blocks and a consolidated layer (B). Here, rafted ice and ice blocks are frozen together. Both sail height (E) and the level ice thickness (D) are key parameters to define other geometrical shape parameters. The thickness of the consolidated layer and the keel depth (F) are depending on geographical location. Multi-year ridges are more rectangular in shape compared to first-year ridges.

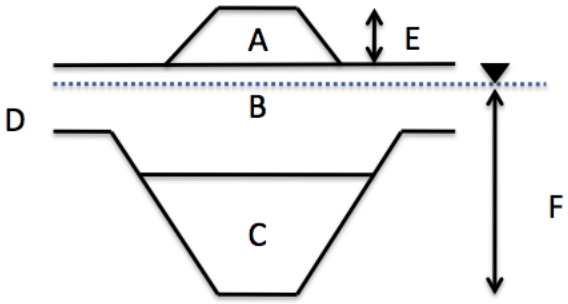

Figure 2.4: Idealized first-year sea ice ridge

Figure 2.5: Iceberg

2.1.3 Compressive strength

The compressive strength of sea ice depends on many parameters such as brine volume, amount of air bubbles, strain rate and type of ice. Uniaxial compressive strength is the most common in ice mechanics and important in the calculations of ice actions on offshore structures.

Uniaxial compressive strength of first-year ice

The uniaxial compresssive strength has its maximum at a strain rate of approximately $\dot{\varepsilon}$ = 10^{-3} sec^{-1}. Here, the ice fails at the transition between ductile and brittle deformation.

Many investigators have studied the compressive strength of small samples of sea ice. It has been found that there are many factors that will affect the compressive strength such as temperature, salinity, density, ice type, crystal size, orientation and the test conditions. Timco and Frederking (Timco & Frederking, 1990, 1991) have developed a model to describe the compressive strength of an ice sheet. The equations are valid for FY-ice and include information regarding temperature, ice salinity, bulk ice density, grain structure, grain structure, loading direction and number of tests.

For horizontally-loaded columnar ice, the uni-axial strength [MPa] is

$$\sigma_c = 37(\dot{\varepsilon})^{0.22}\left[1-\sqrt{\frac{\nu_T}{270}}\right] \tag{2.5}$$

For vertically-loaded columnar ice, the uni-axial strength [MPa] is

$$\sigma_c = 160(\dot{\varepsilon})^{0.22}\left[1-\sqrt{\frac{\nu_T}{200}}\right] \tag{2.6}$$

and for granular ice, the uni-axial strength [MPa] is

$$\sigma_c = 49(\dot{\varepsilon})^{0.22}\left[1-\sqrt{\frac{\nu_T}{280}}\right] \tag{2.7}$$

Where ν_T is given in ‰. The equations give slightly conservative values if the total void volume is replaced by the brine volume fraction v_b and are applicable in the strain rate of $10^{-7}s^{-1}$ to about $2\cdot 10^{-4}s^{-1}$. At higher strain rates brittle failure may occur.

Uniaxial compressive strength of multi-year ice

From measurements of the compressive strength of MY-ice (Timco & Frederking, 1986; Sinha, 1984), it has been found that MY-ice has almost the same strength as FY-ice if the ice is very cold (i.e. -20 °). However, when the ice is warmed up during the summer season, MY-ice can be considerable stronger than FY-ice. The reason for this is that as the temperature of MY- ice increases, there are only small differences in the brine volume.

There is little data existing on small-scale uni-axial compression tests conducted on ridges. Therefore, there is no clear justification for lowering the compressive strength of the consolidated layer when comparing it to level ice.

2.1.4 Tensile strength

Tensile strength is a fundamental property of sea ice because it defines the maximum tensile stress the ice can withstand before failure. Often when observing large areas of sea ice open leads can be observed. This phenomenon is often a result of tensile failure of ice. The tensile strength is important for predicting large-scale ice movements and local ice forecasting.

The tensile strength is almost independent of the strain rate in the range of ε = 10^{-5} sec^{-1} to 10^{-3} sec^{-1} and is in the vertical direction (of columnar grained ice) about twice as high as in the horizontal direction. Typical values are given in Table 2.3 (ISO 19906, 2010).

Table 2.3: Typical tensile strength values

Temperature	Ice type	Salinity	Action direction	
			Vertical	Horizontal
-10°C	Sea Ice	4-6 ‰	1.7 MPa	0.9 MPa
-10°C	Baltic Ice	0.2 ‰	2.2 MPa	1.0 MPa

Based on Table 2.3 the tensile strength [MPa] can be expressed as below where v_b is the brine volume fraction.

$$\sigma_t(vertical) = 2.2\left(1 - \sqrt{\frac{v_b}{0.31}}\right) \tag{2.8}$$

$$\sigma_t(horizontal) = 1.0\left(1 - \sqrt{\frac{v_b}{0.14}}\right) \tag{2.9}$$

There is a very small number of measurements of the tensile strength of MY- ice. From the few tests that are conducted large deviations in strength are found due to variations of the structure of the different samples. In general, MY- ice is stronger, higher tensile strength, compared to first-year ice.

2.1.5 Flexural strength

The flexural strength of ice is used for estimating ice actions on sloping structures and defined as the extreme fibre stress in tension. Many real sea ice failures occur in flexure which is the reason why it is important to measure the flexural strength of the ice. Examples are pressure ridge formation, icebreaking vessel failing ice and bending of ice on conical-shaped structures.

The strength of sea ice is depending on several parameters such as temperature, the loading direction of the ice, the ice grain structure, the grain size, the test type (simple beam test or cantilever beam test), the loading rate, ice salinity and brine volume. Because the flexural strength is a function of many different parameters, it is challenging to make a strong correlation between the strength of the ice and the above-given sample characteristics. Several researchers have related the strength of the ice to the brine volume or the total porosity of the ice. This because it is generally assumed that as the total porosity in the ice increases, the strength should decrease because there is less "solid ice" that has to be broken. From a comprehensive analysis of the problem (Timco & O'Brien, 1994) it has been shown that for FY-ice the below-given equation (only valid for cold and growing ice) yields for flexural strength.

Where;

σ_f	Flexural strength of ice [MPa]
v_b	Brine volume (expressed as a brine volume fraction)

$$\sigma_f = 1.76e^{-5.88\sqrt{v_b}} \tag{2.10}$$

For sea ice, the flexural strength is normally ranging from 0.3 MPa to 0.5 MPa in the winter season while it decreases to 0.2 MPa during the summer (ISO 19906, 2010).

Only a few tests have been conducted on MY-ice compared to FY-ice. MY-ice has low salinity and thus higher strength values compared to FY-ice at the same temperature. However, the strength values will never exceed values for freshwater since there is some salt present.

2.1.6 Friction coefficient

The ice actions acting on sloping and conical structures are affected by frictional effects. The friction coefficient, μ, between ice and different material surfaces has been established based on both laboratory and in field tests. Examples of surfaces tested are concrete and steel of various conditions (corroded, smooth, painted, low-friction coating).

The influence of different parameters has been investigated in laboratory conditions. The parameters are; static vs. kinetic friction, normal action, relative velocity, surface roughness, ice temperature and surface lubrication by the sea water.

The main findings from tests are;

- The static friction coefficient can be up to five times greater than the kinetic friction coefficient at v = 0.1 m/sec
- The kinetic friction coefficient decreases with increasing contact pressure
- The coefficient of friction increases with a decrease of the sliding velocity and also with a decrease of temperature
- The sea water that can be present at the ice-structure interface does not significantly influence the kinetic friction

Table 2.4 (based on (Saeki et al., 1986; Mäkinen et al., 1994)) shows how the kinetic friction coefficient varies between different materials, surfaces and sliding velocities.

Table 2.4: Measured values of kinetic friction coefficient

Construction material	Influence of sliding velocity					
	$v_s \leq 0.01$ m/s		$v_s = 0.1$ m/s		$v_s = 0.5$ m/s	
	Mean	SD	Mean	SD	Mean	SD
Smooth steel	0.10	0.02	0.05	0.01	0.05	0.01
Smooth concrete	0.12	0.02	0.05	0.015	0.05	0.01
Corroded steel	0.15	0.03	0.10	0.03	0.10	0.03
Rough concrete	0.22	0.05	0.10	0.03	0.10	0.03

(The results presented above are taken from A.8.2.8.6 (ISO 19906, 2010).)

In addition to the ice-structure friction, an ice-to-ice coefficient, μ_i, is involved in the ice action calculations later presented in Chapter 3. Typical values for kinetic ice-to-ice friction (μ_k) and static ice-to-ice friction (μ_s) are respectively 0.03 and 0.1 (Løset et al., 2006).

2.1.7 Shear strength of ridge keels

The strength of a ridge keel is often in the literature characterized by two parameters known as internal friction (ϕ) and cohesion (c).

Values of published internal friction angle range between 10° and 80° (ISO 19906, 2010) . The reason for the large variation is consolidation; in tests it is challenging to distinguish between what part of the shear strength is due to friction and what part due to cohesion. Consolidation can increase the cohesion in a short time after the floes are brought together and put under pressure. In ice action calculations an internal friction angle in the range of 20° and 40° is normally accepted.

The rubble cohesion is normally ranging from 0 to 100 kPa (ISO 19906, 2010) in the literature. A FY-ridge has typically a cohesion of 5-10 kPa. Zero cohesion may occur for example after the keel fails while the rubble is clearing the structure. Higher cohesion is associated with partly consolidated layer. The cohesion increases linearly from the bottom of the keel where the value is zero.

The temperature inside the ice ridge determines the depth of the consolidated layer and its strength, which depends on the brine volume and the temperature.

2.1.8 Elastic and strain modules

The commonly used relationship between stress (σ) and strain (ε) during elastic behavior is known as the elastic modulus (E) of the material;

$$\sigma = E\varepsilon \tag{2.11}$$

An increase in the value of E with decreasing temperature and brine volume is to expect (Peschanskii, 1960) for FY-ice. As a result, there will be a seasonal variation of the E-modulus. From dynamic measurements performed by Langleben and Pounder (Langleben & Pounder, 1963) it appeared that E [GPa] decreased linearly with the brine volume ;

$$E = 10 - 0.0351\nu_b \tag{2.12}$$

Representative E-Moduli values used in design ice actions are ranging from 2 to 6 GPa. To compare, E-modules for fresh water is in the range of 9 to 10 GPa (ISO 19906, 2010).

2.1.9 Ice density

One important and unique property for H_2O is the density. As the temperature of the water drops below the freezing point the density decreases. Consequently, in engineering applications it is very important to have knowledge of the ice density. Two main reasons for this are;

- The density and size of the ice block determine the weight of the ice. This is important in situations like ride-up of ice sheets on a sloping structure. The weight of the ice will determine the loads involved in the ice-structure interaction.
- When ice is displaced under the waterline, the resultant buoyancy force is proportional to the difference in the density between the ice and the seawater.

Measurements done by a large number of researchers show that the sea ice density ranges from 720 kg/m^3 to 920 kg/m^3 (ISO 19906, 2010). In-situ measurements have shown that there is a difference in the ice density above and below the waterline. Above waterline the ice density ranges from 840 kg/m^3 and 910 kg/m^3 for FY-ice and between 720 kg/m^3 and 910 kg/m^3 for MY-ice. The density is more consistent below the waterline. Here typical values range from 900 kg/m^3 to 920 kg/m^3 for both FY-ice and MY-ice.

2.1.10 Ice salinity and porosity

Ice salinity is normally given as the fraction by weight of the salt contained in a unit mass. Normally it is given as the ratio of grams per kilograms of seawater in parts per thousand (‰). There is usually some variation of the salinity with depth within the ice sheet. The depth dependence of the salinity changes during the winter as the temperature drops and the salt tends to migrate downwards through the ice.

Cox and Weeks (Cox & Weeks, 1974) examined the average salinity of growing FY-ice (this equation does not apply for decaying ice). They concluded that there was a consistent variation with the ice thickness (h_i). A general expression that relates the bulk salinity of the ice to its ice thickness as given below.

$$S_i = 4.606 + \left[\frac{91.603}{h_i}\right] \tag{2.13}$$

The ice thickness is given in cm, up to a maximum value of 200 cm. With this simple calculation it is assumed that there is no salinity variation with depth through the ice sheet, which is a reasonable first approximation for sea ice. Kovacs (Kovacs, 1996a) did also compile salinity values of MY-ice. He developed a relationship between the bulk salinity and the floe thickness (h_{Fi});

$$S_i = 1.85 + \left[\frac{80217.9}{h_{Fi}^2}\right] \tag{2.14}$$

where the floe thickness is in cm, up to a maximum value of 900 cm.

During the spring and the summer season when the temperature and solar radiation increase, the sea ice thickness decreases rapidly. As the thickness decreases also the strength of the ice sheet decreases. At the temperature of approximately -8 °C, the great majority of the solid salt present in the ice at low temperatures has dissolved back to liquid phase. When the ambient

temperature increases further, the brine pockets rapidly increase in size and ”brine drainage channels” are formed. The channels increase the permeability of the ice which results in a desalination of the ice.

There have only been a few direct measurements of the porosity of an ice ridge. According to measurements of both keel and sail porosity in the Sakhalin region (Beketsky et al., 1996) , the average porosity of the sail in the Baltic is 0.19 and for the keel 0.29. In the Sakhalin region, the average sail and keel porosities are 0.33 and 0.22 respectively.

2.2 Failure modes

The failure between a drifting ice sheet and a structure is a function of various parameters such as ice thickness, presence of ice ridges, ice velocity, ice temperature and geometry of both ice and structure (Løset et al., 2006).

Structure geometry is important for determining the ice actions. Key factors are the structure type (multi-leg, mono-leg or caisson), vertical or sloping waterline geometry, the plan shape of the structure and the plan dimensions.

The *profile of the structure* will highly affect the ice actions. In Figure 2.7, both a vertical and a sloping structure are shown. The vertical structure is generally subjected to greater forces than a sloping structure for similar waterline dimensions (discussed further in Chapter 4). However, this may not always be the case if ice rubble accumulates on the sloping wall and a crushing failure takes place instead of flexural failure.

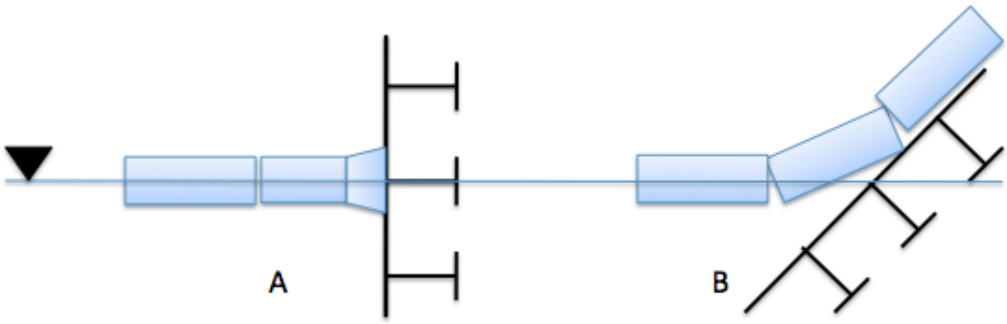

Figure 2.6: Crushing failure (A) and Flexural failure (B)

The *cross-section form of a structure* is usually not important when determining the ice action.

The *structures size* is on the other hand an important factor that governs the actions. Experiments and observations show that the effective pressure (the total action divided by the nominal contact area) for narrow structures is higher than for a wide one. A structure with waterline diameter less than 5 m is defined as a *narrow structure* while structures with waterline diameter $>>$ 5 m are considered as *wide structures* (ISO 19906, 2010).

A brief description of the most important failure modes is given under the figure.

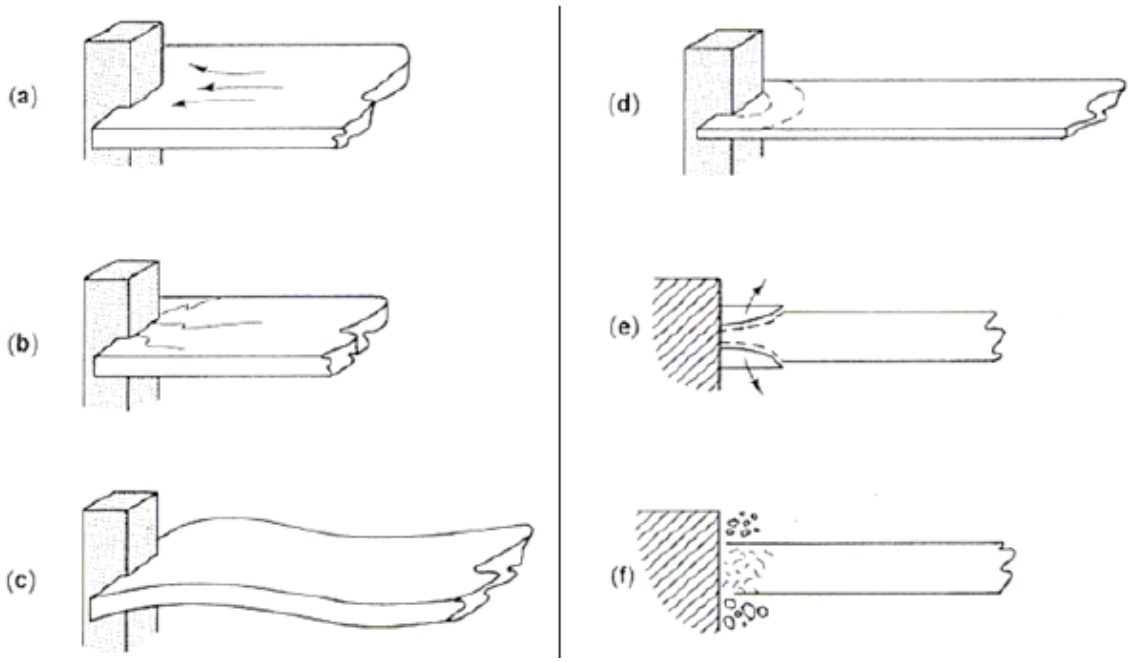

Figure 2.7: Failure modes and cracking on a vertical surface (Løset et al., 2006)

- *Creep (a)* means that ice flows around the body without cracking. The contact between ice and body is perfect, i.e. the whole surface facing the ice drift is in contact with the ice.
- *Radial cracks (b)* are associated with tensile failure. They occur when the stress level reaches a critical value and especially at high aspect ratios. For rectangular structures they radiate from the structure's corners. Cracks may also form in front of the structures if the cross-section is cylindrical.
- *Buckling (c)* can take place at higher drift speeds and is especially characteristic for thin ice and wide structures. This type of failure is often associated with circumferential or radial crack formation.
- *Circumferential cracks (d)* may form due to elastic buckling or due to an out-of-plane bending moment caused by the eccentric action condition.
- *Spalling-formation (e)* of out-of-plane horizontal cracks, which grow away from the contact zone and divide the ice sheet into several layers.
- *Brittle crushing (f)* takes place when the stresses inside the ice sheet reach the compressive strength of ice. Crushing is more likely to occur for high drift velocities. The crushing process often controls the design action.
- *Bending* is the main failure mode when looking at failure of ice against inclined structures. Since the tensile strength of ice is significantly lower than the compressive strength, the ice loads acting on an inclined surface are normally lower than for a vertical structure.

2.3 Load scenarios

Different scenarios of ice-structure interaction have to be considered in the design of an offshore structure (Løset et al., 2006) . Four scenarios are described below;

- Limit stress
- Limit momentum
- Limit force
- Splitting

All four scenarios correspond to the situation when one of the parameters reaches the utmost value. The ice can not withstand the action that exceeds its bearing capacity (e.g. strength).

Limit stress scenario corresponds to the situation when the stress (compressive, shear, tensile, flexure, buckling) reaches some critical value. This scenario is often the one that controls the maximum action.

The limit momentum scenario predominates when the kinetic energy of the ice feature is insufficient for the structure to penetrate significantly into the ice which causes the ice feature to come to a halt. This phenomenon can most often be seen during ridge action on the structure. Often are the limit momentum actions less than the limit stress actions if the floe is less than 5 km in size (CAN/CSA-S472/92, 1992). The consequent behavior of the floe after halt is of great importance. If the structure is not very wide and the ice concentration is low, the floe may later travel around the obstacle. The actions corresponding to the limit momentum scenario may not exceed those corresponding to the limit stress scenario. However, if the ice concentration is high and the ice is trapped, the feature can not travel round the structure. In this case, the limit force scenario develops.

The limit force scenario develops if a strong ice field is trapped in front of a wide structure and transmits the actions exerted by the surrounding ice features, wind and current. An example of this is when the actions from the surrounding features, wind and current are accumulated over the halted feature's surface and are transmitted to the structure. If the magnitude of the action is large enough, the structure will start to penetrate into the ice.

The splitting scenario develops when a moderately large ice feature hits the structure. If the structure corner is directed against the ice floe motion this is likely to occur.

3 LITERATURE STUDY ON ISO 19906

A review of the new ISO 19906 standard on Arctic Offshore Structures (ISO 19906, 2010) is given in this chapter based on the existing methodology for estimation of level ice loads on structures with sloping waterline geometry. Two methodologies are assessed, namely;

- Ralston's methodology
- Croasdale's methodology

In addition, a review of the methodology recommended for estimation of the global ice load on vertical structures is given.

Only an introduction to Ralston's and Croasdale's methodology is given. A more detailed description and discussion of each term in the algorithms with respect to physics and trigonometry behind the terms in the equations is given in the master thesis by Fredrik R. Larsen (Larsen, 2011).

3.1 Sloping structures

There are several types of sloping structures and they differ both in design and geometry. Two different methodologies for calculating the ice action loads are presented below. The first method, Ralston's methodology, is suitable for narrow conical structures while the second method, Croasdale's methodology, is based on elastic beam bending and more appropriate for wider structures.

Ice action on sloping structures has been studied during several field programmes such as Kemi-1 lighthouse in 1983-86 in the Gulf of Bothnia, two piers of the Confederation Bridge since 1997, jacket production platforms in the Bohai Sea, the Kulluk downward breaking floating structure in the Beaufort Sea, and an experimental tower at Mombetsu in Japan. A large variation in the first-year ice conditions was experienced including level ice, first-year ice ridges and rubble fields. The results and observations from the field measurement programmes have been used as benchmarks for verification of theoretical model in addition to ice criteria for newly built conical and sloping structures.

A sloping structure breaks the oncoming ice sheet either upwards or downwards where the resulting ice action has both a horizontal and a vertical load component.

Ice interaction with a sloping surface is a complex process and involves failure of intact ice, ride-up/down of broken ice and accumulation of the ice rubble on the slope, ref. Figure 3.8.

A. Two ice sheets encounter the structure.

B. The ice sheets separate but are still in contact with each other. The upper sheet is being push upwards along the inclined surface wall and may fail again into smaller blocks.

C. As more and more ice sheets are pushed up against the wall, parts of the blocks fall down.

D. If the weight of the accumulated ice on the ice surface reaches some level, parts or all of the blocks will submerge.

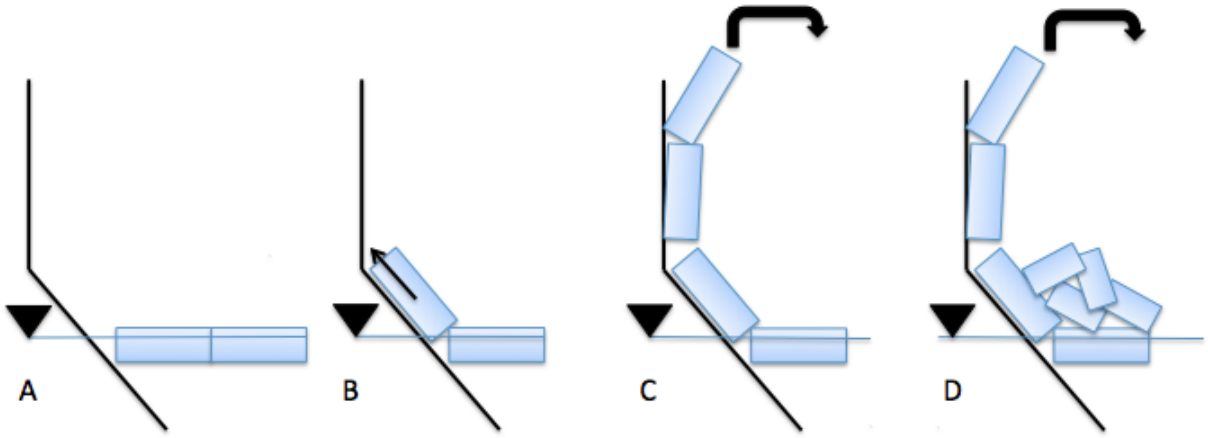

Figure 3.8: Processes in the interaction between an upward sloping structure and sheet ice

The maximum ice action load is a function of several parameters including bending, compressive and shear strengths of the ice sheet, friction coefficient between the ice sheet and the structure, ice properties, rubble height etc.

Figure 3.9 illustrates interaction between an ice sheet and an upward-breaking structure.

Where;

- N Component normal to the structure surface
- α Inclination angle of the structure surface from the horizontal
- μ Coefficient of kinetic friction between the ice and structure surface

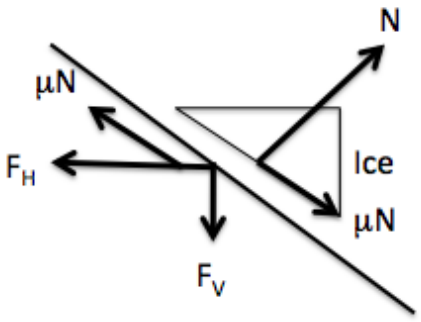

Figure 3.9: Ice action components on a sloping structure (2D)

The horizontal and vertical components, F_H and F_V, of ice action are given by:

$$F_H = N \sin\alpha + \mu N \cos\alpha \tag{3.15}$$

$$F_V = N \cos\alpha - \mu N \sin\alpha \tag{3.16}$$

The relationship between F_H and F_V is

$$F_V = \frac{F_H}{\xi} \tag{3.17}$$

where;

$$\xi = \frac{\sin\alpha + \mu\cos\alpha}{\cos\alpha - \mu\sin\alpha}$$

Symbols used in the calculations are;

E	Elastic modulus
g	Acceleration due to gravity
h	Thickness of the ice sheet
H_B	Horizontal action on the cone due to ice breaking
H_L	Load required to push the sheet ice through the ice rubble on the top of the advancing ice sheet prior to breaking it
H_P	Load required to push the sheet ice through the ice rubble
H_R	Horizontal action on the cone due to ride up
H_T	Load to turn the ice block at the top of the slope
V_B	Vertical action on the cone due to ice breaking
V_R	Vertical action on the cone due to ride up
w	Waterline diameter of the cone or width of a sloping structure
σ_f	Flexural strength of the ice sheet
ρ_i	Density of ice
ρ_w	Density of water
ν	Poisson ratio

Notice that the flexural strength will depend upon the size of the ice specimen that is used to obtain this parameter. Consequently, the parameter σ_f should be adopted from the field test where the specimen size is comparable to the design condition.

3.1.1 Ralston's methodology

Ralston's methodology is based on theory of plasticity and is suitable for narrow conical structures, typically less than 5 m at the waterline (ISO 19906, 2010). The model considers action due to the flexural failure of the ice sheet and the ride-up actions due to ice pieces and is valid for an upward breaking cone. To make it valid for a downward breaking structure ρ_i must be replaced by (ρ_i- ρ_w).

The following functions are defined for the solution;

$$f = \sin\alpha + \mu E_1 \cos\alpha \tag{3.18}$$

$$g_r = \frac{\sin\alpha + \frac{\alpha}{\cos\alpha}}{\frac{\pi}{2}\sin^2\alpha + 2\mu\alpha\cos\alpha} \tag{3.19}$$

$$h_v = \frac{f\cos\alpha - \mu E_2}{\frac{\pi}{4}\sin^2\alpha + \mu\alpha\cos\alpha} \tag{3.20}$$

$$W = \rho_i g h_r \cdot \frac{w^2 - w_T^2}{4\cos\alpha} \tag{3.21}$$

Where;

w_T	Top diameter of the cone
h_r	Ice ride-up thickness ($h_r \geq h$)

The parameters E_1 and E_2 are the complete elliptical integrals of the first and second kind defined as;

$$E_1 = \int_0^{\frac{\pi}{2}} \left(1 - \sin^2\alpha \sin^2\eta\right)^{-0.5} \, d\eta \tag{3.22}$$

$$E_2 = \int_0^{\frac{\pi}{2}} \left(1 - \sin^2\alpha \sin^2\eta\right)^{0.5} \, d\eta \tag{3.23}$$

When a single sheet thickness is assumed, the horizontal ride up action H_R and the vertical ride up action V_R can be calculated by;

$$H_R = W \cdot \frac{\tan\alpha + \mu E_2 - \mu f g_r \cos\alpha}{1 - \mu g_r} \tag{3.24}$$

$$V_R = W\cos\alpha\left(\frac{\pi}{2}\cos\alpha - \mu\alpha - f h_v\right) + H_R h_v \tag{3.25}$$

The horizontal breaking action H_B and the vertical breaking action V_B are given by;

$$H_B = \frac{\sigma_f h^2}{3} \cdot \frac{\tan\alpha}{1 - \mu g_r} \cdot \left[\frac{1 + Y x ln x}{x - 1} + G(x-1)(x-2)\right] \tag{3.26}$$

$$V_B = H_B h_v \tag{3.27}$$

Y	2.711 for Tresca yielding
Y	3.422 for Johansen yielding

and

$$G = \frac{\rho_i g w^2}{4\sigma_f h}$$

$$X = 1 + \left(3G + \frac{Y}{2}\right)^{-0.5} \tag{3.28}$$

The total action components in the horizontal and vertical directions are evaluated respectively as;

$$F_H = H_B + H_R \tag{3.29}$$

$$F_V = V_B + V_R \tag{3.30}$$

3.1.2 Croasdale's methodology

When the ice is interacting with the structure, the flexural failure components can be evaluated considering the ice sheet as an elastic beam resting on elastic foundation. Three-dimensional effects are included as well as the presence of rubble on the face of the structure. Also this methodology can be used for downward breaking slopes by replacing ice weight in air by ice buoyancy in water.

The horizontal action component is determined by;

$$F_H = \frac{H_B + H_P + H_R + H_L + H_T}{1 - \frac{H_B}{\sigma_f l_c h}} \tag{3.31}$$

The breaking load is calculated as;

$$H_B = 0.68\xi\sigma_f \cdot \left(\frac{\rho_w g h^5}{E}\right)^{0.25} \cdot \left(w + \frac{\pi^2 L_c}{4}\right) \tag{3.32}$$

Where

$$L_c = \left[\frac{Eh^3}{12\rho_w g(1-\nu^2)}\right]^{0.25} \tag{3.33}$$

L_c is the characteristic length of an elastically supported ice beam. The last term in H_B,

$$\left(w + \frac{\pi^2 L_c}{4}\right)$$

takes the 3D effects at the surface ends into account.

$$H_P = w h_r^2 \mu_i \rho_i g \cdot (1-e) \cdot \left(1 - \frac{\tan\theta}{\tan\alpha}\right)^2 \cdot \frac{1}{2\tan\theta} \tag{3.34}$$

Where;

h_r	Rubble height
μ_i	Ice-to-ice friction coefficient
e	Porosity of the ice rubble
θ	Angle the rubble makes with the horizontal

The load component H_R is given by;

$$H_R = wP \cdot \frac{1}{\cos\alpha - \mu\sin\alpha} \tag{3.35}$$

Where;

$$P = 0.5\mu_i \cdot (\mu_i + \mu) \cdot \rho_i g \cdot (1-e) \cdot h_r^2 \sin\alpha \cdot \left(\frac{1}{\tan\theta} - \frac{1}{\tan\alpha}\right) \cdot \left(1 - \frac{\tan\theta}{\tan\alpha}\right) +$$

$$0.5 \cdot (\mu_i + \mu) \cdot \rho_i g \cdot (1-e) \cdot h_r^2 \cdot \left(\frac{\cos\alpha}{\tan\alpha}\right) \cdot \left(1 - \frac{\tan\theta}{\tan\alpha}\right) + h_r h \rho_i g \cdot \left(\frac{\sin\alpha + \mu\cos\alpha}{\sin\alpha}\right) \tag{3.36}$$

H_L is given by;

$$H_L = 0.5wh_r^2\rho_i g \cdot (1-e) \cdot \xi \cdot \left(\frac{1}{\tan\theta} - \frac{1}{\tan\alpha}\right) \cdot \left(1 - \frac{\tan\theta}{\tan\alpha}\right) + 0.5wh_r^2\rho_i g \cdot (1-e) \cdot \xi \tan\phi \cdot \left(1 - \frac{\tan\theta}{\tan\alpha}\right)^2 + \xi c w h_r \cdot \left(1 - \frac{\tan\theta}{\tan\alpha}\right) \tag{3.37}$$

Where;

c	Cohesion angle of the ice rubble
ϕ	Friction angle of the ice rubble

H_T is given by;

$$H_T = 1.5wh^2\rho_i g \cdot \left(\frac{\cos\alpha}{\sin\alpha - \mu\cos\alpha}\right) \tag{3.38}$$

The total length of the circumferential crack, l_w, can be calculated as

$$l_c = w + \frac{\pi^2}{4} \cdot L_c \tag{3.39}$$

As can be seen in Equation 3.31, the total load components are functions of the breaking load component (H_B), load component required to push the sheet ice through the ice rubble (H_P), load component to push the ice blocks up the slope through the ice rubble (H_R), load required to lift the ice rubble on the top of the advancing ice sheet prior to breaking it (H_L) and the load to turn the ice block at the top of the slope (H_T).

The prediction of the ice action from the two methods presented above depends on the height of the rubble pile. This height will depend upon the slope angle and the width of the cone. Frictional effects due to snow or surface roughness will also influence the height of the rubble pile.

In the latter described model, the loads are also sensitive to the angle of repose chosen for the rubble pile. This angle determines the volume of the ice rubble together with the rubble height. The force to drive the oncoming ice through this pile and upwards increases rapidly with the volume. The repose angle is usually determined based on experience and observations. In general, the angle should not be less than $10\,^\circ$ of the structure's slope angle (α - $10\,^\circ \leq \theta \leq \alpha$) and for high rubble piles an angle of $5\,^\circ$ less than the slope angle (α - $5\,^\circ \leq \theta \leq \alpha$) will give a realistic volume of rubble on the slope. If θ is equal to α, a single layer of ice is riding up the slope. If the angle of the repose is greater than the slope angle, the model will fail because the rubble volume becomes negative.

3.2 Vertical structures

An ice sheet interacting with a vertical structure is likely to fail in crushing and not bending which is the case for a sloping structure. Crushing refers to a complex compressive failure process, involving the development of a damaged layer as well as the sequential development of flakes or spalls and horizontal splits or cleavage cracks.

When an ice sheet is crushing against a vertical structure, the global ice action normal to the surface can be expressed by (ISO 19906, 2010);

$$F_G = p_G \cdot A_N \tag{3.40}$$

Where;

p_G	Ice pressure averaged over the nominal area associated with the global action
A_N	Nominal contact area

The nominal contact area is the projected area of the intact ice feature on the structure and the product of the ice thickness and the width of the ice sheet. The global ice action can therefore be rewritten as;

$$F_G = p_G \cdot h \cdot w \tag{3.41}$$

The ice pressure is often the most important and critical parameter when designing offshore structures against ice actions. The pressure is influenced by the temperature of the ice, the nominal contact area, the shape or aspect ratio of the contact area, the nature of the contact, the relative speed and displacements between the ice and structure and the compliance of the structure.

Full-scale measurements have been conducted in the Cook Inlet, the Beaufort Sea, Baltic Sea and Bohai Sea where the data obtained have been used to determine upper bound ice pressure values for scenarios where a first-year or multi-year ice acts against a vertical structure. Based on the studies, an equation for calculating the global ice pressure has been established;

$$p_G = C_R \left(\frac{h}{h_1}\right)^n \cdot \left(\frac{w}{h}\right)^m \tag{3.42}$$

where;

p_G	Global average ice pressure [MPa]
w	Projected width of the structure (equal to the waterline diameter of the structure) [m]
h	Ice thickness [m]
h_1	Reference thickness of 1 m [m]
m	Empirical coefficient equal to -0.16
n	Empirical coefficient, equal to -0.5 + h/5 for h $<$ 1.0 m, and to -0.30 for h $\geq$ 1.0 m
C_R	Ice strength coefficient [MPa]

Equation 3.42 applies for rigid structures with an aspect ratio, $\frac{w}{h}$, greater than 2.

Equations 3.41 and 3.42 can be used in a probabilistic analysis. First one has to determine a probability density function for the ice thickness and strength parameter, C_R. In a deterministic analysis, C_R can be assumed to be equal to 2.8, based on first-year and multi-year data from the Beaufort Sea (Blanchet, 1998; Timco & Johnston, 2004; Wight, 1998). This value may be conservative as it potentially includes some magnification due to the compliance of the structure in the referenced data from the Beaufort Sea (Jefferies et al., 2008).

Another data series from a stiff structure in the Baltic Sea showed that C_R = 1.8 in conditions where the ice speed was higher than 0.1 m/s and the maximum waterline displacements in the direction of the ice action were approximately 0.4 % of the ice thickness (Kärnä et al., 2006). Under the conditions, C_R did not exhibit magnification due to the compliance of the structure.

4 SLOPING VS. VERTICAL STRUCTURES

A comparison of the horizontal and vertical loads acting on the sloping structures shown in Figure 4.10 has been performed. The first structure breaks the oncoming ice downwards while the second structure breaks the ice upwards. Both methodologies for estimation of ice loads on sloping structures presented in Chapter 3 are used, namely Ralston's and Croasdale's methodology.

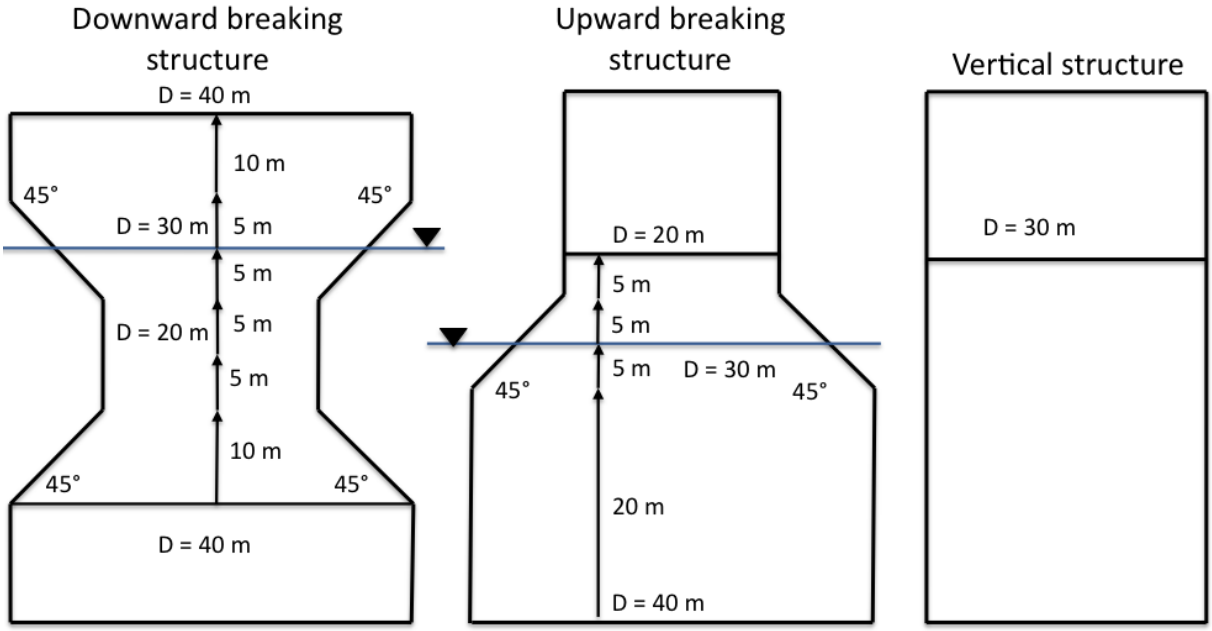

Figure 4.10: Downward breaking, upward breaking and vertical structure

The loads calculated are compared to the crushing load acting on the vertical structure also shown in Figure 4.10. Notice that all three structures have a waterline dimeter of 30 m. The purpose for the comparison is to justify the use of sloping structures.

4.1 Static load estimate

The geometrical parameters of the structures are seen in Figure 4.10. Target ice properties used in the calculations are given on page 24.

Notice that the greater part of the input is given in Appendix A. The parameters that have been assumed by the student are the following; rubble height (h_r) , density of the water (ρ_i), ice-to-ice coefficient (μ_i) and the angle the rubble makes with the horizon (θ).

All the symbols are earlier explained in Chapter 3 and given in the nomenclature on page XIX.

Parameter	Value
α [°]	45
θ [°]	35
μ [-]	0.15
μ_i [-]	0.03
ν [-]	0.3
ρ_i [kg/m^3]	900
ρ_w [kg/m^3]	1025
σ_f [MPa]	0.5
ϕ [°]	35
c [Pa]	8000
e [-]	0.3
E [GPa]	3
g [m/s^2]	9.81
h [m]	1
h$_r$ [m]	2

4.1.1 Sloping structures

Table 4.5 gives the horizontal load (F$_X$), vertical load (F$_Z$) and the resultant load (F$_{RES}$) for both an upward- and a downward-breaking structure. Notice that the results are only valid for the structures and ice conditions presented in Appendix A . The resultant load is calculated by Pythagoras;

$$F_{RES} = \sqrt{F_X^2 + F_Z^2} \tag{4.43}$$

Table 4.5: Forces acting on an upward and a downward sloping structure

Direction	Ralston's methodology			Croasdale's methodology		
	F$_X$	F$_Z$	F$_{RES}$	F$_X$	F$_Z$	F$_{RES}$
	[MN]	[MN]	[MN]	[MN]	[MN]	[MN]
Up	0.8	1.1	1.4	3.1	2.3	3.8
Down	1.6	1.4	2.1	1.7	1.3	2.1

The ice loads calculated, in all three directions, vary between Ralston's methodology and Croasdale's methodology. The resultant load obtained with Ralston's methodology is almost three times less for upward breaking compared to Croasdale's methodology. When comparing the results obtained for downward breaking, the two methododologies give more or less the same results for the given structure geometry and ice conditions.

It can also be seen that the loads calculated for downward breaking are less than the loads for upward breaking. A discussion for possible reasons for the deviations obtained are given in Chapter 4.1.3.

4.1.2 Vertical structures

The equation for calculating the crushing load acting on a vertical structure was earlier given in Chapter 3;

$$F_G = C_R \left(\frac{h}{h_1}\right)^n \cdot \left(\frac{w}{h}\right)^m \cdot h \cdot w \tag{4.44}$$

C_R, h_1, n and m were explained earlier in Chapter 3.2 and therefore only listed here.

C_R	2.8 MPa
h_1	1 m
n	-0.3
m	-0.16

The ice thickness (h) is 1 m and the diameter of the vertical structure (w) is 30 m. With the given input, the ice action load becomes;

$$F_G = p_G \cdot h \cdot w = 2.8MPa \left(\frac{1m}{1m}\right)^{-0.3} \cdot \left(\frac{30m}{1m}\right)^{-0.16} \cdot 1m \cdot 30m = 48.7MN \tag{4.45}$$

4.1.3 Discussion

Possible reasons for the results obtained are the following;

- Firstly, it was seen that the loads calculated with Ralston's and Croasdale's methodology are not of same magnitude for the upward breaking structure. The resultant loads are almost three times higher for Croasdale's methodology than for Ralston's. Results obtained for downward breaking are on the other hand in the same range.

  Ralston's methodology considers actions due to the flexural failure of the ice sheet and the ride-up actions due to ice pieces and is according to the ISO 19906 not suitable for structures with a waterline diameter greater than 5 m. Croasdale's methodology considers the ice sheet as an elastic beam resting on elastic foundation. Also, three-dimensional effects are included as well as the presence of rubble on the face of the structure. A deviation in the results obtained for the two methodologies was therefore expected in advance, however in what degree was unknown.

- When comparing the downward breaking structure with the upward breaking structure with same waterline diameter it can be seen from Table 4.5 that upward breaking gives higher loads. Both the vertical and horizontal load components are lower for a downward breaking structure compared to an upward breaking structure. In case of downward breaking, the vertical component of the ice action is directed upwards and the effective shear resistance is therefore reduced at the structure-seabed interface.

  The fact that a downward breaking structure has lower ice actions loads can also be shown mathematically. In Chapter 3, it was pointed out that the equations for calculating the ice action are valid for an upward breaking structure, but can also be utilized for a downward breaking structures if ρ_i is replaced by (ρ_w - ρ_i). Typically values for the density [1] are given in the table below.

[1] The values are taken from the module "Ice 1" lectured by Gunnar Furnes at NTNU Fall 2010

Table 4.6: Typical values for density of H_2O

Density	Value
ρ_w [kg/m^3]	1020
ρ_i [kg/m^3]	917
ρ_w - ρ_i [kg/m^3]	103

To get an understanding of the implications of replacing ρ_i by (ρ_w-ρ_i) it is convenient to study Equation 3.21. The total action components are sums of the ride-up action load (HR and VR) and the breaking load (HB and VB). The ride-up action components are functions of the density and will be affected by reducing the density from 917 kg/m^3 (upward breaking) to 103 kg/m^3 (downward breaking). However, the breaking load components are not affected.

When looking at the equation for calculating HR and VR, it can be seen that an upward breaking structure will have almost 9 times greater contribution than a downward breaking structure if all other parameters are equal, ref. equation below.

$$\frac{\rho_i}{\rho_w - \rho_i} = \frac{917\frac{kg}{m^3}}{1020\frac{kg}{m^3} - 917\frac{kg}{m^3}} \approx 9 \tag{4.46}$$

The factor of 9 accounts for the ratio between the forces to lift an ice floe out of the water and to submerge it completely into the water. The effective weight of the ice pieces below the water is much smaller than the weight above the water, and therefore clearing forces are smaller.

- Based on the above-given results it can be concluded that the ice-action loads acting on a vertical structure are significantly higher than the loads acting on an inclined structure with same waterline diameter. While the calculated resultant load for an upward and downward breaking structure with an inclination angle of 45° is respectively 3.8 MN and 2.1 MN (Croasdale's methodology), the load acting on a vertical structure is calculated to be 48.7 MN.

  Ice failure against a vertical structure is related to crushing forces while the failure against a sloped walled structure is related to flexural bending. It has successfully been proven that the ice-action loads are considerably lower for sloping structures compared to vertical structures (for the given structure geometry and ice conditions).

4.2 Gravity based structures vs. floating structures

Floating structures

It has already been proven in the above-given discussion regarding waterline geometry that there is a benefit of having a sloping geometry in the waterline. According to the results based on Croasdale's methodology, the resultant ice action force acting on an upward breaking structure (B) of 45° is 3.8 MN. For a downward structure (A) with the same inclination angle and waterline diameter the force is reduced to 2.1 MN. To compare, the ice action force acting on a vertical structure (C) with the same waterline diameter as for the sloped structures is 48.7 MN.

For a floating structure it should be kept in mind that;

- A downward breaking structure gets lifted up in the water as a result of an upward acting resultant load. This is the reason why a downward breaking structure is the best solution for a floating concept.
- An upward breaking structure is on the other hand pushed downwards in the water as a result of a downward acting resultant load. This leads to a reduction in free board and is therefore a less attractive solution.
- The high crushing loads acting on a vertical structure lead to high tension in the mooring lines. A vertical structure is not recommended as a floater in the given ice conditions.

The red arrows in Figure 4.11 illustrate the magnitude of the resultant ice action load. The load acting on the vertical structure is considerably larger than the resultant loads acting on the structures with sloped waterline geometry.

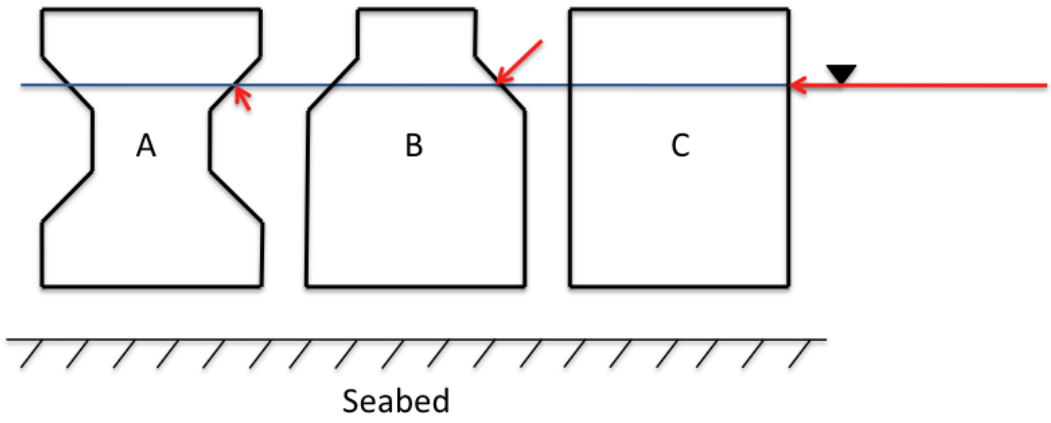

Figure 4.11: Floating structures

Gravity based structures

Figure 4.12 illustrates an upward (B) and a downward breaking structure (A). Both structures are gravity based structures which means that they sit on the seabed by their own weight. Normally is the friction between the structures and seabed sufficient to keep it in place both with respect to horizontal forces and overturning moment. Skirts can be included to improve the structure's stability against sliding.

The green arrows illustrate where the resultant forces are acting for both platforms. When applying a sloping geometry in the waterline for a gravity based structure the following should be kept in mind;

- The resultant force acting on a downward breaking structure contributes to an overturning moment which makes the platform *less stable*. The green arrow tries to push the platform over.
- The resultant force acting on an upward breaking structure *improves the overall stability* of the structure. This green arrow pushes the structure down into the seabed.

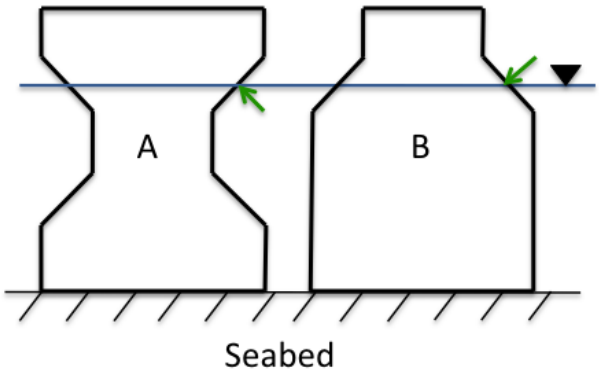

Figure 4.12: Gravity based structures

It is believed that an upward breaking structure is a better solution than a downward breaking structure when looking at gravity based structures.

5 NUMERICAL MODEL

A MATLAB-script has been developed for the time-domain analysis of an upward breaking structure, see Figure A.44 in Appendix A. The script is based on Croasdale's methodology described in Chapter 3.1.2.

5.1 Breaking length of ice sheet

In order to calculate the ice-action loads in the time-domain it is necessary to know the breaking length of the advancing ice sheet. Chapter 5.1.1 gives a detailed description of how the breaking length can be calculated by simplifying the ice-structure problem. The problem can by simplified by saying that the ice sheet is a beam resting on elastic foundation (the theory is taken from (Timoshenko, 1956; Timoshenko & Goodier, 1951)).

5.1.1 Beam on elastic foundations

The level ice-structure interaction has been studied as a simple beam problem on elastic foundation to take the buoyancy from the seawater into account. The beam has only one dimension which is the x-axis. The purpose for this simplified analysis is to find the most reasonable weakest point, hence the breaking length, on the ice sheet which is assumed to be semi-infinite.

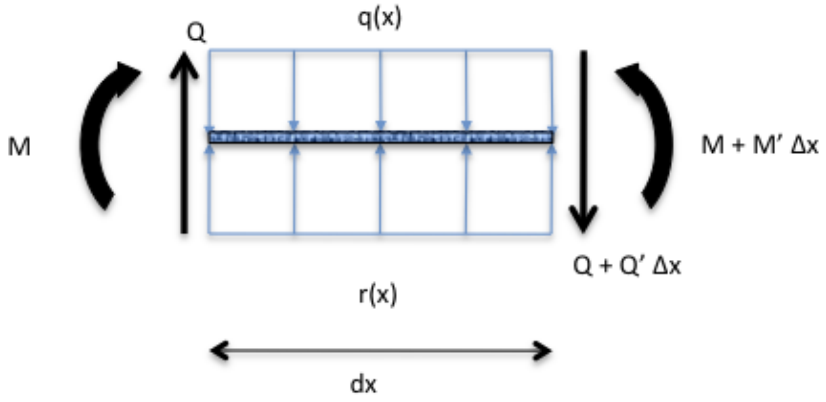

Figure 5.13: Forces acting on a beam element on an elastic foundation

Equation of the beam on elastic foundation

Figure 5.13 illustrates the forces acting on a beam element resting on elastic foundation. In addition to the distributed load q(x), the beam is subjected to r(x) which is the foundation pressure. The vertical condition for equilibrium of a differential beam element is

$$Q + Q'dx - Q + qdx - rdx = 0 \Rightarrow (Q' + q - r)dx = 0 \tag{5.47}$$

$$\Rightarrow Q' = -q + r \tag{5.48}$$

The moment condition of equilibrium is

$$M - M - M'dx + Qdx + (q - r)dx \cdot \frac{dx}{2} = 0 \tag{5.49}$$

$$\Rightarrow \left[-M' + Q + (q - r) \overbrace{\frac{dx}{2}}^{\approx 0} \right] dx = 0 \tag{5.50}$$

$$\Rightarrow Q = M' \tag{5.51}$$

By combining Equation 5.48 and Equation 5.51, we obtain the equilibrium equation of a beam element on an elastic foundation.

$$M'' = -q + r \tag{5.52}$$

Equation 5.52 differs from the equation of a normal beam due to the foundation pressure *r*. The following relationships commonly used in normal beam-theory are also valid in the case of an elastic foundation.

The relationship between rotation and deflection

$$\varphi = v' \tag{5.53}$$

the relationship between curvature and deflection

$$\kappa = -v'' \tag{5.54}$$

the relationship between bending moment and curvature

$$M = EI\kappa \tag{5.55}$$

and the relationship between shear force and bending moment.

$$Q = M' \tag{5.56}$$

Foundation model

A foundation model is necessary when describing the relationship between the deflection v(x) of the beam and the foundation pressure r(x). The so called *Winkler foundation* (Winkler, 1867) model assumes that the foundation pressure is directly proportional to deflection. This simple assumption is a satisfactory approximation in many practical cases.

$$r(x) = kv(x) \tag{5.57}$$

where *k* is the so-called foundation modulus and denotes the reaction per unit length when the deflection is equal to unity.

Differential equation of the beam on elastic foundation

By combining Equation 5.54 and Equation 5.55 we get

$$M = -EIv'' \tag{5.58}$$

By inserting Equation 5.58 and Equation 5.57 into the equilibrium equation, we get

$$(EIv'')'' + kv = q \tag{5.59}$$

which is the differential equation for a beam resting on an elastic foundation. For a uniform beam (EI = constant) the equation becomes

$$EIv^{(4)} + kv = q \tag{5.60}$$

This can be expressed as

$$v^{(4)} + 4\beta^{(4)}v = \frac{q}{EI} \tag{5.61}$$

where;

$$\beta = \sqrt[4]{\frac{k}{4EI}}$$

$$k = \rho g$$

$$I = \frac{1 \cdot t^3}{12}$$

The general solution of Equation 5.61 is

$$v(x) = \overline{v}(x) + v_0(x) \tag{5.62}$$

where $\overline{v}$(x) is the general solution to the homogenous part of the equation

$$v^{(4)} + 4\beta^4 v = 0 \tag{5.63}$$

and v_0(x) is one particular solution of the full equation 5.61. The general solution to Equation 5.63 can be expressed as

$$\overline{v} = e^{-\beta x}(B_1 \cos \beta x + B_2 \sin \beta x) + e^{\beta x}(B_3 \cos \beta x + B_4 \sin \beta x) \tag{5.64}$$

In particular cases the above-given constants must be determined from the known conditions at certain points. The form of particular solution v_0(x) is determined by the distributed load q(x). In the case of a concentrated load, v_0(x) = 0.

Semi-infinite solution to the beam on elastic foundation

If the beam resting on elastic foundation is long enough, βL $\geq$ 5, the edge disturbance due to the supports of the beam ends or by the concentrated loads are local enough to be solved without taking the disturbance of the other edge into account. As a result, this case can be solved as a so called semi-infinite problem.

The semi-infinite solution to the beam on elastic foundation is the sum of the general solution given in Equation 5.64 to the homogenous equation and the particular solution v_0(x).

Equation 5.64 can also be expressed by

$$\overline{v} = e^{\pm\beta x}\,(C_1 cos\beta x + C_2 \sin \beta x) \tag{5.65}$$

where the upper sign corresponds to the positive x-axis (x $\geq$ 0) and the lower sign to the negative x-axis (x $\leq$ 0). We then get a solution to the problem in terms of the constant of integration

$$v(x) = e^{\pm\beta x}\,(C_1 cos\beta x + C_2 \sin \beta x) + v_0(x) \tag{5.66}$$

where the constant are determined by the boundary conditions.

Simplified Ice-structure problem

By help of the equations derived above, the level ice-structure interaction can be modeled as a semi-infinite beam resting on an elastic foundation due to the buoyancy from the seawater, ref. Figure 5.14.

Figure 5.14: Simplified model for ice-structure interaction

The right end of the beam is far enough (βL ≥ 5) for the theory of the semi-infinite beam to be applied. The equations required to determine deflection, bending moment and shear force are given below.

$$v(x) = e^{-\beta x}\left(C_1 cos\beta x + C_2 \sin \beta x\right) \tag{5.67}$$

$$v'(x) = -\beta e^{-\beta x}\left[(C_1 - C_2)\cos \beta x + (C_1 + C_2)\sin \beta x\right] \tag{5.68}$$

$$M(x) \equiv -Elv''(x) = 2EI\beta^2 e^{-\beta x}\left(C_2 \cos \beta x - C_1 \sin \beta x\right) \tag{5.69}$$

$$Q(x) \equiv M'(x) = 2EI\beta^3 e^{-\beta x}\left[-\left(C_1 + C_2\right)\cos \beta x + (C_1 - C_2)\sin \beta x\right] \tag{5.70}$$

Boundary conditions at the left end of the beam:

$$M(0) = 0, Q(0) = -P \tag{5.71}$$

Determining the constants of integration:

$$M(0) \equiv 2EI\beta^2 C_2 = 0 \Rightarrow \underline{C_2 = 0} \tag{5.72}$$

$$Q(0) \equiv -2EI\beta^3(C_1 + C_2) = C_1 \Rightarrow \underline{\frac{P}{2EI\beta^3}} \tag{5.73}$$

Deflection, bending moment, and shear force:

$$v(x) = \frac{P}{2EI\beta^3} e^{-\beta x}\cos \beta x \tag{5.74}$$

$$M(x) = -\frac{P}{\beta} e^{-\beta x}\sin \beta x \tag{5.75}$$

$$Q(x) = Pe^{-\beta x}(\sin \beta x - \cos \beta x) \tag{5.76}$$

Dimensionless expressions:

$$\frac{v(x)EI\beta^3}{P} = \frac{1}{2} \cdot e^{-\beta x}\cos \beta x \tag{5.77}$$

$$\frac{M(x)\beta}{P} = -e^{-\beta x}\sin\beta x \tag{5.78}$$

$$\frac{Q(x)}{P} = e^{-\beta x}(\sin\beta x - \cos\beta x) \tag{5.79}$$

Notice that the deflection, bending moment and shear force are functions of k, E and I which are determined by geometry and material properties of the ice sheet. The length of the ice sheet has to be larger than $\frac{5}{\beta}$ for semi-infinite theory to be valid, but is not involved directly in the calculations.

Results

Input used in the calculations;

Parameter	Value
E [GPa]	4
ρ_w [kg/m^3]	1025
g [m/s^2]	9.81

The level ice-structure interaction has been analyzed as a simple beam problem where the buoyancy from the seawater is taken into account by saying that the beam is resting on an elastic foundation. The interaction point marked in Figure 5.14 is introduced in the simple calculations as a concentrated load *P* at x = 0.

The maximum bending moment (BM) for three different thicknesses are calculated, respectively for 0.5 m, 1 m and 1.5 m. Where the maximum BM is acting, it is reasonable to assume that the ice sheet will fail. The results are given in Table 5.7. The fourth column is showing L_c for the same three ice thicknesses (see Equation 3.33). This parameter corresponds to the characteristic length that is used in the ice-action load calculation in Chapter 3.1.1 where the ice sheet is also considered as an elastic beam on elastic foundation.

Table 5.7: Results from simple beam test

Ice thickness [m]	Max BM [$\frac{M(x)\beta}{P}$]	Crack length [m]	L_c [m]
0.5	-0.3224	9	8.2
1.0	-0.3224	15	13.8
1.5	-0.3223	20	18.7

As can be seen in Table 5.7 the crack lengths that correspond to the three different ice thicknesses are 9 m, 15 m and 20 m. As expected, the crack length increases as the thickness of the ice sheet is increased. The crack lengths calculated analytically are close to the characteristic lengths used in Croasdale's methodology.

Alternatively to the above-described method for estimating the breaking length is to solve the problem as a semi-infinite plate, instead of beam, resting on an elastic foundation. A new analytical closed form solution has been established (Lubbad & Løset, 2010) to simulate the process of ship-ice interaction in real time.

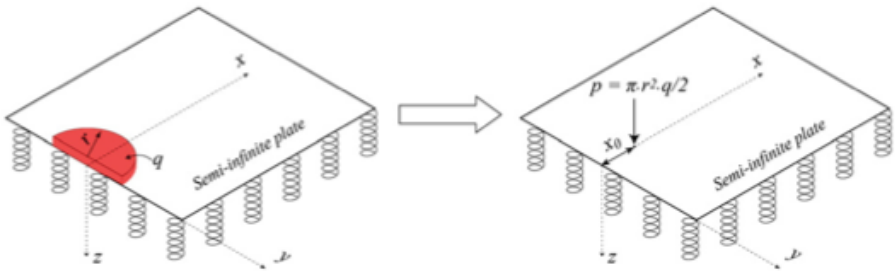

Figure 5.15: Idealized ice sheet as a semi-infinite plate resting on an elastic foundation and subjected to a uniform distribute load

q is the distributed load per unit area and r is the radius of the loaded area. This analytical method for estimating the breaking length will not be covered in this thesis as it will focus on Croasdale's methodology.

5.2 Breaking period of ice sheet

The breaking period, T, can be calculate directly from Equation 5.80 if the breaking length and the velocity of the ice sheet are known. T is shown in Figure 5.16.

Where;

F	Ice action
τ	Duration of loading/unloading cycle
t	Time
T	Period of ice action

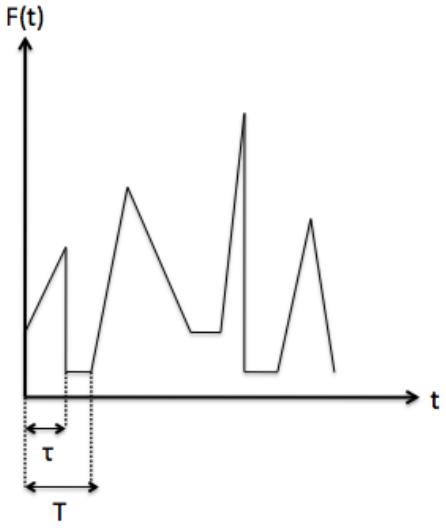

Figure 5.16: Idealized time history of the ice action loads

The time-varying action, F(t), is a function of the structure's geometry in addition to the frictional actions involved. The period between the ice actions, T, is given by;

$$T = \frac{l_b}{v} \tag{5.80}$$

Where;

- l_b Breaking length of the ice sheet
- v Velocity of the oncoming ice sheet

l_b is a function of ice thickness, ice strength, structure geometry and drift velocity and is normally in the range of 3 to 10 times the ice thickness. This ratio decreases typically with increasing ice thickness and ice velocity. The ratio between τ and T normally varies between 0.3 and 1.0 (ISO 19906, 2010).

5.3 Assumptions made in the numerical model

In order to be able to develop a MATLAB-script for calculating the ice forces, assumptions regarding rubble accumulation and geometry have to be made. Also the period (explained in Chapter 5.2) for each single ice component must be assumed. Notice that the assumptions are based on the best available material which was readily available at the time. Model test videos have not been involved in the process of making the script.

The force components (explained in section 3.1.2) related to the build-up of ice rubble are H_P, H_R and H_L. They are all (except H_R, see section 5.3.2) assumed to be equal to zero as long as there is only a single layer of ice on the sloping plane. H_T is also equal to zero until the first ice block starts to tip over at the top of the sloping plane.

The time the first oncoming ice sheet uses to reach the top of the sloping plane is a function of the velocity of the ice sheet, inclination angle and the length of the sloping plane. According to the geometry given in Figure 5.17, the length of the sloping plane can be calculated by simple trigonometry;

$$\frac{Height}{Length} = \frac{5m}{x} = \sin(45) \rightarrow x = \frac{5m}{\sin 45} = 5\sqrt{2}m \approx 7.1m \tag{5.81}$$

Example: If the velocity of the ice sheet is 1 m/s, H_P, H_L and H_T start to act after 7. 1 s.

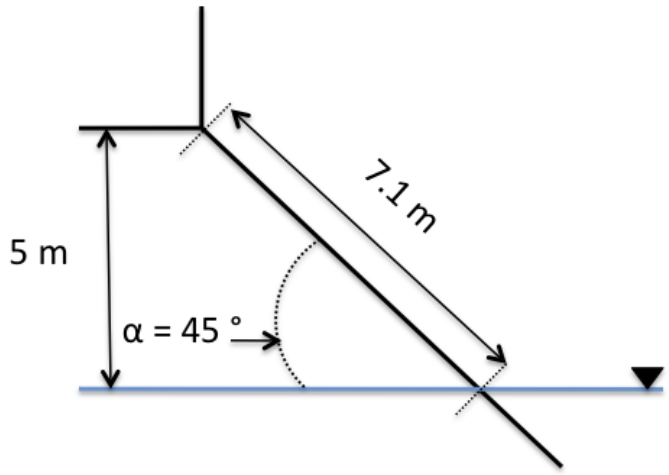

Figure 5.17: Waterline geometry of sloping structure

5.3.1 Geometry of ice rubble

The assumed rubble geometry is shown in Figure 5.18. The parameters involved are the following;

h	Ice thickness
h_r	Rubble height
α	Inclination angle
θ	Angle the rubble surface makes with the horizon

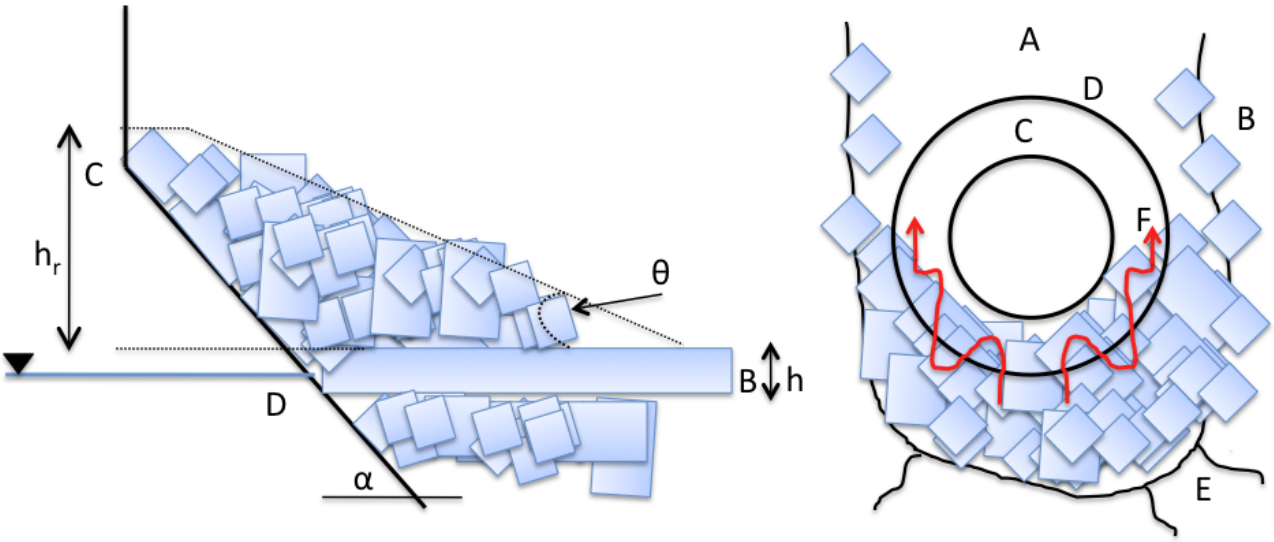

Figure 5.18: Ice rubble pile geometry

The letters A - F marked in the figure are representing;

A	Open water in wake of structure
B	Encroaching ice sheet
C	Top of sloping face of structure
D	Waterline of structure
E	Cracks forming in encroaching ice sheet
F	Clearing of ice rubble blocks around the structure

The two red arrows are representing how it is believed that an ice sheet is transported around the structure from the moment when it hits the structure the first time. How each ice sheet is transported first up the inclined wall and then further around the structure is challenging to predict without any visual tools available. It has therefore been assumed that from the moment the rubble starts to accumulate it takes 50 seconds before a constant rubble volume is obtained. It is expected that this value has to be corrected when the MATLAB-script is compared to real model test data provided by Aker Solutions, see Chapter 7. As soon as the rubble has reached a maximum volume it is believed that the rubble volume is more or less constant. In the script developed it is assumed that the ice breaking period and the rubble accumulation period before failure are independent of each other.

When only a single layer of ice rides up the slope (no rubble present), $\theta = \alpha$. As the rubble starts to accumulate, θ drops until it reaches a minimum value. The angle should not be less than the

structure's slope angle minus 10° (ISO 19906, 2010). Angles steeper than the inclination angle correspond to a negative rubble volume.

The inclination angle for the given structure geometry is 45°. Accordingly, it is believed that θ decreases from 45° to 35° during the time it takes from the first ice block falls down from the top of the sloping wall until the rubble volume has reached its maximum.

The rubble height, h_r, is assumed to be 5 m which is the height of the sloping plane from the waterline (see Figure 5.17).

5.3.2 Load components

Breaking Force, H_B

The characteristic length, L_C, of the ice sheet has been calculated from Equation 3.33 for two different ice thicknesses and velocities. The corresponding breaking periods are calculated by Equation 5.80 and presented in Table 5.8. It is assumed that L_C is a reasonable estimate for the breaking length as the calculated values are close to the values obtained in the analysis given in Chapter 5.1.

Table 5.8: Estimated breaking period (T_{H_B})

Test no.	Velocity [m/s]	Ice thickness [m]	L_C [m]	T_{H_B} [s]
1	0.5	1	12.9	25.8
2	1	1	12.9	12.9
3	0.5	1.5	17.4	34.8
4	1	1.5	17.4	17.4

At this stage, is it assumed that H_B acts as an impulse load once during the breaking period.

Example: When looking at Test no. 1 it is assumed that the structure is subjected to H_B at t = 0 and every 25.8th second.

Force to push the advancing ice sheet through the ice rubble, H_P

H_P is related to the rubble volume resting on the advancing ice sheet as shown in Figure 5.19. It is assumed that H_P = 0 until the rubble starts to accumulate.

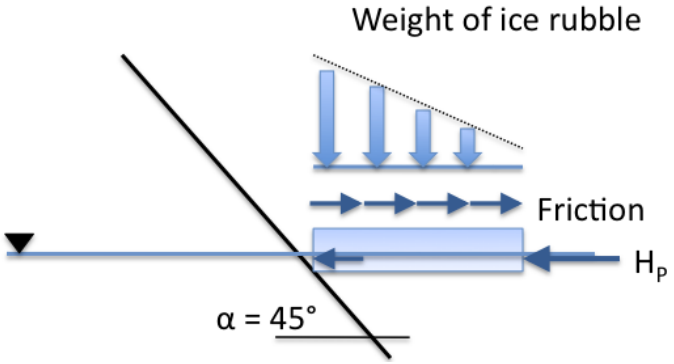

Figure 5.19: Force necessary to push the ice sheet through the ice rubble, H_P

H_P is a function of the rubble volume, hence θ. The time it takes from the first ice block falls down from the top of the sloping plane until the rubble volume is constant is assumed to be

50 s. During this period H_P increases from zero to its maximum. After the rubble volume has reached a constant value, H_P is kept constant at the maximum value.

Additional force to push the ice blocks up the slope through the ice rubble, H_R

H_R is the additional force to push the ice blocks up the slope through the ice rubble. When studying Equation 3.36 where P is calculated, it can be seen that when θ is equal to α, only the last term of the equation will contribute to H_R. As soon as θ starts to drop after the first ice block has reached the top of the sloping plane all three terms in Equation 3.36 are contributing. It is assumed that during 50 s, H_R has increased from zero to a maximum value. After the rubble volume has reached a constant value, H_R is kept constant at the maximum value.

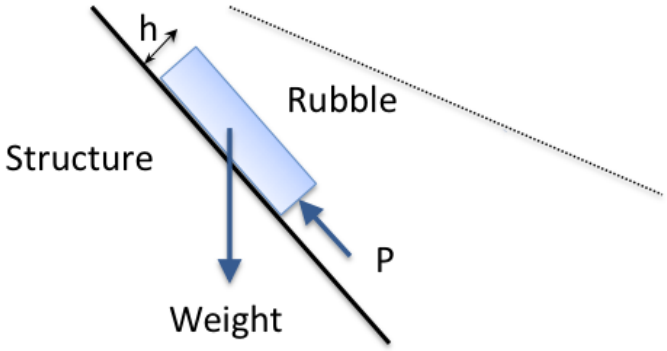

Figure 5.20: Forces acting on ice block pushed up the slope through ice rubble, H_R

Force required to lift the ice rubble on top of the advancing ice sheet prior to breaking it, H_L

H_L is the additional force necessary to lift the ice rubble on the top of the oncoming ice sheet prior to breaking it. H_L is equal to zero if there is no rubble present. As soon as the rubble starts to build-up, θ decreases and the load increases. The load is at its maximum when θ is at its minimum at 35°. H_L is kept constant at its maximum value as soon as the rubble has reached a constant volume. It is assumed that it takes 50 s for the rubble to reach a constant volume.

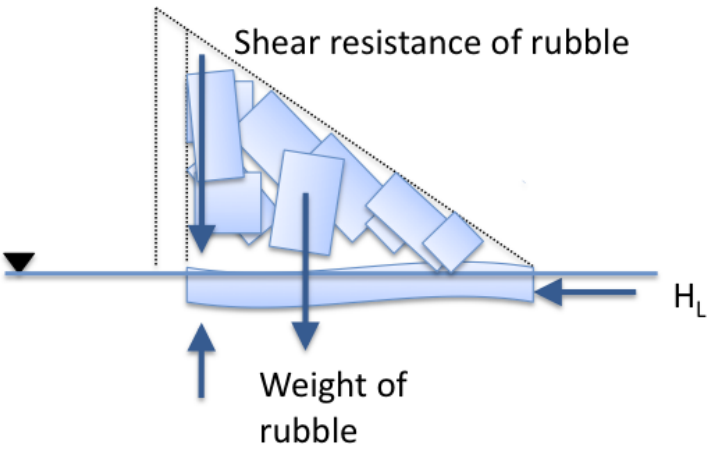

Figure 5.21: Additional force needed to overcome weight of ice rubble, H_L

Force to turn the ice blocks at the top of the slope, H_T

The given structure, see Figure A.44, has a vertical superstructure at the top of the slope. H_T is the force necessary to rotate the ice blocks into a vertical orientation. It is assumed that secondary failures have reduced the block size to three times its thickness, 3h.

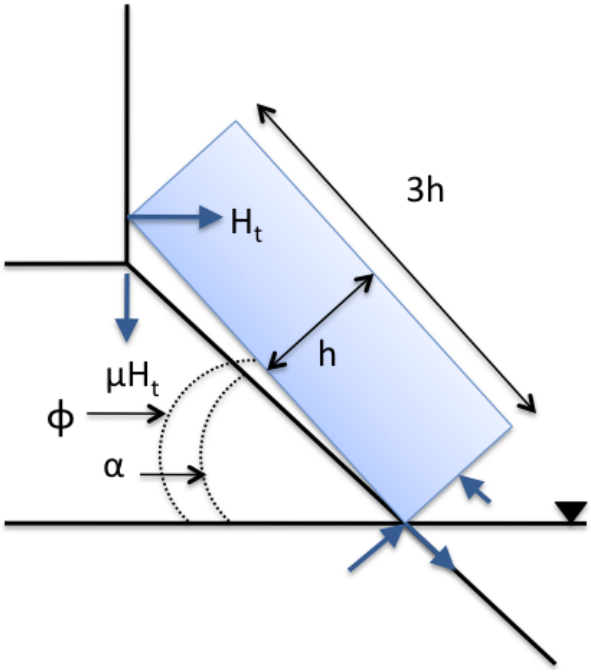

Figure 5.22: Forces involved in turning an ice block at top of slope, H_T

ϕ is the angle between the horizon and the ice sheet. When the ice sheet is resting on the plane, ϕ is equal to the inclination angle and the load is at its maximum. As soon as the ice block starts to turn, ϕ increases and the load decreases. It is assumed that ϕ_{max} = 90° which corresponds to H_T = 0. The load is assumed to repeat itself after it has reached ϕ = 90°.

The period of the turning process is calculated from the velocity of the ice and the distance the ice block is moving before it falls over. The distance is assumed to be 3h.

$$T_{H_T} = \frac{3h}{velocity} \tag{5.82}$$

H_T is assumed to act as soon as the first ice sheet has reached the top of the sloping plane.

6 PRE-SIMULATION OF ICE MODEL TESTS

6.1 Pre-simulation

A pre-simulation of the ice model test campaign shown in Table 6.9 has been performed. The numerical model used was earlier presented in Chapter 5 and based on Croasdale's methodology described in Chapter 3.1.2. Assumptions regarding rubble geometry, accumulation scenario etc. are clearly stated in Chapter 5 and will not be repeated here.

The purpose for performing a pre-simulation is to see how the ice-action loads are varying with time in addition to identifying the maximum forces acting on the structure.

The results obtained in the pre-simulation are later compared to an ice model test campaign performed by Aker Solutions where the structure geometry and target ice properties are similar to the ones used in the calculations. Time series measured and videos recorded during the campaign have been provided the student. The purpose for this has been to correct the numerical model used in the pre-simulation in agreement with the observations made.

6.2 Ice test campaign analysed in the pre-simulation

Table 6.9 below shows the unique combination of velocity and ice thickness for the four ice model tests in the campaign. The structure considered is an upward breaking structure and shown in Figure A.44, see Appendix A. All geometrical parameters are given by the figure.

Table 6.9: Ice test campaign

Test no.	Velocity [m/s]	Ice thickness [m]
1	0.5	1.0
2	1.0	1.0
3	0.5	1.5
4	1.0	1.5

The target mechanical and physical ice properties used in the calculations are given in Table 6.10.

Table 6.10: Target mechanical and physical properties of level ice

Test no.	Ice thickness [m]	Flexural strength [MPa]	Ice density [kg/m^3]	Ice-structure friction	Poisson's ratio	E-Module [GPa]	Cohesion [kPa]	Internal angle of friction	Porosity
1 & **2**	*1*	0.5	900	0.15	0.3	3	8	35	0.3
3 & **4**	*1.5*	0.5	900	0.15	0.3	3	8	35	0.3

The following values have been assumed in the calculations;

Rubble height (h_r, see Figure 5.18)	5 m
Ice-to-ice friction (u_i)	0.03
Sea water density (ρ_w)	1025 kg/m^3

The assumed breaking period (T_{H_B}) for the ice sheet, load build-up period (equal to T_{H_P}, T_{H_R} and T_{H_L}) and turning period (T_T) are summarized in Table 6.11.

Table 6.11: Assumed periods of the load components used in Croasdale's methodology

Test no.	Period [sec]				
	T_{H_B}	T_{H_P}	T_{H_R}	T_{H_L}	T_{H_T}
1	25.8	50	50	50	6
2	12.9	50	50	50	3
3	34.9	50	50	50	9
4	17.4	50	50	50	4.5

Example: When looking at Test no. 1 the following is assumed;

- H_B acts as an impulse load every 25.8th s. The component is a function of the characteristic length of the oncoming ice sheet and the velocity of it, see Chapter 5.3.2.
- H_P, H_R and H_L are all functions of the rubble volume resting on the oncoming ice sheet. It it assumed that it takes 50 s from the rubble starts to accumulate until a more or less constant volume is obtained, see Chapter 5.3.2. This period is also referred to as the load build-up period.
- H_T is a function of the ice thickness and the velocity. It is assumed that it takes 6 s to turn the ice block from the sloping wall into a vertical position which makes it to fall down, see Chapter 5.3.2.

6.3 Results from pre-simulation

The following is calculated in the pre-simulation;

- Horizontal load (F_X): Maximum, minimum and mean value.
- Vertical load (F_Z): Maximum, minimum and mean value.
- Resultant load (F_R): Maximum, minimum and mean value.
- Angle the maximum, minimum and mean resultant load makes with the horizon (θ).

All the results presented are based on the stabilized part of the time series which means that the rubble volume is more or less constant.

The estimated horizontal, vertical and resultant loads are shown numerically in Table 6.12 and visually in Figure 6.23 (exemplified with ice test no. 1) .

Table 6.12: Results from pre-simulation

	Test no.											
	1			**2**			**3**			**4**		
	Max.	**Min.**	**Mean**	**Max.**	**Min.**	**Mean**	**Max.**	**Min.**	**Mean**	**Max.**	**Min.**	**Mean**
	[MN]			**[MN]**			**[MN]**			**[MN]**		
$\mathbf{F}_X$	6.7	3.8	4.0	6.7	3.8	4.0	10.3	5.0	5.5	10.3	5.0	5.5
$\mathbf{F}_Z$	4.9	2.8	2.9	4.9	2.8	2.9	7.6	3.7	4.1	7.6	3.7	4.1
$\mathbf{F}_R$	8.3	4.7	4.9	8.3	4.7	4.9	12.8	6.3	6.8	12.8	6.3	6.8
θ	36.2°	36.4°	35.9°	36.2°	36.4°	35.9°	36.4°	36.5°	36.7°	36.4°	36.5°	36.7°

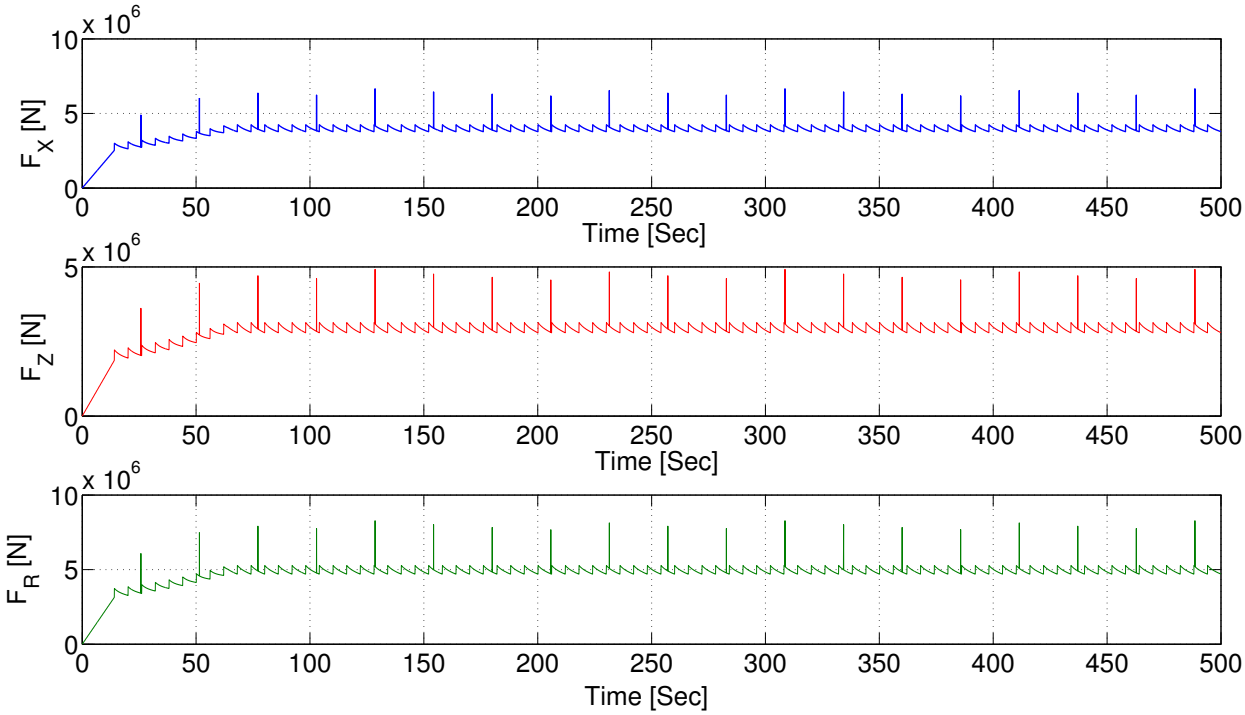

Figure 6.23: Calculated time series of ice test no. 1

The results are summarized below.

- Tall peaks are observed in the time series shown. This is a result of assuming that the breaking component (H_B) is an impulse load.
- The mean loads are much closer to the minimum loads than the maximum loads.
- Ice test no. 3 and no. 4 result in higher ice loads compared to the two first tests due to thicker sea ice.
- The horizontal load component is greater than the vertical component for all four cases.
- The statistics from the pre-simulation show that the forces acting on the structure are equal for ice test no. 1 and no. 2, and for ice test no. 3 and no. 4. This is a result of not including the ice velocity in Croasdale's methodology. However, the velocity has been included in the time-domain MATLAB-model developed by the student, but for the assumptions made it becomes clear that the loads calculated are unaffected by the velocity. It is believed that this is incorrect and has to be corrected for in Chapter 8 after studying the time series and videos recorded by Aker Solutions.

7 ICE MODEL TEST ANALYSIS

In order to gain an increased knowledge regarding ice loads acting on a structure with inclined waterline geometry, a campaign has been carried out in the Aker Arctic Technology ice model tank on behalf of Aker Solutions. The main purpose has been to define the total loads in different ice conditions, and to describe both the ice loads and the failure scenario as a function of time. Chapter 7 summarizes the main findings from the campaign as well as the model test set-up and measurement techniques for determining the actual ice properties. A report, videos and time series measured during the tests are provided the student.

In total, 21 ice model tests are included in the campaign performed. Only *four* tests are highlighted and presented in this master thesis, see Table 7.13.

7.1 Set-up and measurement analysis

The four tests were performed in fixed configuration in two different level ice conditions, 1.0 m and 1.5 m thick ice, as towing tests with a constant speed of 0.5 m/s and 1.0 m/s, see Table 7.13.

Table 7.13: Ice model test matrix (Full Scale)

Ice test no.	Velocity [m/s]	Ice thickness [m]
1	0.5	1
2	1	1
3	0.5	1.5
4	1	1.5

As seen in Figure 7.24, the hull is designed with a 45° upward breaking angle in the waterline allowing the level ice to fail in a flexural mode and to further transport the broken ice pieces around the hull.

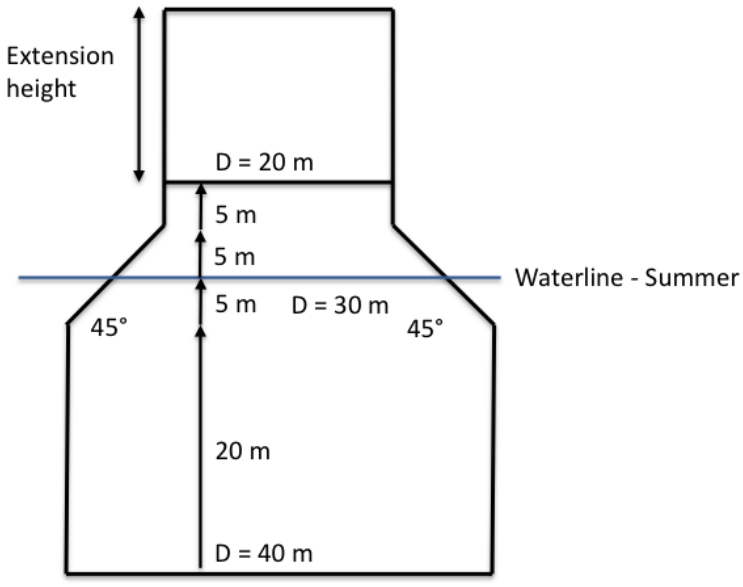

Figure 7.24: Dimensions of the upward breaking structure (Full Scale)

Measured friction coefficient between the model's surface and the ice was about 0.050. The model test basin utilized for the test campaign has the following parameters (Full Scale);

- Length [m]	Total	76
	Test	60
- Width [m]		6.5
- Depth [m]		2.3
- Shallow water possibility [m]	Depth	0 - 0.8
	Length	26

There are in total 60 frames along the longitudinal axis of the test basin, hence one frame per meter.

Scaling

In the test campaign the model was scaled down by use of Froude scaling in order to obtain equality between inertia and gravity forces. The relationship between the model and full scale is 1:30 (λ = 30). See list below for conversion from full scale (s) to model scale (m).

Beam	B_s	$=$	$\lambda \cdot B_m$
Coefficient of friction	m_s	$=$	m_m
Draught	T_s	$=$	$\lambda \cdot T_m$
Force	F_s	$=$	$\lambda^3 \cdot F_m$
Ice Strength	S_s	$=$	$\lambda \cdot S_m$
Ice Thickness	H_s	$=$	$\lambda \cdot H_m$
Length	L_s	$=$	$\lambda \cdot L_m$
Modulus of Elasticity	E_s	$=$	$\lambda \cdot E_m$
Time	t_s	$=$	$\sqrt{\lambda} \cdot t_m$
Velocity	V_s	$=$	$\sqrt{\lambda} \cdot V_m$

Measurements

Horizontal and vertical forces acting on the structure have been measured with a six-component balance, which consist of two relatively stiff rings placed above another. The rings are interconnected through six force transducers, three in the vertical direction and three in the horizontal direction. During the measurements all force components are transmitted via the transducers first to the lower ring thereafter to the upper ring. A schematic plan of the measuring arrangement is shown below. Notice that the structure shown breaks the oncoming ice downwards, but has the same arrangement as an upward breaking structure.

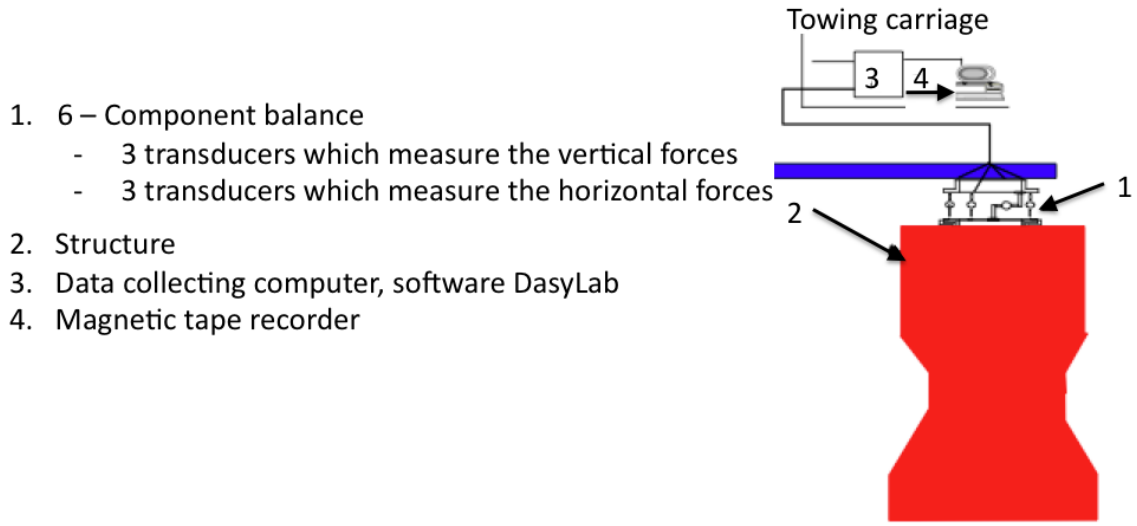

Figure 7.25: A schematic plan of the measuring arrangement

- **Ice properties**

  The ice properties measured from the level ice are the flexural strength (σ_f), ratio between Young's modulus and the flexural strength (E/σ_f), density of ice (ρ_i), ice thickness (h_i) and compressive strength of ice (σ_c).

  – The ice thickness was also measured after the tests.

  – Flexural strength has been determined based on a cantilever beam test. One pair of beams was taken in advance of the tests.

  – The compressive strength was measured from two ice sheets and compared to results from previous tests.

  – Young's modulus of elasticity was measured daily before the tests by an infinite plate bending test.

  – The density of the ice was not measured in advance of every test due to constant density of model ice.

  In addition to the above-given ice properties the length and the width of the level ice were estimated daily after the tests. The tensile strength, ice salinity, Poisson's ratio, ice-to-ice friction, cohesion, friction angle of the ice rubble and porosity are on the other hand not measured. Here, the student has to assume appropriate values for the comparison study in Chapter 8 where the MATLAB-script is to be corrected based on the actual time series provided by Aker Solutions .

- **Visual observations**

  Videos of the ice model tests were recorded from four different angles; from the carriage, side of the test basin, through the windows in the sides and under the basin (underwater views). The model was painted with a visible scale to make the estimation of ride up height and submersions easier.

7.1.1 Measured ice properties

During the period of ice testing, 13-16 February, 2007, the above-listed ice properties were measured. The target values for the four days are presented in Table 7.14. Notice that the properties are given in model scale (see Chapter 7.1 for conversion to full scale).

Table 7.14: Target ice properties (Model Scale)

Measurement no.	**Date**	h_i **[mm]**	σ_f **[kPa]**	**E /** σ_f **[-]**
1	13.02.2007	50	18	> 1000
2	14.02.2007	33	18	> 1000
3	15.02.2007	33	18	> 1000
4	16.02.2007	50	18	> 1000

- **Measured values of the flexural strength**

  The flexural strength has been measured at different frames along the longitudinal axis of the test basin. The measured values shown in Table 7.15 are average model scale values of the flexural strength based on measurements from both starboard and port side of the test basin. As can be seen in the table, the measured values are ranging from 18.05 to 25.64 kPa while the target value was 18 kPa.

Table 7.15: Achieved values for flexural strength [kPa] (Model Scale)

Frame no.	**Measurement no.**			
	1	**2**	**3**	**4**
	[kPa]	[kPa]	[kPa]	[kPa]
16	25.28	19.12	24.00	20.46
28	22.67	24.21	22.26	18.05
40	20.68	24.06	25.64	19.51

- **Measured values of the Young's modulus**

  The measured values of the ratio between the Young's modulus and the flexural strength are ranging from 755.5 to 2865.3 (Model Scale) while the target was to achieve a value greater than 1000. In measurement no. 2 and no. 3 where the ice thickness target was 33 mm the measured ratio is greater than 1000. The measured ratio is less than 1000 for measurement no. 1 and no. 4 where the target ice thickness was 50 mm.

Table 7.16: Achieved values for E/σ_f [-] (Model Scale)

		h_i [mm]	Weight [g]	Deflection [mm]	E [kPa]	σ_f ave. [kPa]	E / σ_f
Measurement no.	**1**	52	100	0.0877	15167.63		
		52	200	0.1703	16071.17		
					15619.40 (ave.)	20.68	755.5
	2	33.5	100	0.0763	74822.78		
		33.5	200	0.1663	63032.38		
					68927.58 (ave.)	24.06	2865.3
	3	33	100	0.1333	25655.32		
		33	200	0.2567	27693.38		
					26674.35 (ave.)	25.64	1040.5
	4	53	100	0.0820	16373.50		
		53	200	0.1667	15853.74		
					16113.62 (ave.)	19.51	826.0

- **Measured values of the ice density**

  The density of the ice was measured the first and second day. Table 7.17 shows the results.

Table 7.17: Achieved values for ice density [kg/m^3] (Model Scale)

Measurement no.			
1	**2**	**3**	**4**
[kg/m^3]	[kg/m^3]	[kg/m^3]	[kg/m^3]
920.22	925.74	-	-

- **Measured values of the ice thickness**

  The ice thickness has been measured on both starboard (SB) and port (P) side of the test basin at 52 different frames along the longitudinal axis of the basin. At each frame an average value of the measured ice thicknesses is calculated. The measurements are presented statistically where an overall average thickness has been calculated on both starboard and port side of the basin. Also, the standard deviation (SD) has been calculated in addition to the difference from the target values which were 30 mm and 50 mm, ref. Table 7.14.

Table 7.18: Achieved values for ice thickness [mm] (Model Scale)

	Measurement no.							
	1		**2**		**3**		**4**	
	SB	**P**	**SB**	**P**	**SB**	**P**	**SB**	**P**
Average	47.06	46.82	32.66	32.68	32.98	33.21	49.38	49.85
SD	4.31	4.17	1.37	1.56	1.05	1.46	2.18	1.90
SD/Ave.	9.16 %	8.91 %	4.20 %	4.78 %	3.19 %	4.39 %	4.42 %	3.81 %
Diff. from the target	-5.9%	-6.4 %	-1.0 %	-1.0 %	-0.1 %	0.6 %	-1.2 %	-0.3 %

- **Measured values of the compressive strength**

  The compressive strength has been measured both the first and the fourth day, see results in Table 7.19. Measurements show that there were variations in the compressive strength during the period of ice model testing.

Table 7.19: Achieved values for compressive strength [kPa] (Model Scale)

		Velocity	Force		Pressure		σ_c (total force)	
			mean	peak, mean	mean	peak, mean	mean	peak
		[mm/s]	[N]	[N]	[bar]	[bar]	[kPa]	[kPa]
Measurement no.		5	48.58	74.85	-	-	22.09	34.03
		20	58.3	98.40	-	-	26.50	44.74
		50	66.08	102.76	-	-	30.04	46.72
	1						**26.21**	**41.83**
						σ_f	**20.68**	
						σ_c / σ_f	**1.27**	**2.02**
		5	37.01	57.97	-	-	11.92	18.67
		20	41.34	64.34	-	-	13.31	20.72
		50	46.7	77.13	-	-	15.04	24.84
	4						**13.42**	**21.41**
						σ_f	**18.36**	
						σ_c / σ_f	**0.73**	**1.17**

- **Discussion**

  Not all of the ice properties needed for the numerical model presented in Chapter 5 are measured during the ice test campaign, namely the tensile strength, ice salinity, Poissons ratio, ice-to-ice friction, cohesion, friction angle of the ice rubble and porosity.

  For the measured ice properties, there is a variation in the number of measurement within the prepared ice sheet. The ice thickness is measured at 52 different frames along the longitudinal axis of the test basin on both port and starboard side. To compare, the flexural strength was only measured at four (notice, only three measurements are presented in this report due to poor quality of the ice at the fourth frame) different frames. Eight measurements of the E-modules are presented. The ice density was only measured twice due to more or less constant model ice density.

  As a result of not measuring the ice properties over the whole ice sheet, it is uncertain whether the presented values are representative for the whole ice sheet. There may be areas in the ice where the ice properties have different values from the given ones due to poor ice quality. This kind of information would be very useful when studying the time series from the model tests as identified peaks may be a result of a suddenly reduction/increase of an ice property due to poor ice quality.

  All the measured ice properties show deviations from the target values given in Table 7.14. The properties are not only varying from one day to another, but also within the prepared ice sheet. This can be seen clearly in AARC REPORT A-372 (Mattsson, 2007) provided by Aker Solutions. In general, the measured values for the flexural strength are too large while the measured values for ice thickness are too small compared to the target values.

  The target ice properties used in the pre-simulation and later in Chapter 8 are given in Appendix A.

7.1.2 Fixed vs. moored set-up

In deep waters it is believed (Dalane et al., 2009) that a moored structure solution is more adequate than a fixed structure one. A floating platform can be designed with different open water and ice waterline which optimizes the concept for both conditions. Another important benefit with a floating concept is that the mooring system can be disconnected in case of extreme ice features or to avoid iceberg impact, giving the platform the possibility to move away from the initial location.

Ice model tests on both moored and floating platforms were performed at Hamburg Ship Model Basin (HSVA) on behalf of Aker Solutions during the period of 9-12 June, 2009 (Bruun et al., 2009). The main differences experienced and observed between the two concepts from the model tests are summarized below.

- In general, the ice-structure interaction pressure is different from the two tested concepts.
- A moored structure is free to move in all rigid-body modes defined for a floating body; described by three translational modes referred to as surge, sway and heave, and three rotational degrees of freedom referred to as roll, pitch and yaw. From the model tests it was seen that the surge motion dominates. A fixed platform is on the other hand not able to neither displace not rotate.
- The stiffness in the mooring lines and the mass of the structure are not taken into account in a fixed model test.
- A moored platform requires a sufficient distance between the basin bottom and the bottom of the hull to avoid hydrodynamic effects due to near bottom position.
- An ice model test with a moored platform requires deeper test basin compared to a test of a fixed structure.
- In the case of a moored platform, the ice loads may be affected by the platform motions (pitch and surge) which results in an increase of the angle of interaction with the cone and therefore reducing the efficiency in breaking the ice in bending.

7.2 Analysis of test results

Four ice model tests are presented in Table 7.13, all with an unique combination of ice thickness and velocity. Basic statistics are calculated for all tests based on the time series from the model tests. Also a sensitivity study is presented where the purpose is to see how the ice action loads are affected by the variation in ice thickness and velocity.

Notice: All results presented below are in Full Scale.

7.2.1 Basic statistics

Basic statistics are estimated for the four tests based on the time series provided by Aker Solutions. The statistics are valid for the part of the time series where the ice action loads are more or less stabilized. When looking at plots (see Figure B.45 to Figure B.48 in Appendix B) of the time series it is obvious that the loads are not stabilized at the same time for the four ice model tests mainly due to variation in velocity. The stable part for each ice model test is given in Table 7.20.

Table 7.20: Time interval of stabilized loads [sec] (Model Scale and Full Scale)

	Ice test no.			
	1	**2**	**3**	**4**
Model	100-200 sec.	40-80 sec.	60-160 sec.	30-80 sec.
Full Scale	547-1095 sec.	219-438 sec.	328-876 sec.	164-438 sec.

- The **Maximum load** is the highest load measured
- The **Minimum load** is the lowest load measured
- The **mean load** is the average load measured and calculated by;

$$\overline{x} = \frac{1}{n}\sum_{i=1}^{n} x_i \tag{7.83}$$

- The **Standard Deviation** (SD) shows how much variation or "dispersion" there is from the mean value. A low standard deviation indicates that the data points tend to be very close to the mean, whereas high standard deviation indicates that the data are spread out over a large range of values.

$$SD = \sqrt{\frac{1}{n-1}\sum_{i=1}^{n}(x_i - \overline{x})^2} \tag{7.84}$$

- The **mean zero up-crossing period** (T_0) is estimated from the stabilized part of the time series and corresponds to the period between each time the measured load is up-crossing the mean load indicated in red, see Figure 7.26. Due to rubble failure, the period is varying considerably during the time series especially for the horizontal load component. For example in ice test no. 2, the measured horizontal load did not cross the mean load more than once during a period of 100 s. The presented values are only average values and are not representative for the whole time series.

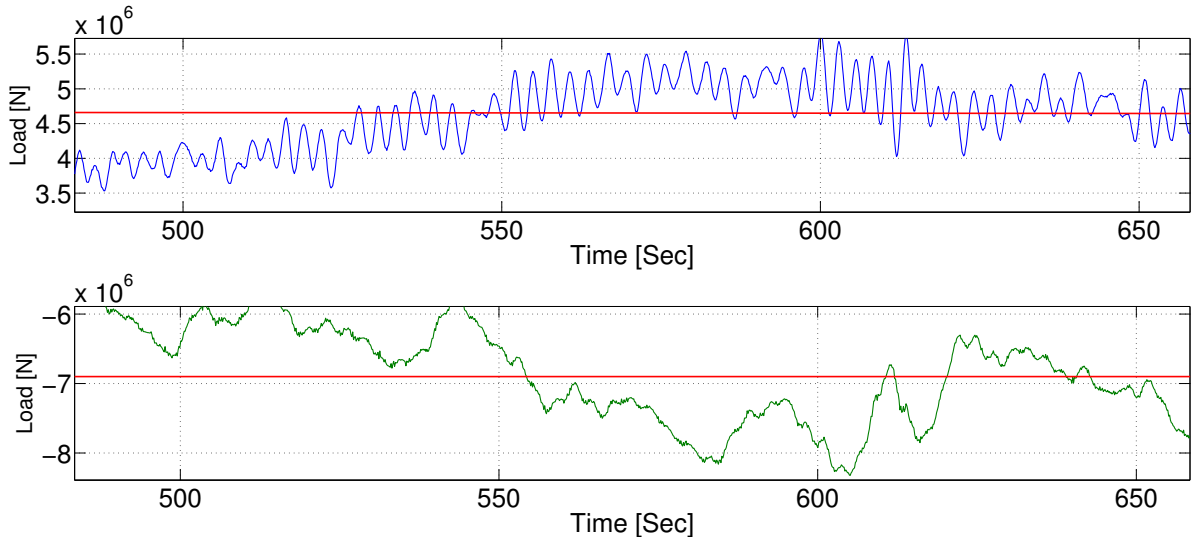

Figure 7.26: Zero up crossing period - Ice test no. 1 (Full Scale)

Results

Notice that the forces in the vertical direction are negative due to the definition of the coordinate system, see Figure 7.27.

Table 7.21: Basic statistics from the ice test campaign [MN] (Full Scale)

	Ice test no.							
	1		**2**		**3**		**4**	
	$\mathbf{F}_x$	$\mathbf{F}_z$	$\mathbf{F}_x$	$\mathbf{F}_z$	$\mathbf{F}_x$	$\mathbf{F}_z$	$\mathbf{F}_x$	$\mathbf{F}_z$
Max. [MN]	5.8	-8.3	6.2	-8.6	7.4	-10.7	7.3	-11.2
Min. [MN]	2.9	-5.4	5.1	-7.3	0.9	-2.8	4.0	-6.9
Mean [MN]	4.7	-6.9	5.7	-8.0	4.5	-7.4	5.7	-9.0
SD [MN]	0.4	0.5	0.2	0.2	1.2	1.7	0.6	0.7
T_0 [sec]	4.2	25.4	7.2	18.0	6.5	17.1	16.16	11.6

The statistics show that;

- The vertical force is larger than the horizontal force for all tests.
- Ice test no. 3 and no. 4 give highest maximum forces (ice thickness is 1.5 m).
- Ice test no. 2 and no. 4 give the largest mean forces (velocity is 1 m/s).
- The standard deviations is larger for ice test no. 3 and no. 4 compared to no. 1 and no. 2. This can also be seen in the time series attached in Appendix B.
- For the first three ice tests, the zero up-crossing period is much larger for the vertical load compared to the horizontal load. However, it is mentioned above that the values presented are not representative for the whole time series as the identified periods vary due to rubble failure.

7.2.2 Resultant forces

The coordinate system used when calculating the resultant forces and the corresponding angle with the horizon, θ, is given in Figure 7.27. Notice that the positive vertical axis is pointing upwards and the positive horizontal axis is pointing to the left which is the direction of the moving ice sheet.

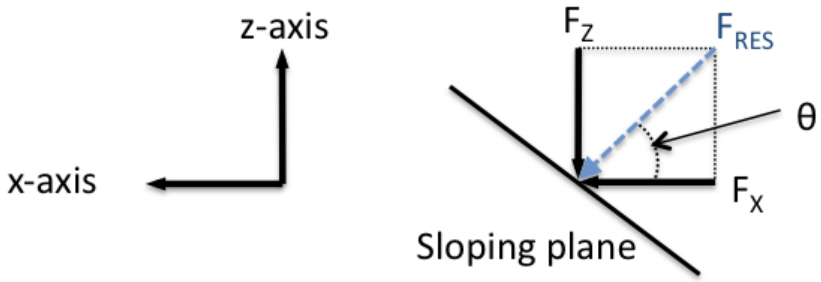

Figure 7.27: Coordinate system used in Chapter 7.2.2

According to the coordinate system are the forces measured negative in the vertical direction and positive in the horizontal direction. The resultant forces and corresponding angle with horizon, θ, are given as positive values.

Table 7.22: Resultant forces and angle with the horizon [MN] (Full Scale)

	Test no.							
	1		**2**		**3**		**4**	
	$\mathbf{F}_{RES}$ **[MN]**	θ **[deg]**	$\mathbf{F}_{RES}$ **[MN]**	θ **[deg]**	$\mathbf{F}_{RES}$ **[MN]**	θ **[deg]**	$\mathbf{F}_{RES}$ **[MN]**	θ **[deg]**
Max.	10.2	55.1	10.6	54.0	13.0	55.4	13.2	56.6
Min.	6.1	61.9	8.9	55.0	3.0	73.1	8.0	59.8
Mean	8.3	55.7	9.9	54.5	8.7	58.5	10.7	57.7

From Table 7.22 it becomes apparent that the maximum resultant forces occur in Test no. 3 and no. 4 (ice thickness is 1.5 m) while the minimum resultant forces occur in Test no. 1 and no. 3 (velocity is 0.5 m/s). The maximum mean forces are observed in Test no. 2 and no. 4 (velocity is 1.0 m/s).

7.2.3 Sensitivity of ice thickness and velocity

Table 7.23 presents the four sensitivity tests performed where the ice model tests have been compared to each other. The purpose for this is to investigate the sensitivity of thick ice vs. thin ice and high velocity vs. low velocity. Notice how only one parameter is varied during each sensitivity test.

Example: In sensitivity test I, ice model test no. 1 and no. 2 are compared. Here the ice thickness is 1 m for both tests while the velocity is increased from 0.5 m/s to 1 m/s, hence the purpose is to investigate the sensitivity of the ice velocity.

Table 7.23: Sensitivity test matrix (Full Scale)

Sensitivity test no.	Ice model test no.	Ice thickness [m]	Velocity [m/s]
I	1	1	0.5
	2	1	1
II	1	1	0.5
	3	1.5	0.5
III	2	1	1
	4	1.5	1
IV	3	1.5	0.5
	4	1.5	1

The ice thickness is referred to as either thin (1 m) or thick (1.5 m), while the velocity is referred to as either high (1 m/s) or low (0.5 m/s).

The main findings from the sensitivity tests are the following;

The main findings from the four sensitivity tests (ST) are given below. Plots utilized in the comparison study are included in Appendix B, see Figure B.49 to Figure B.56. Notice that the loads measured during the four tests were earlier presented in Table 7.21 and Table 7.22.

- **Sensitivity of ice thickness (ST II and ST III)**
  - The ice loads stabilize faster for the thick ice than for the thin ice. When studying the load history from ST II one can see that after approximately 300 s the ice loads for the thick ice are following more or less the same trend. To compare, the thin ice uses about twice the time until the same trend can be seen. The same tendency, however not as clearly, can be observed in ST III where the thin ice uses about 250 s while the thick ice uses 200 s to stabilize.
  - The standard deviation calculated is greater for the thick ice compared to the thin ice. This is even more clear when looking at the low-velocity ice in ST II.
  - Thick ice results in greater forces than thin ice.
- **Sensitivity of velocity (ST I and ST IV)**
  - The time it takes until the ice loads are more or less stabilized is significantly shorter for the high-velocity ice compared to the low-velocity ice. This trend is even more clear in ST I where the ice thickness is 1 m compared to ST IV where the ice is 1.5 m. The low-velocity ice is stabilized after approximately 600 s and 300 s respectively for ST I and ST IV. To compare, the high-velocity ice is stabilized after 250 s and 200 s.
  - The calculated standard deviation is larger for the low-velocity ice compared to the high-velocity ice. This is even more clear when looking at ST I.
  - The high-velocity ice gives slightly higher ice action loads than the low-velocity ice in both sensitivity tests.

Table 7.24 summarizes how the maximum, minimum and mean resultant forces (earlier presented in Table 7.22) vary with increasing velocity (ST I and ST IV) and increasing ice thickness (ST II and ST III). When looking at the mean forces, it becomes very clear that the forces are more sensitive to an increase in velocity than an increase in ice thickness. The statistics are based on the stabilized part of the time series.

Example: In sensitivity test no. I, the velocity is increased from 0.5 m/s to 1 m/s while the ice thickness is kept constant at 1 m. From the table it can be seen that an increase in velocity means that both the maximum, minimum and the mean load of the resultant force increase by respectively 4%, 46% and 19%.

Table 7.24: Results from sensitivity tests (Full Scale)

Sensitivity test no.	Comments	F_{RES}		
		Max.	Min.	Mean
I	h = 1 m v increases from 0.5 m/s to 1 m/s	+4%	+46%	+19%
II	v = 0.5 m/s h increases from 1m to 1.5 m	+27%	-51%	+5%
III	v = 1 m/s h increases from 1 m to 1.5 m	+25%	-10%	+8%
IV	h = 1.5 m v increases from 0.5 m/s to 1 m/s	+2%	+167%	+23%

7.2.4 Observations from ice model test videos

Videos from the ice model tests have been studied in detail to be able to describe the ice breaking periods, ice breaking lengths, rubble accumulation, geometry etc. Table 7.25 summarizes the main findings from the videos.

Notice that the table is only based on visual observations and assumptions made by the student and shall not be used as design values. It should also be pointed out that the videos from test no. 3 and no. 4 are filmed far away from the structure compared to the other two tests. Consequently it has been much more challenging to estimate the breaking length and rubble angle for respectively test no. 3 and no. 4.

Table 7.25: Average values observed in the ice model test videos (Full Scale)

Ice model test no.	Duration of load build-up [s]	Breaking length [m]	Breaking period [s]	Rubble angle [deg]	Rubble failure period [s]	Rubble height [m]
1	280	3	6	30	61	6
2	93	2	2	35	33	7
3	175	3.75	7.5	31	130	6
4	66	6	6	33	84	7

- The duration of load build-up indicates the time it takes from the first ice sheet collides with the structure until the ice loads are stabilized due to more or less constant rubble volume. It was seen in the videos that this period differs significantly between the four tests mainly due to the variation in velocity. Ice model test no. 4 (high-velocity and thick ice) uses only 66 s from the first ice sheet breaks until a more or less constant rubble volume is obtained. To compare, ice model test no. 1 (low-velocity and thin ice) uses 280 s to obtain the same rubble volume.

  The relative velocity of the structure decreased during the build up of ice loads. The measured velocity was positive at all time, hence the structure was constantly moving towards the ice sheet and packing the rubble.

- Figure 7.28 shows how the breaking length and rubble angle is estimated. The observed breaking lengths are ranging from 2 m to 6 m.

When only a single layer of ice is being pushed upwards the sloping wall, the angle of the rubble is equal to the inclination angle. As soon as the rubble starts to accumulate the rubble angle decreases until a more or less constant rubble volume is obtained. The rubble angles have been calculated by simple geometry with help from screen shots taken from the ice model test videos and ranging from 30° to 35°. Even though the angles are roughly estimated it is reasonable to believe that the they are within an acceptable range (ISO 19906, 2010).

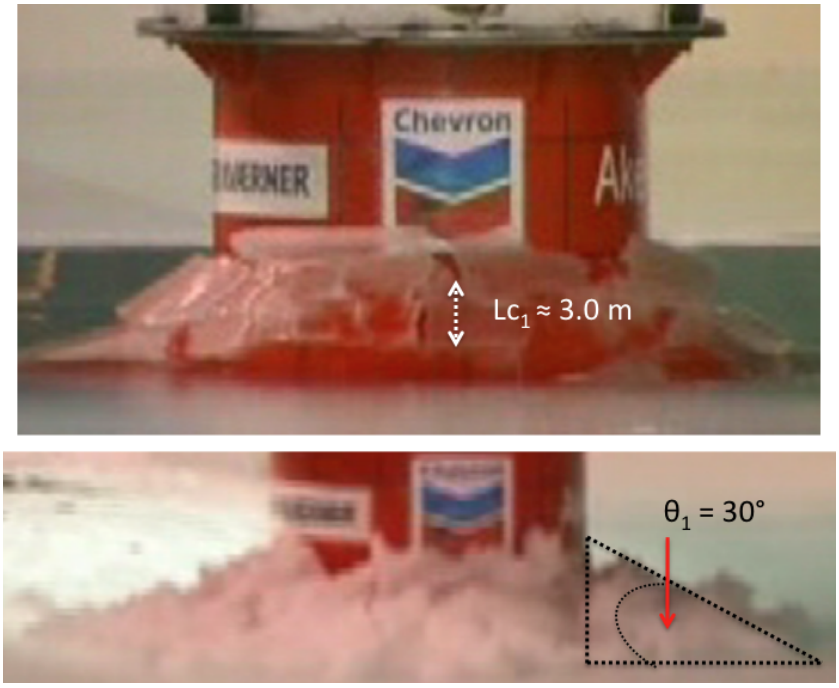

Figure 7.28: Estimate of breaking length and rubble angle (ice test no. 1)

See Appendix C for ice test no. 2, no. 3 and no. 4.

- Figure 7.29 shows how the rubble failure period is estimated (exemplified here with test no. 1) for the four tests. It is believed that the eight identified tops in the figure correspond to maximum rubble volume. The period between each top is therefore assumed to be the rubble failure period.

  The observed periods are ranging from 33 s to 130 s.

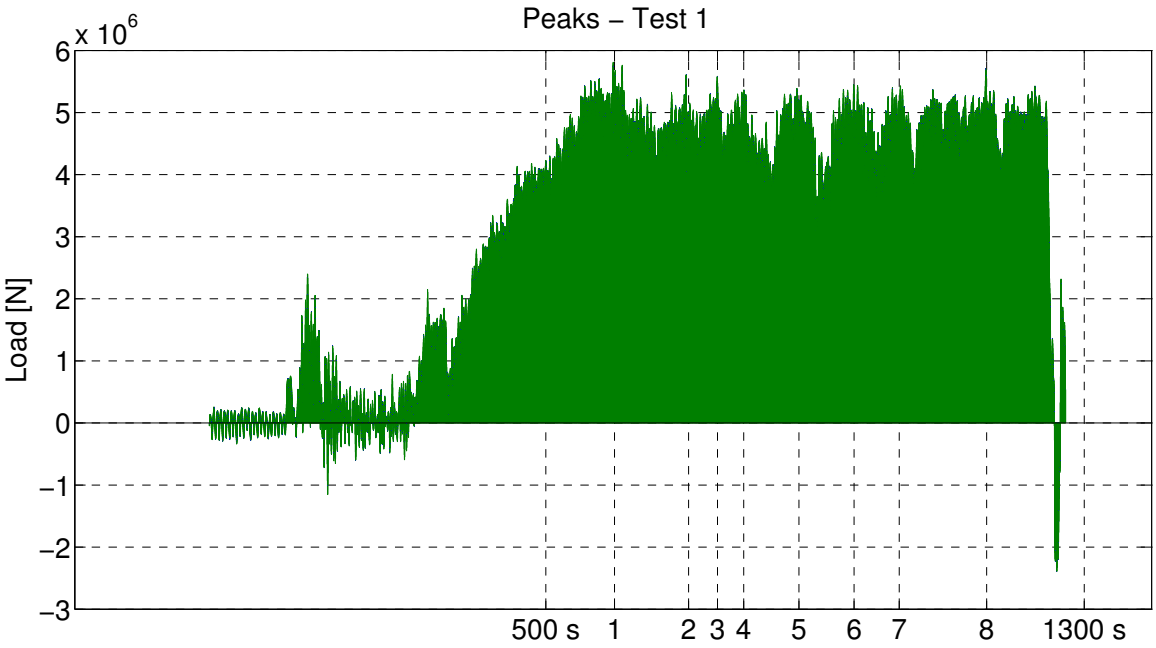

Figure 7.29: Estimate of rubble failure period (ice test no. 1)

- Figure 7.30 shows how the rubble height is estimated. From the videos and pictures from the model tests it can be seen that the rubble height is slightly higher for ice model test no. 2 and no. 4 where the velocity is 1 m/s. It is estimated that an average value of the rubble height is approximately 6 m for ice model test no. 1 and no. 3, while it is 7 m for ice model test no. 2 and no. 4.

Figure 7.30: Estimate of rubble height (ice test no 1)

See Appendix C for ice test no. 2, no. 3 and no. 4.

From the videos it can be seen that at some time during the model test the rubble fails. This leads to a reduction in rubble height and rubble volume. This will again lead to an increase in rubble angle.

- An illustration of the ice transport is given in Figure 7.31 indicated with red arrows.

  When the drifting ice interacts with the sloping structure the ice breaks into small ice blocks with a breaking period dependent on the drift velocity and the thickness of the ice. The broken ice is immediately being pushed upwards the sloping wall until it reaches the top of the inclined plane. At this point the ice is further pushed into a vertical position which makes it to fall down as indicated in the figure. Further the ice sheets are transported around the structure on both sides. According to screen shots taken from the videos the major part of the ice is accumulated above the waterline. Only a small amount of ice is trapped below the waterline.

  Based on the videos it is reasonable to believe that circumferential breaking pattern was governing the failure mode followed up by radial breaking pattern.

  There have not been observed any significant differences in the ice transport for the four tests disregarded the ice velocity.

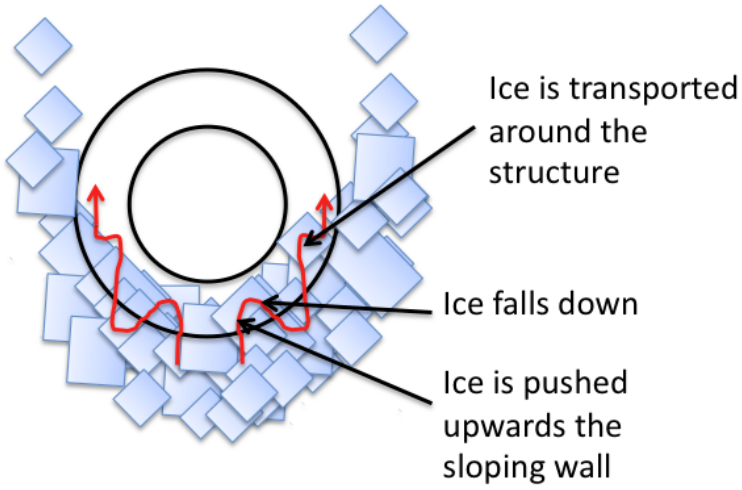

Figure 7.31: Ice transport (Birdview)

8 COMPARISON STUDY OF TIME SERIES

Based on the activities earlier performed in Chapter 6 and Chapter 7 the results obtained with the MATLAB-script, for all the four ice model tests, are to be compared with the measured ice load time series provided by Aker Solutions.

The comparison study is divided into two parts. In the first part, three different cases (Case 1, Case 2 and Case 3 (a and b [2])) are compared to the measured time series. Here, the purpose is to study the sensitivity of ice properties in addition to identify the correction factor(s) between the numerical model and the measured time series.

In the second part of the comparison study Case 1 and Case 4 are compared to the measured time series. The purpose has been to investigate the validity of performing numerical simulations compared to performing ice model tests.

All cases are summarized in Table 8.26. Notice that the input in Case 3.a and Case 3.b is equal, see footnote. A general discussion of the results obtained is given in Chapter 8.5.

Table 8.26: Comparison study matrix

Case no.	Ice properties		Breaking period		Ice transport		Ice accumulation	
	Target	Measured	Assumed	Identified	Assumed	Identified	Assumed	Identified
1	x		x		x		x	
2		x		x	x		x	
3.a		x		x		x		x
3.b		x		x		x		x
4	x			x		x		x

For all four ice model tests the following is calculated;

- Horizontal load (F_X): Maximum, minimum and mean value.
- Vertical load (F_Z): Maximum, minimum and mean value.
- Resultant load (F_R): Maximum, minimum and mean value.
- Angle the maximum, minimum and mean resultant load makes with the horizon (θ).

All the results presented in this chapter are in full scale and based on the stabilized part of the time series, hence after the load build-up has stabilized.

The input needed for the calculations is given in Chapter 8.1.

For all four cases presented, the time series calculated for ice test no. 1 (see Table 8.27 and Table 8.28 for input) is included. The intension for this is to visually compare the time series calculated to the measured ones presented in Chapter 8.2.

8.1 Ice properties, rubble geometry and accumulation scenarios

The predicted and obtained actual ice thickness, ice velocity and flexural strength are given in Table 8.27.

[2]Case 3.b differs from Case 3.a by reducing the horizontal and vertical load by identified factors, see page 66

Table 8.27: Ice properties - Predicted and measured (Full Scale)

		Ice model test no.			
		1	**2**	**3**	**4**
Ice thickness [m]	Measured	0.98	0.98	1.44	1.48
	Predicted	1.0	1.0	1.5	1.5
Ice velocity [m/s]	Measured	0.49	0.99	0.49	0.99
	Predicted	0.5	1.0	0.5	1.0
Flexural strength [kPa]	Measured	720	693	615	579
	Predicted	500	500	500	500

In addition, the density of the ice, E-modules and ice/structure-friction have been measured.

- The average value of the measured ice density is 925.74 kg/m^3 while the target value was 900 kg/m^3 (both in Full Scale).
- Due to variations in the measured E-modulus (see Table 7.16), average values are used in the calculations. The values calculated for the 1.0 m thick ice and 1.5 m thick ice are respectively 1.43 GPa and 0.48 GPa (both in Full Scale). The target ratio between the E-modulus and the flexural strength was $\geq$1000. This is obtained for ice test no. 1 and no. 2, not for no. 3 and no. 4.
- The ice-structure friction measured is 0.050 while the target was 0.15.

The identified and assumed values of the rubble height, breaking period of the ice, load build-up period, rubble failure period and the angle the rubble make with the horizon are given in Table 8.28.

Table 8.28: Ice transport and rubble scenarios - Predicted and identified (Full Scale)

		Ice model test no.			
		1	**2**	**3**	**4**
h$_r$ [m]	Identified	6	7	6	7
	Assumed	5	5	5	5
T$_B$ [sec]	Identified	6	2	7.5	6
	Assumed	25.8	12.9	34.8	17.4
T$_{RB}$ [sec]	Identified	280	93	175	66
	Assumed	50	50	50	50
T$_{RF}$ [sec]	Identified	61	33	130	84
	Assumed	0	0	0	0
θ [deg]	Identified	30	35	31	33
	Assumed	35	35	35	35

Where;

h$_r$	Rubble height
T$_B$	Average breaking period of the ice
T$_{RB}$	The time it takes from the first ice sheet collides with the structure until a more or less constant rubble volume is obtained (load build-up)
T$_{RF}$	Average rubble failure period
θ	The angle the rubble makes with the horizon

It is important to keep in mind that the so-called *identified* values are based on observations from the model test videos and should not be used as design values.

8.2 Measured time series

The measured horizontal and vertical loads for ice test no. 1 are presented in Figure 8.32. Basic statistics for all four tests can be found in Table 8.29. A thorough description of the ice model tests is given in Chapter 7 and will therefore not be given here.

Table 8.29: Results from measured time series (Full Scale)

	Test no.											
	1			**2**			**3**			**4**		
	Max.	**Min.**	**Mean**	**Max.**	**Min.**	**Mean**	**Max.**	**Min.**	**Mean**	**Max.**	**Min.**	**Mean**
	[MN]			**[MN]**			**[MN]**			**[MN]**		
$\mathbf{F}_X$	5.8	2.9	4.7	6.2	5.1	5.7	7.4	0.9	4.5	7.3	4.0	5.7
$\mathbf{F}_Z$	8.3	5.4	6.9	8.6	7.3	8.0	10.7	2.8	7.4	11.2	6.9	9.0
$\mathbf{F}_R$	10.2	6.1	8.3	10.6	8.9	9.9	13.0	3.0	8.7	13.2	8.0	10.7
θ	55.1°	61.9°	55.7°	54.0°	55.0°	54.5°	55.4°	73.1°	58.5°	56.6°	59.8°	57.7°

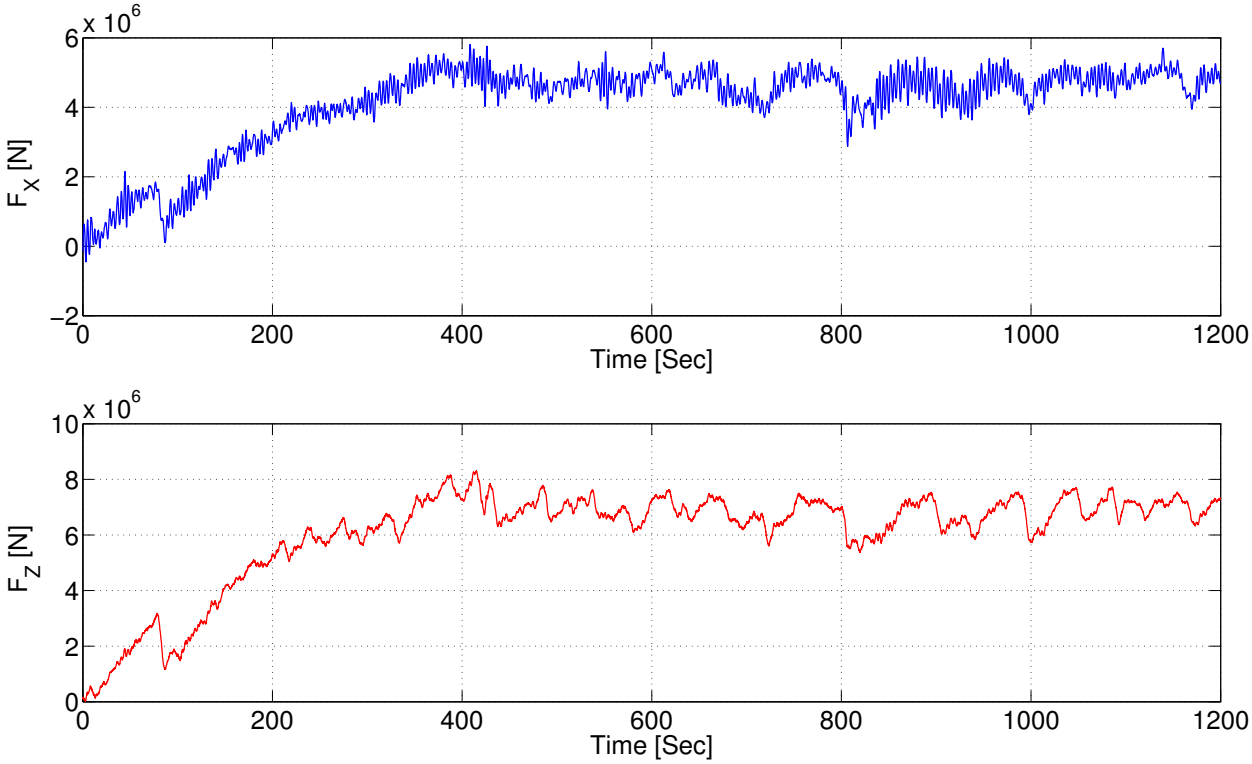

Figure 8.32: Measured time series of ice test no.1 (Full Scale)

8.3 Comparison study - Part 1

In Part 1 of the comparison study three cases are compared to the measured time series. Case 1, Case 2 and Case 3 (a and b) are based on the MATLAB-script earlier utilized in the pre-simulation in Chapter 6. However, the script has been modified in Case 2 and Case 3 (a and b) in agreement with the description of the cases below.

The purpose for the comparison is to investigate the sensitivity of ice properties, rubble geometry and accumulation scenarios.

The use/input of the developed MATLAB-script for the three cases are the following;

- **Case 1:** Use of MATLAB-script with target ice properties and assumed ice transport and accumulation scenario.
- **Case 2:** Use of MATLAB-script with actually obtained ice properties and identified average breaking period of the ice, and assumed ice transport and accumulation scenario.
- **Case 3.a :** Use of MATLAB-script corrected for actual measured ice properties, identified average breaking periods of the ice and geometry of ice accumulation and transport on the structure.
- **Case 3.b :** In addition to the input given for Case 3.a, the total horizontal and vertical load shall be corrected with a *correction factor* in order to obtained loads in the same range as the measured loads presented in Chapter 8.2.

The results from the three cases are discussed in Chapter 8.3.5.

8.3.1 Case 1

In Case 1, the target ice properties are used as input, see Table 8.27, combined with the assumed ice transport and accumulation scenario described in Chapter 5.3 which is summarized in Table 8.28. The results are given in Table 8.30. Case 1 is equal to the pre-simulation presented in Chapter 6.

Table 8.30: Results from Case 1 (Full Scale)

	Test no.											
	1			**2**			**3**			**4**		
	Max.	**Min.**	**Mean**	**Max.**	**Min.**	**Mean**	**Max.**	**Min.**	**Mean**	**Max.**	**Min.**	**Mean**
	[MN]			**[MN]**			**[MN]**			**[MN]**		
$\mathbf{F}_X$	6.7	3.8	4.0	6.7	3.8	4.0	10.3	5.0	5.5	10.4	5.0	5.5
$\mathbf{F}_Z$	4.9	2.8	2.9	4.9	2.8	2.9	7.6	3.7	4.1	7.7	3.7	4.1
$\mathbf{F}_R$	8.3	4.7	4.9	8.3	4.7	4.9	12.8	6.3	6.8	12.9	6.3	6.8
θ	36.2°	36.4°	35.9°	36.2°	36.4°	35.9°	36.4°	36.5°	36.7°	36.5°	36.5°	36.7°

Figure 8.33 shows the calculated time series for ice test no. 1.

It was assumed in Case 1 that the breaking component, H_B, in Croasdale's methodology is an impulse load, hence the peaks.

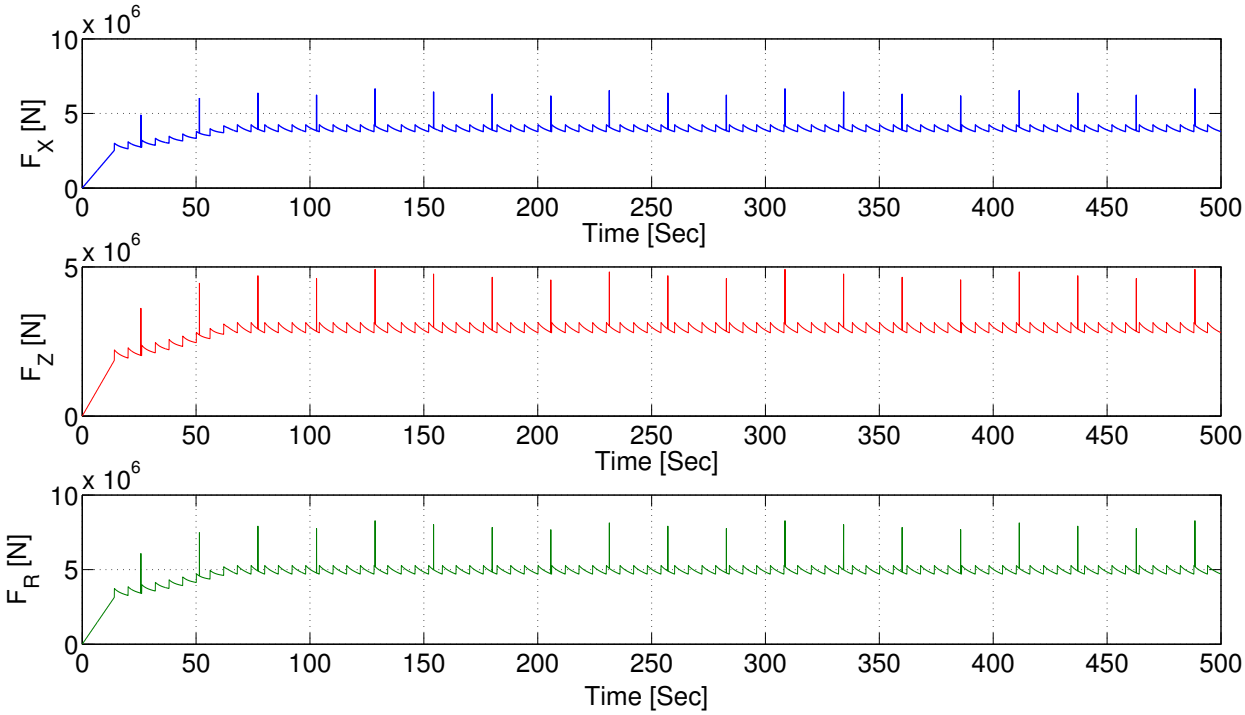

Figure 8.33: Calculated time series of ice test no. 1 - Case 1 (Full Scale)

8.3.2 Case 2

The actually obtained ice properties and the identified average breaking period of the ice are used as input in Case 2 combined with the assumed ice transport and accumulation scenario (see Table 8.27 and Table 8.28). The results are summarized in Table 8.31.

Case 2 differs from Case 1 by using the identified ice properties and breaking length, hence the purpose for Case 2 is to investigate the sensitivity of ice properties.

Table 8.31: Results from Case 2 (Full Scale)

	Test no.											
	1			**2**			**3**			**4**		
	Max.	**Min.**	**Mean**	**Max.**	**Min.**	**Mean**	**Max.**	**Min.**	**Mean**	**Max.**	**Min.**	**Mean**
	[MN]			**[MN]**			**[MN]**			**[MN]**		
$\mathbf{F}_X$	8.2	3.1	3.3	13.1	3.1	3.5	16.8	4.0	4.5	12.3	4.1	4.6
$\mathbf{F}_Z$	7.4	2.8	3.0	11.9	2.8	3.1	15.2	3.7	4.1	11.1	3.7	4.2
$\mathbf{F}_R$	11.1	4.1	4.4	17.7	4.1	4.7	22.6	5.4	6.1	16.5	5.6	6.2
θ	42.1°	42.1°	42.3°	42.3°	42.1°	42.3°	42.1°	42.8°	42.3°	42.1°	42.1°	42.4°

Figure 8.34 shows the calculated time series for ice test no. 1.

Like in Case 1, it was assumed in Case 2 that the breaking component, H_B, in Croasdale's methodology is an impulse load. However the period between the peaks is reduced compared to Case 1 due to reduction in the breaking period.

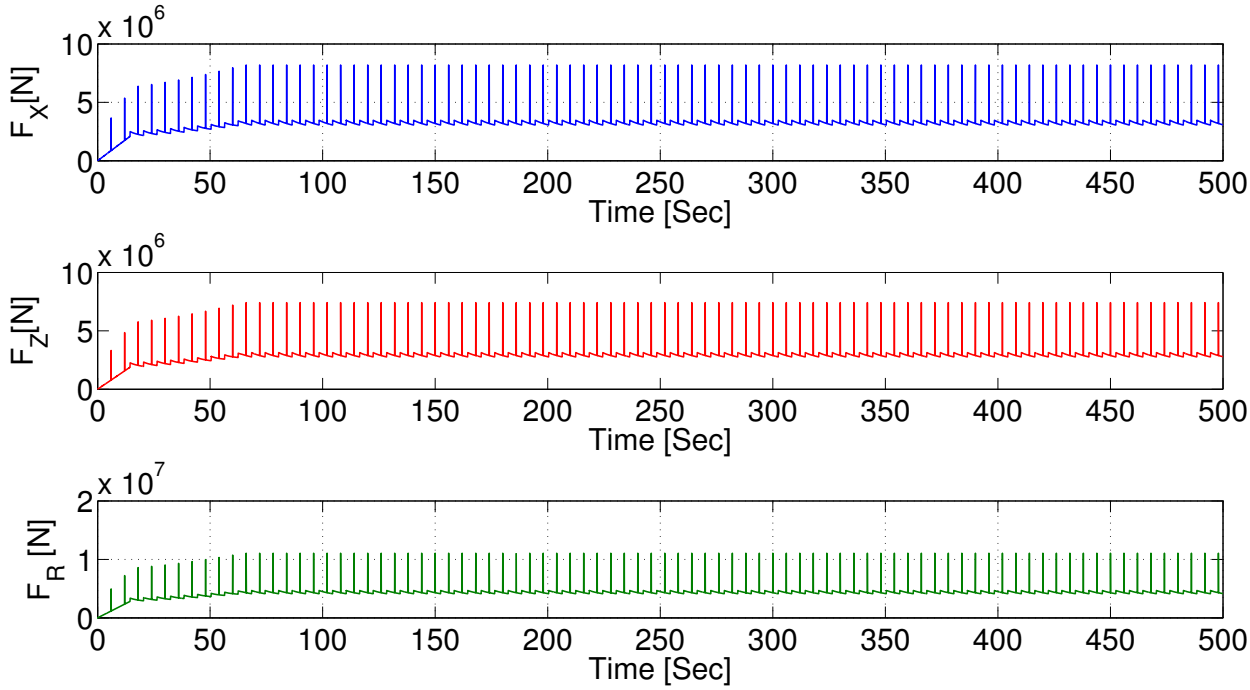

Figure 8.34: Calculated time series of ice test no. 1 - Case 2 (Full Scale)

8.3.3 Case 3.a

Case 3.a differs from Case 2 by using the observed rubble geometry, ice transport and rubble accumulation scenario in the script. The purpose for Case 3.a is to identify the correction factor(s) between the numerical model and the measured time series. The following is corrected for;

- **Ice Properties**
  - Actually measured ice properties used are summarized in Chapter 8.1.
- **Load components**
  - **General comments:**

    The total horizontal and vertical loads calculated by Croasdale's methodology (see Chapter 3.1.2) are functions of the five load components H_B, H_P, H_R, H_L and H_T. The time series provided by Aker Solutions only present the total horizontal (F_X and F_Y) and vertical load (F_Z), hence not each load components separately. This has made the correction of each load component challenging.

    It was first assumed that the duration of the load build-up (T_{RB} ref. Table 8.28) was 50 s for all four tests. From the videos it became clear that the low-velocity (v = 0.5 m/s) tests use in general more time to achieve a constant rubble volume compared to the high-velocity (v = 1 m/s) tests. The actually measured periods are also given in Table 8.28.

    It was also assumed that after reaching the maximum rubble volume both H_P, H_R and H_L were constant at its maximum value. Rubble failure was in other words not taken into account. When observing the time series it was possible to identify that the rubble fails with a varying period. An average rubble failure period has therefore been used in the corrected MATLAB-script.

In order to take the reduction in the rubble volume due to rubble failure into account *reduction factors* have been introduced to the MATLAB-script. This is explained further below.

- **Reduction factor**
  - **Rubble failure**

    Rubble failure corresponds to a reduction in the rubble volume which affects the loads. The true reduction in rubble volume has been very challenging to estimate based on the videos. To deal with the uncertainties regarding the magnitude of the rubble reduction, a reduction factor has been introduced in the script. This factor determines the magnitude of the reduction in rubble volume during one rubble failure period.

    Example: If the reduction factor is 0.1 and the rubble failure period is 60 seconds the scripts makes sure of reducing the load component linearly by 10% during 60 seconds.

    H_R, H_P and H_L are assumed to be reduced 10% during one rubble failure period, hence the reduction factor is 0.1.

    The reduction factor is estimated from a process of trial and error where the calculated time series have been compared to the time series actually measured both visually and numerically.

    Another way of including the reduction in rubble volume in the script is to increase the rubble angle. Notice that a rubble angle greater than the inclination angle corresponds to a negative rubble volume, hence $\theta_{MAX} = 45°$.

  - **Other**

    H_T is the force necessary to rotate the ice blocks into a vertical orientation, ref. Figure 5.22. It was first assumed that the load dropped from its maximum to zero during one turning period. After studying the time series it is believed that this is only the case for the first turning. As soon as the rubble has started to accumulate it is assumed that the load is only reduced 50%, not 100% as first believed, during the turning period. Hence a reduction factor of 0.5 is used.

    The breaking component, H_B, was first assumed to act as an impulse load once during the breaking period. This can be seen very clearly in the plots from the pre-simulation in Chapter 6. After studying the time series it is assumed that H_B is contributing during the whole breaking period. Exactly how H_B is varying has been challenging to understand based on the time series measured. By visually comparing the calculated and measured time series it seems reasonable to believe that the load component is reduced in the range of 10% during the breaking period. The reduction factor used is in other words 0.1.

    All the five load components are shown i Figure 8.35 below. The rubble failure period, starting at 300 s, can clearly be seen when looking at H_R (blue) , H_P (red) and H_L (green). H_T and H_B are shown in pink and yellow.

After correcting the model in agreement with the identified rubble accumulation scenario, ice transport etc. the loads calculated were not in the same range as the measured loads, see Figure 8.36. Both the horizontal and the vertical load are too large.

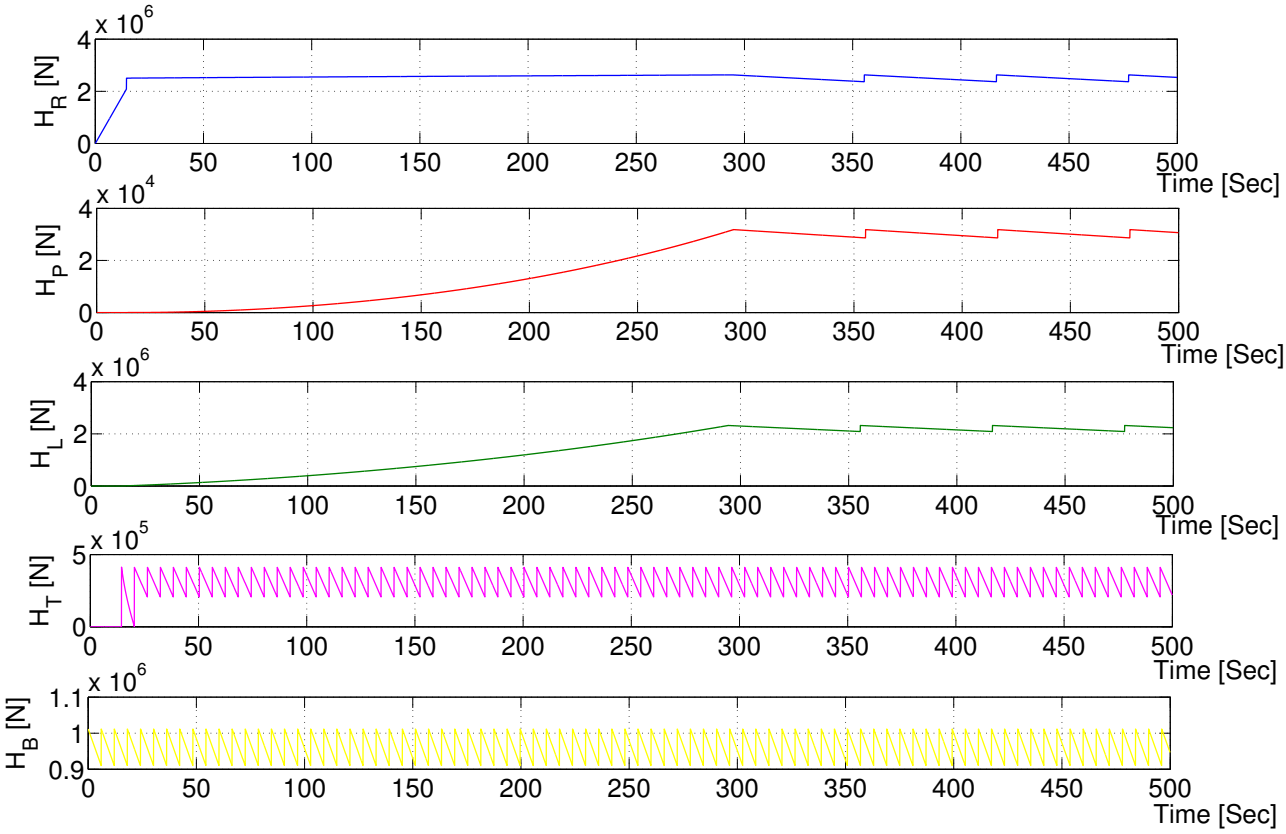

Figure 8.35: All load components in horizontal direction - Ice test no. 1 (Full Scale)

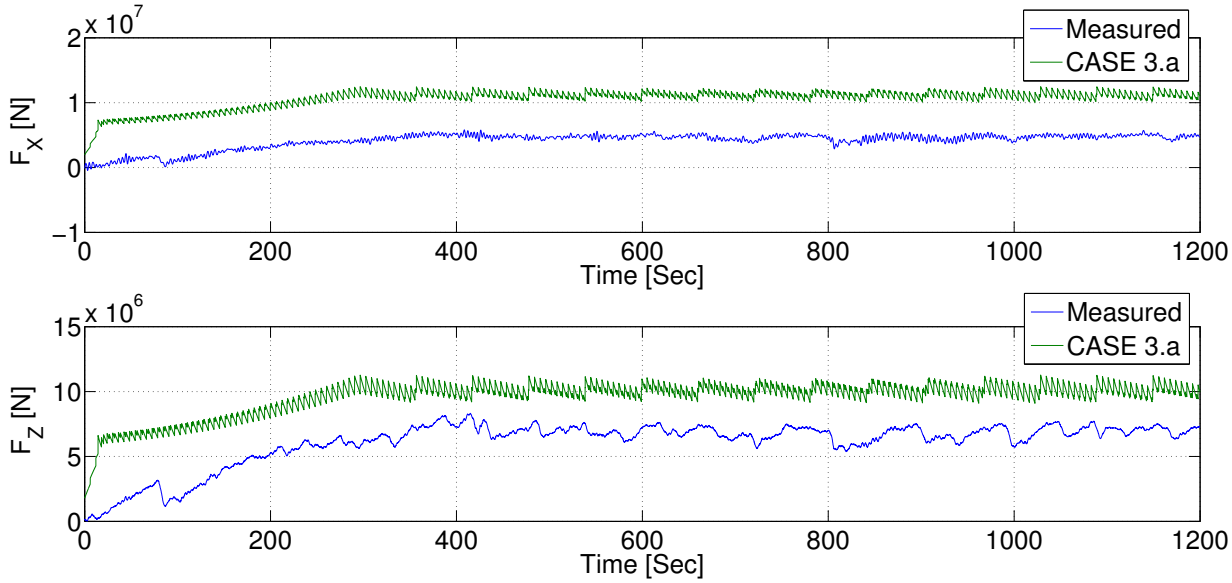

Figure 8.36: Case 3.a vs. measured time series - Ice test no. 1 (Full Scale)

8.3.4 Case 3.b

In order to obtain statistics in the same range as the measures loads, the total horizontal loads were divided by 3 and the total vertical loads were divided by 1.5, see Figure 8.37. Apart from this, Case 3.b is equal to Case 3.a.

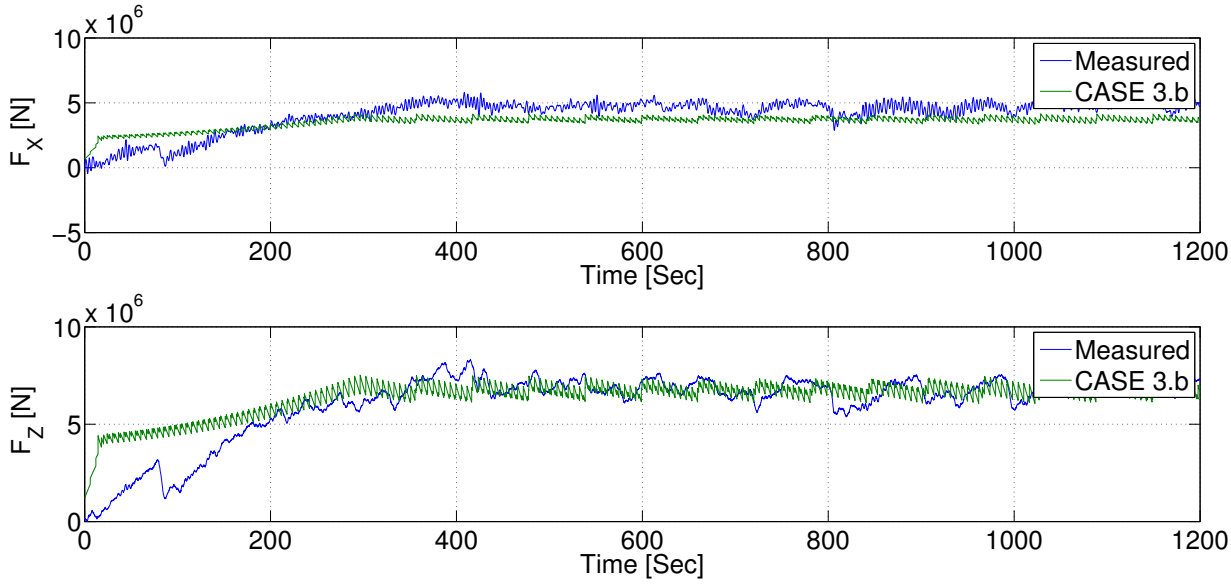

Figure 8.37: Case 3.b vs. measured time series - Ice test no. 1 (Full Scale)

The results from Case 3.b is given in Table 8.32.

Table 8.32: Results from Case 3.b (Full Scale)

	Test no.											
	1			**2**			**3**			**4**		
	Max.	**Min.**	**Mean**	**Max.**	**Min.**	**Mean**	**Max.**	**Min.**	**Mean**	**Max.**	**Min.**	**Mean**
	[MN]			**[MN]**			**[MN]**			**[MN]**		
$\mathbf{F}_X$	4.1	3.4	3.7	6.1	4.3	5.2	7.1	5.1	6.2	5.6	4.5	5.0
$\mathbf{F}_Z$	7.5	6.1	6.8	11.1	7.7	9.4	12.8	9.2	11.2	10.1	8.2	9.1
$\mathbf{F}_R$	8.6	7.0	7.7	12.6	8.8	10.8	14.7	10.5	12.8	11.6	9.4	10.4
θ	61.3°	60.9°	61.4°	61.2°	60.8°	61.0°	61.0 °	61.0 °	61.8°	61.0°	61.2°	61.2°

Figure 8.39 shows the calculated time series for ice test no. 1.

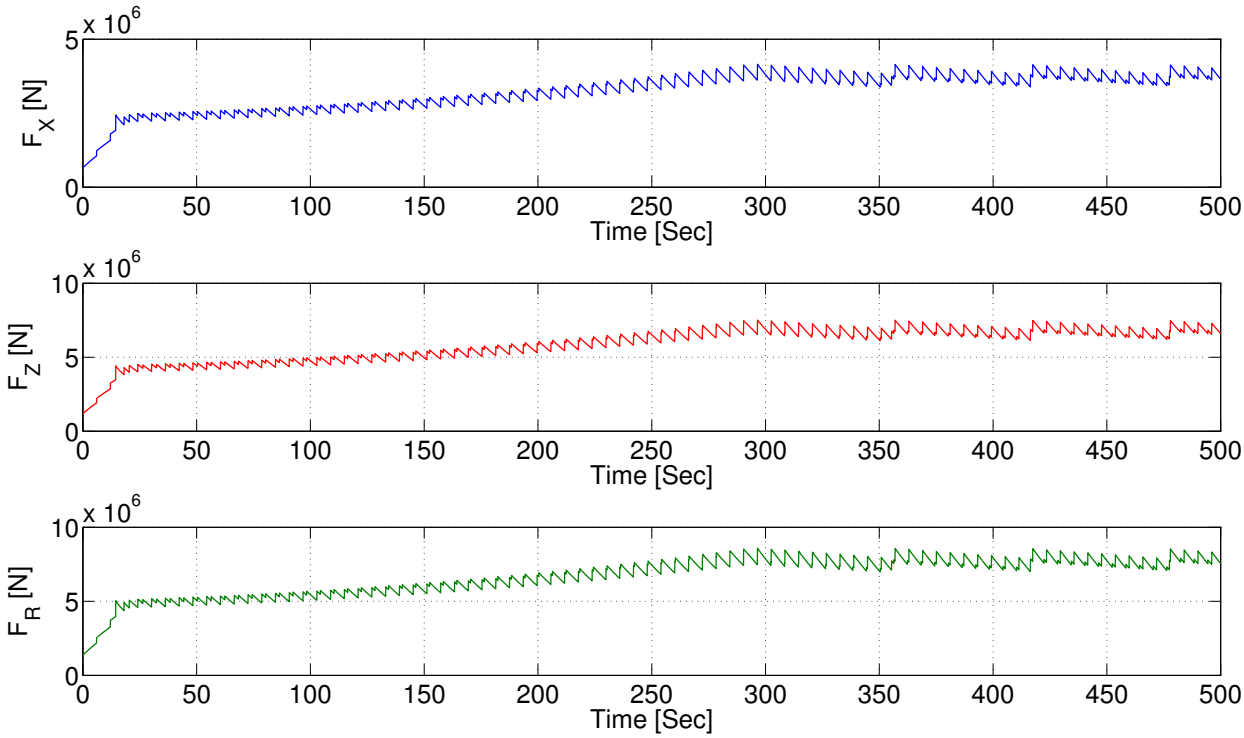

Figure 8.38: Calculated time series of ice test no. 1 - Case 3.b (Full Scale)

8.3.5 Results

The three cases show deviations from the measured loads, both numerically and visually. The main findings from the first part of the comparison study are;

- When comparing Case 1 and Case 2 it can be seen that the maximum loads are larger for Case 2 (higher peaks). However, the mean loads calculated are slightly larger for Case 1. Hence, by introducing the measured ice properties and identified breaking length the mean loads decrease for all four tests. Also the angle between the horizon and the loads presented are larger for Case 2 compared to Case 1.
- The forces in the horizontal direction are larger than the forces in the vertical direction in Case 1 and Case 2. This is in contrast with the loads calculated in Case 3.b.
- Case 3.a is visually more similar to the measured time series compared to the two first cases. However, both the horizontal and vertical loads are too large compared to the measured loads. In Case 3.b, the loads calculated in Case 3.a are reduced in order to better correlate the magnitude of the measured loads. The horizontal load is reduced by a factor of 3 while the vertical load is reduced by a factor of 1.5.
- Neither Case 1, Case 2 nor Case 3 include the random rubble failure behavior that is observed in the measured time series.

Both the horizontal, vertical and resultant loads for all three cases are plotted in Figure 8.39. It can clearly be seen that the three time series differ as described in the above-given discussion.

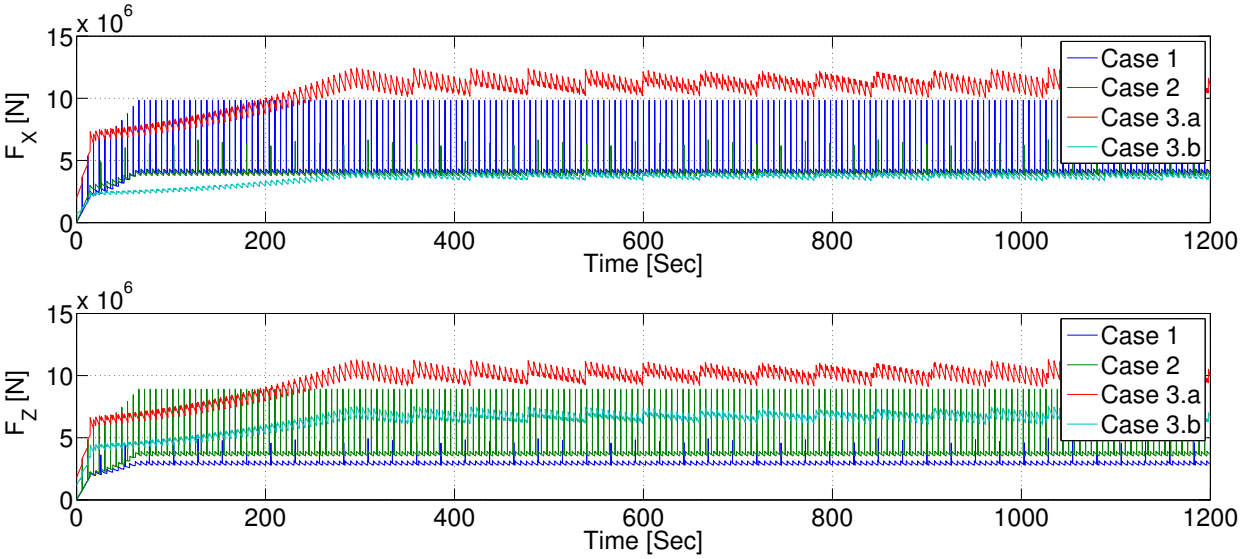

Figure 8.39: F_X, F_Z for Case 1, Case 2, Case 3.a and Case 3.b (ice test no.1)

Possible reasons for the deviations observed are discussed in Chapter 8.5.

8.4 Comparison study - Part 2

In the second part of the comparison study a fourth case is introduced. Case 4 is to be compared to Case 1 (see Chapter 8.3.1) and the measured time series. In conformity with Case 1, Case 4 is based on the MATLAB-script used in the pre-simulation given in Chapter 6, however the input differs as seen below;

- Use of MATLAB-script with the target ice mechanical properties and, identified average breaking periods of the ice and geometry of the ice transport on the structure.

  Notice: The only difference between Case 4 and Case 3.b is that the target ice properties are used instead of the actually measured ice properties. The identified breaking period, ice transport and accumulation scenario are described in Chapter 8.3.3. Also the same correction factors that were used in Case 3.b are used in Case 4; the horizontal load is reduced by a factor of 3 and the vertical load is reduced with a factor of 1.5.

Results obtained for Case 1, Case 4 and the measured time series are given in respectively Table 8.30, Table 8.33 and Table 8.29.

8.4.1 Case 4

Table 8.33 and Figure 8.40 present the results obtained from Case 4.

Table 8.33: Results from Case 4 (Full Scale)

	Test no.											
	1			**2**			**3**			**4**		
	Max.	**Min.**	**Mean**	**Max.**	**Min.**	**Mean**	**Max.**	**Min.**	**Mean**	**Max.**	**Min.**	**Mean**
	[MN]			**[MN]**			**[MN]**			**[MN]**		
$\mathbf{F}_X$	4.8	3.9	4.3	7.3	5.2	6.2	5.9	4.7	5.3	5.3	4.4	4.8
$\mathbf{F}_Z$	7.1	5.7	6.4	10.8	7.8	9.2	8.7	7.0	7.8	7.8	6.4	7.1
$\mathbf{F}_R$	8.6	6.9	7.7	13.0	9.4	11.1	10.5	8.4	9.4	9.4	7.8	8.6
θ	56.0°	55.6°	56.1°	55.9°	56.3°	56.0°	55.9°	56.1°	55.8°	55.8°	55.5°	55.9°

Notice: the horizontal load is reduced by a factor of 3 while the vertical load is reduced by a factor of 1.5 in Case 4.

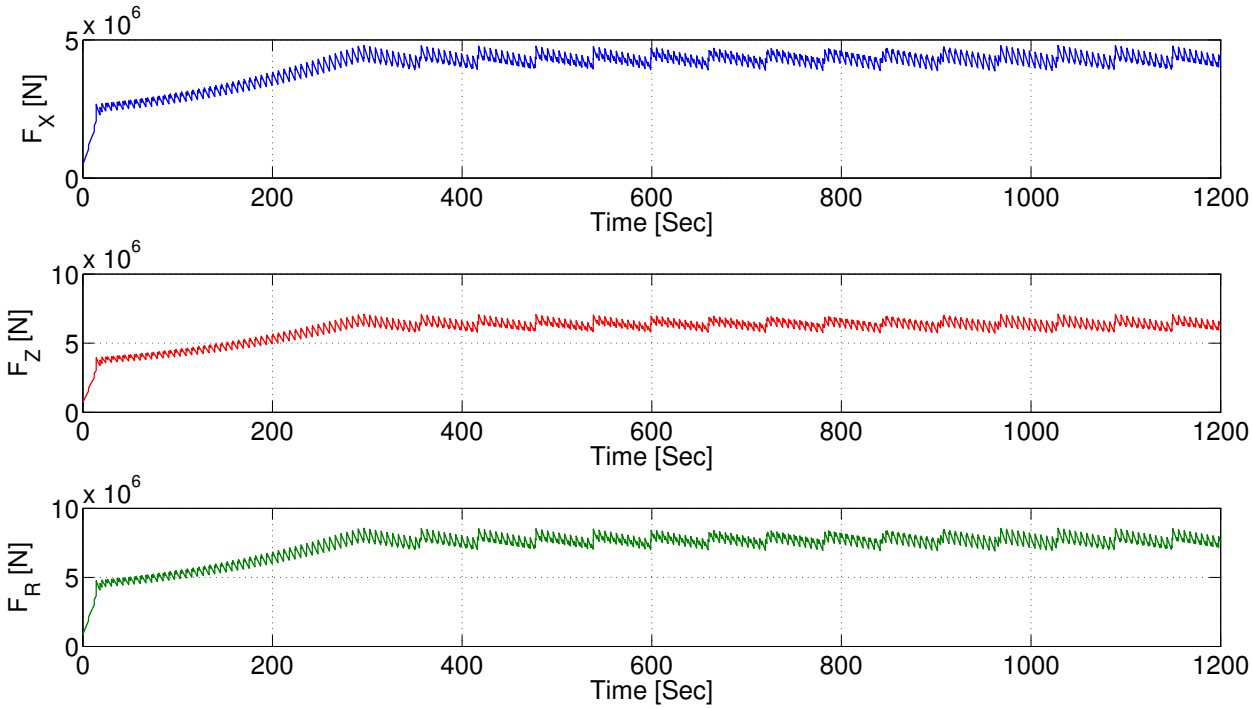

Figure 8.40: Calculated time series of ice test no. 1 - Case 4 (Full Scale)

8.4.2 Results

Like in the first part of the comparison study, deviations, both numerically and visually, between Case 1, Case 4 and the measured time series are observed. The main findings from the second part of the comparison study are;

- Case 4 is more similar to the measured time series compared to Case 1 both numerically and visually.
- The mean loads in the horizontal direction calculated in Case 1 are more or less in the

same range as the loads in Case 4. However, when comparing the vertical loads, Case 4 gives loads 2-3 higher than Case 1.

- The forces in the horizontal direction are larger than the forces in the vertical direction in Case 1. This is in contrast with the loads calculated in Case 4.
- The angle the mean loads make with horizon, θ, is in the range 54.5° - 58.5° for Case 4 and the measured time series. To compare, the angles in Case 1 are in the range 35.9° - 36.7°.
- Neither Case 1 nor Case 4 include the random rubble failure behavior that is observed in the measured time series.

Both the horizontal, vertical and resultant loads for Case 1 and Case 4 are plotted in Figure 8.41.

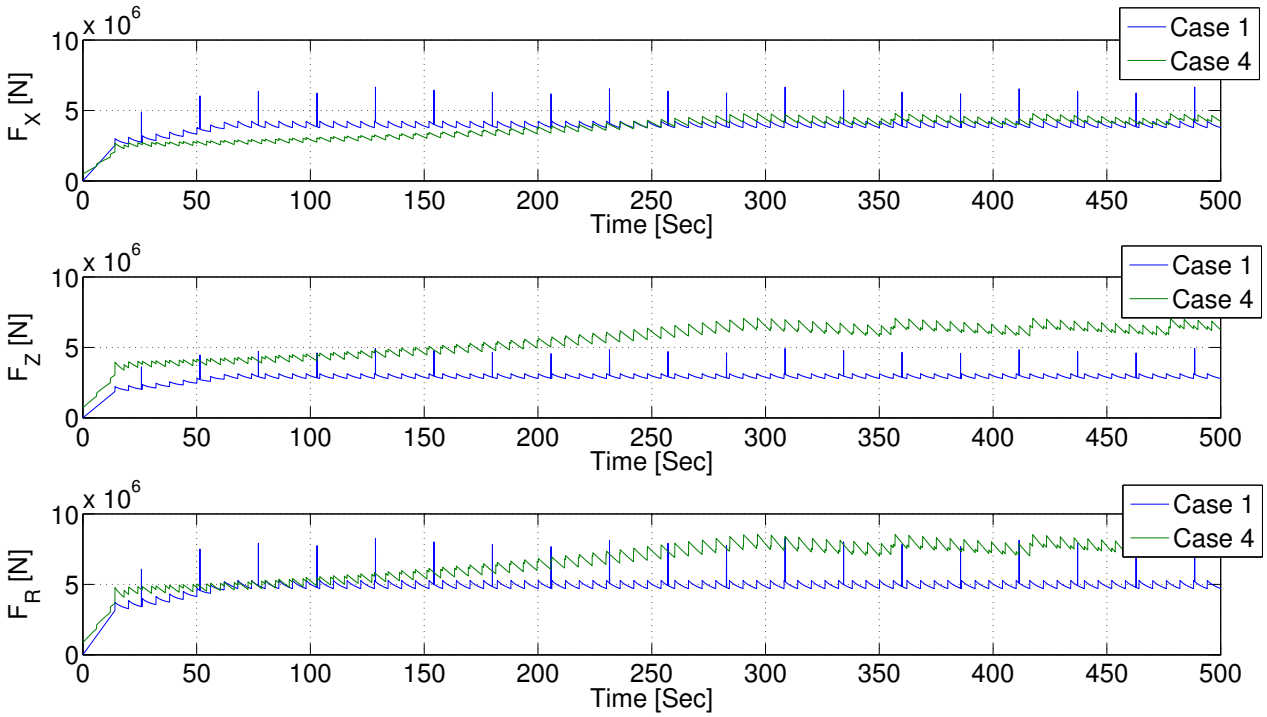

Figure 8.41: F_X, F_Z, F_{RES} for Case 1 and Case 4 (ice test no. 1)

The purpose for this comparison was to investigate the validity of using a numerical model in order to describe the ice action loads compared to performing an ice model test. Case 4 which is the model corrected for actually identified breaking period, rubble geometry, rubble accumulation and ice transport is closer correlated, both numerically and visually, to the measured time series compared to Case 1. However, it is not recommended to replace ice model testing with numerical simulations based on the results obtained. Possible reasons for the deviations observed between the calculated and the measured time series are discussed in Chapter 8.5.

8.5 Discussion

The identified deviations between the four cases and the measured time series may be a result of the following;

- The assumed breaking periods (calculated by Equation 3.33) used in Case 1 are too large compared to the observed breaking periods from the model test videos. While the as-

sumed breaking periods were in the range of 12.9 s - 34.8 s, the measured periods were only in the range of 2 s - 7.5 s.

- It was first assumed that the breaking load acts as an impulse load (used in Case 1 and Case 2). Accordingly, H_B is equal to zero in the intervals between each breaking period. When looking at Equation 3.31 where the horizontal load is calculated it can be seen that when $H_B = 0$, the total load will decrease significantly compared to case where $H_B > 0$ (if all other terms in the equations are kept constant).
- The load build-up period was assumed to be 50 s for all four test in Case 1 and Case 2, hence independent on velocity. From the videos it can clearly be seen that the load build-up period is significantly larger for the low-velocity (0.5 m/s) tests compared to the high-velocity (1 m/s) tests. The periods identified are ranging from 93 s to 280 s.
- Rubble failure was not taken into account in the calculations in Case 1 and Case 2. This because it was assumed that the rubble volume was constant after the load build-up. As a result for this assumptions H_P, H_R and H_L were kept constant at their maximum value after the load build-up.

  In Case 3 (a and b) and Case 4, an average value of the observed rubble failure period has been introduced to the numerical model.
- The numerical models used for all four cases are very theoretical while an ice failure process in its nature is a random process. This means that the numerical models developed give the same results over and over again as long as the input is kept unchanged. In a real ice failure process there will be a variation in the measured ice loads. One example for this is the rubble failure period which was assumed to be constant in Case 3 (a and b) and Case 4 (and not even included in Case 1 and Case 2). When later observing the measured time series it was seen that the period was varying during the whole test within a certain interval. A possible solution for including the variation in rubble failure period in the numerical simulations is to make use of a Monte-Carlo simulation which makes sure of randomly varying the rubble failure period within the observed interval.
- The horizontal and vertical loads calculated by Croasdale's methodology are both functions of five load components, namely H_B, H_P, H_R, H_L and H_T (described in Chapter 5.3). It has been challenging to understand the behavior and contribution of each component as the measured time series only present the total horizontal and vertical loads. In order to deal with this problem the following is suggested;
  - The breaking length of the ice sheet is an important parameter for the numerical simulations. To identify this parameter from the videos has been very challenging due to the distance between carriage and camera. It is therefore suggested that in addition to the ice tests already performed a test where the purpose is only to identify the breaking length should be included. Here, the distance between the carriage and the camera should be minimized.
  - Also a test where the rubble angle is measured should be included in order to optimize the numerical model.
- There are several weaknesses in the numerical model. Examples are;
  - The rubble height is assumed to be constant during the whole test in the numerical simulation. According to the videos this is not correct for a real model test.
  - The angle the rubble makes with the horizon varies in the videos as a result of rubble failure. When the rubble volume reduces the angle increases. This is not taken into account in the calculations.

- It is assumed in the numerical simulations that H_P, H_R and H_L are equally affected by the rubble failure. It has not been possible to prove/disprove this assumption with help from the videos and the measured time series.
- It was first assumed that the accumulated rubble did not affect the turning component, H_T. After observing the videos it is believed that in some way the rubble does affect the load, but how is challenging to conclude. Therefore, a reduction factor has been introduced in the calculations, see Chapter 8.3.3.

Although the calculated time series show deviations from the measured time series, it is reasonable to believe that a numerical simulation of the ice failure process against a sloping structure may give results in the same range as an ice model test. As described above, it is suggested that the numerical simulation includes the random behavior of rubble failure for instance by use of a Monte-Carlo simulation. This will hopefully result in a closer correlation between the calculated and measured time series.

9 CONCLUSION

There have been two main objectives of this master thesis. Firstly, to perform a static load estimate for the ice loads acting on a downward breaking structure, an upward breaking structure and a vertical structure. All structures have a waterline diameter of 30 m. Three different methodologies are assessed and compared. The main findings from the static load estimate are the following;

- The two methodologies, namely Ralston's and Croasdale's methodology, assessed for the calculation of ice loads acting on sloping structures give different results for the upward breaking structure. It is believed that this is a result of not including the presence of rubble on the face of the structure in the first methodology.
- Upward breaking results in higher ice loads compared to downward breaking for a structure of same waterline diameter and inclination angle between the structure's sloping plane and waterline. For the given geometry and ice conditions in Appendix A, the ratio between the estimated resultant forces for the two structures is almost 2.
- A vertical structure is subjected to larger loads than a structure with sloping waterline geometry. The static analysis shows that the loads are more than 10 times higher than for both the upward and the downward breaking structure.

The second objective has been to develop a numerical model based on Croasdale's methodology for estimation of level ice loads on structures with sloping surface in the waterline. A pre-simulation of an ice model test campaign was performed where the numerical model was used. Assumptions regarding ice transport and rubble accumulation scenario were based on the best available material which was readily available at the time. Target ice properties were used in the calculations. The results obtained in the pre-simulation were later compared, both visually and numerically, to a real ice model test campaign with same target ice conditions and structure geometry.

The comparison shows that;

- The mean horizontal loads calculated are in the range 4 MN to 5.5 MN, while the mean vertical loads are in the range 2.9 MN to 4.1 MN.
- While the actually measured horizontal loads are close to the estimated ones, ranging from 4.5 MN to 5.7 MN, are the measured vertical loads in the range 6.9 MN to 9.0 MN.

In order to get a closer correlation between the measured and calculated loads, time series and videos recorded during the test campaign have been studied. It should be mentioned that not all ice properties needed for the numerical model were measured during the tests. Also a variation in the measured properties was seen within the prepared ice sheet. Consequently it is unknown whether the measured ice properties are representative for the whole ice sheet.

Based on the time series and observations from the videos the first-made numerical model has been corrected stepwise. Four different cases are defined in Chapter 8, all with an unique combination of either assumed or measured ice properties, and either assumed or observed breaking period of the ice sheet, rubble geometry and ice transport. The last case, referred to as Case 4, includes the actually observed breaking period of the ice sheet, rubble geometry and ice transport in addition to the target ice properties in the calculations.

Both the actually measured loads and the loads calculated in Case 4 are given below.

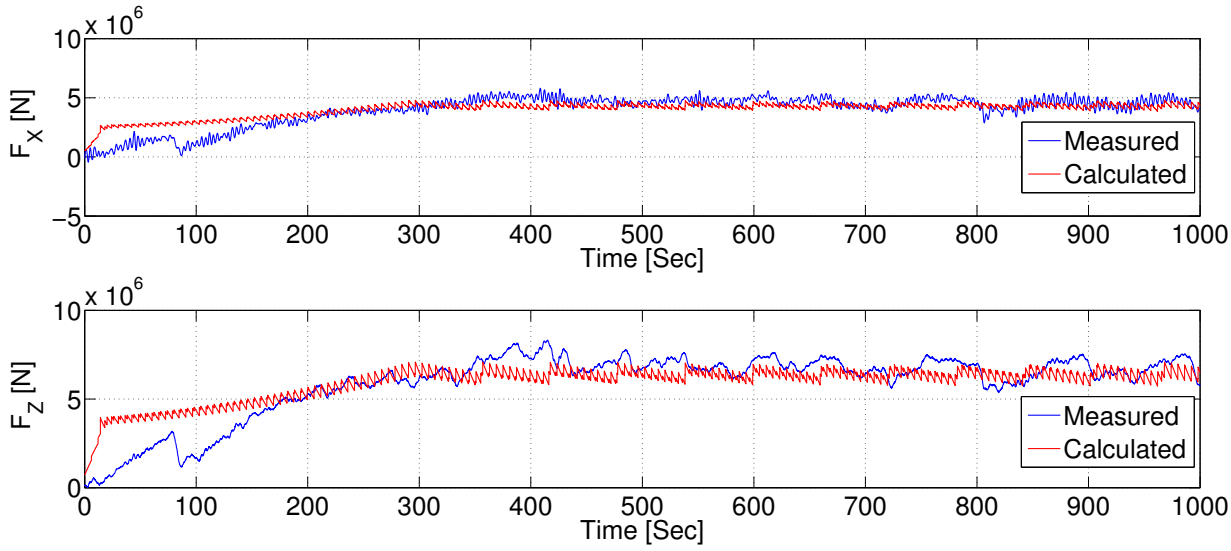

The main differences between the time series calculated and measured are;

- The calculated time series does not take the variation of rubble failure period into account.
- The loads calculated and estimated are more or less in the same range after approximately 300 s where the load build-up has more or less stabilized. However, it was necessary to reduce the total horizontal by a factor of 3 and the vertical load by a factor of 1.5 in the numerical model.
- According to Croasdale's methodology which is the basis for the numerical models developed, the vertical load is less than the horizontal load for the given structure geometry and friction coefficient between the structure and sea ice. This is not in agreement with the measured time series and had to be corrected for.

Although the calculated time series show deviations from the measured time series, it is reasonable to believe that a numerical simulation of the ice failure process against a sloping structure may give results in the same range as an ice model test. However, it is recommended that more time is spent on studying the model test videos in order to get a deeper understanding on how the five load components given in Croasdale's methodology are varying with time. Also, a few more tests should be included in the test campaign where the purpose is to identify important parameters, such as breaking length of the ice sheet and rubble geometry, needed for the numerical simulation.

10 RECOMMENDATIONS FOR FURTHER WORK

The calculated loads involved in the failure process between level ice and a sloping structure show deviations from the actually measured loads for a structure of same geometry. This is a result of many uncertainties in the numerical model developed. The following is suggested to get a closer correlation between the calculated and the measured time series.

Firstly, it is necessary to get a deeper understanding in how each of the five load components in Croasdale's methodology are contributing to the total load. A spectral analysis in WAFO could be helpful in order to divide the forces into categories depending on the frequency of occurrence.

Regarding the reduction in rubble volume during rubble failure, a reduction factor has been introduced in the numerical model. This reduction factor makes sure of reducing the three components depending on the rubble volume, H_P, H_R and H_L, with a certain magnitude during the rubble failure period. The rubble failure period was first assumed to be constant, see Figure 8.35. According to the time series, the rubble failure period is randomly varying within a certain interval. It is suggested that this randomness is included in the numerical model. One approach is to make use of a Monte-Carlo simulation that makes sure of randomly varying the rubble failure period between the minimum and maximum period observed in the time series.

In addition, instead of reducing the load components by use of a reduction factor it is suggested to increase the angle the rubble makes with the horizon instead. The reason for not using this approach in the model is that the quality of the video was too poor to make precise estimations of the rubble angle.

To optimize the numerical simulations a few additional tests in the test basin should be included where the focus is on identifying the breaking length of the ice. The distance between the camera and the structure should be minimized. Also an analytical model to simulate the process of structure-ice interaction by simplifying the problem as a semi-infinite plate resting on an elastic foundation should be included to to get a better insight in how the ice breaking process develops.

The model tests have been recorded on video from four different angles; from the carriage, the side of the test basin in addition to through the window in the sides and under the test basin (underwater views). To get an even better picture of the rubble geometry and accumulation scenario it is suggested that an angle 90° to the moving direction of the carriage is included.

It would be extremely helpful for the numerical calculation if the five load components were estimated during the model tests in addition to the forces and moments already measured.

References

Beketsky, S. P., Astafiev, V. N., & Truskov, P. A. (1996). Structure of Hummocks Offshore Northern Sakhalin. *Proceedings of the 11th Okhotsk Sea Ice Symposium, Hokkaido, Japan*, *2*, 339–342.

Blanchet, D. (1998). Ice loads from first-year ice ridges and rubble fields. *Can. J. Civ. Eng.*, *25*, 206–219.

Bruun, P. K., Husvik, J., Le-Guennec, S., & Hellmann, J.-H. (2009). Ice model test of an Arctic SPAR. *Proceedings of the 20th International Conference on Port and Ocean Engineering under Arctic Conditions*.

CAN/CSA-S472/92 (1992). General requirements, Design Criteria, the Environment and Loads. (p. 87).

Cox, G. F. N., & Weeks, W. F. (1974). Salinity variation in sea ice. *Journal of Glaciology 13 (67)*, (pp. 109–120).

Dalane, O., Løset, S., Aksnes, V., & Aarsnes, J. V. (2009). A moored Arctic floater in first-year sea ice ridges. *Proceedings of the ASME 28th International Conference on Ocean, Offshore and Arctic Engineering OMAE2009*.

Frankenstein, G. E., & Garner, R. (1967). Equations for determining the brine volume of sea ice from -0.5 to -22.9 °c. *J. Glaciology, 6 (48)*, 943–944.

Furnes, G. (2010). Lecture notes in "Ice 1". Ice 1.

ISO 19906 (2010). Petroleum and natural gas industries - Arctic offshore structures. Tech. rep., Geneva, Switzerland.

Jefferies, M., Kärnä, T., & Løset, S. (2008). Field data on the magnification of ice loads on vertical structures. *Proc. 1st IAHR Int. Symp. on Ice Vancouver*, *2*, 1115–1133.

Kärnä, T., Qu, Y., & Yue, Q. J. (2006). Extended Baltic model of global ice forces. *Proc. 18th IAHR Int. Symp. on Ice, Sapporo*.

Kovacs, A. (1996a). Sea Ice Part 1. Bulk salinity versus ice floe thickness. Tech. rep., CREEL Report 96-7, Hanover, NH, USA.

Langleben, M. P., & Pounder, E. R. (1963). Elastic parameters of sea ice. *Kingery, W.D. (Ed.). Ice and snow. MIT Press, USA*, (pp. 69–78).

Larsen, F. R. (2011). *Prediction of ice loads and respons for an Arctic SPAR*. Master's thesis, NTNU.

Løset, S., Shkhinek, K. N., Gudmestad, O. T., & Høyland, K. V. (2006). *Actions from ice on arctic offshore and coastal structures*.

Lubbad, R., & Løset, S. (2010). A numerical model for real-time simulation of ship-ice interaction. *Cold Regions and Technology*.

Mäkinen, E., Liukkonen, S., Nortala-Hoikkanen, A., & Harjula, A. (1994). Friction and hull coatings in Ice Operations. *Proceedings ICETECH '94, Society of Naval Architects and Marine Engineers, March 1984, Calgary, Canada*, *Paper E*.

Mattsson, T. (2007). Model Tests in With Two SPAR Concepts For AKET. Tech. rep.

Melling, H., Reidel, D. A., & Gedalof, Z. (2005). Trends in the thickness and extent of seasonal pack ice. *Canadian Beaufort Sea. Geophysical Research Letters 32 (24)*, (pp. 1–5).

National Snow and Ice Data Center (2009).
URL `http://nsidc.org/seaice/characteristics/difference.html`

Peschanskii, I. S. (1960). Arctic and Antarctic sea ice (R). *Problemy Arktiki i Antarktiki. St. Petersburg, Russia*, *4*, 111–129.

Saeki, H., Ono, T., Nakazawa, N., Sakai, M., & Tanaka, S. (1986). The coefficient of friction between sea ice and various materials used in offshore strucures. *ASME Journal of Energy Resources Technology*, *108*, 65–71.

Sinha, N. K. (1984). Uniaxial compressive strength of first-year and multi-year sea ice. *Canadian Journal of Civil Engineering*, (pp. 82–91).

Timco, G. W., & Frederking, R. M. W. (1986). Confined compression tests; outlining the failure envelope of columnar sea ice. *Cold Regions Science and Technology 12 (1)*, (pp. 13–28).

Timco, G. W., & Frederking, R. M. W. (1990). Compressive strength of sea ice sheets. *Cold regions Science and Technology 17*, (pp. 227–240).

Timco, G. W., & Frederking, R. M. W. (1991). Seasonal compressive strength of Beaufort Sea ice sheets. *Jones S. et al. (Ed) Proceedings IUTAM-IAHR Symposium on Ice/Structure Interaction, St. John's, Nfld. Springer Verlag, Berlin, Heidelber*, (pp. 267–282).

Timco, G. W., & Johnston, M. E. (2004). Ice loads on the caisson structure in the Canadian Beaufort Sea. *Cold Regions and Technology 38*, (pp. 185–209).

Timco, G. W., & O'Brien, S. (1994). Flexural strength equation for sea ice. *Cold Regions Science and Technology 22*, (pp. 285–298).

Timco, G. W., & Weeks, W. F. (2009). A review of the engineering properties of sea ice. *Cold Regions Science and Technology*.

Timoshenko, S. (1956). *Strength of Materials*. Part 2 Advanced Theory and Problems.

Timoshenko, S., & Goodier, J. N. (1951). *Theory of elasticity*.

Wight, B. (1998). Insights from Molikpaq ice loading data: Validation of Low Level Ice Forces on Coastal Structures. *LOLEIF Report No. 1, EU Project, Contract MAS3-CT 97-0098*, (p. 88).

APPENDICES

A INPUT IN NUMERICAL MODEL

Target mechanical and physical ice properties

Table A.34: Target mechanical and physical level ice properties used in Chapter 4

	Ice thickness [m]	Flexural strength [MPa]	Ice density [kg/m^3]	Ice-structure friction	Poisson's ratio	E-Module [GPa]	Cohesion [kPa]	Internal angle of friction	Porosity
Data	1	0.5	900	0.15	0.3	3	8	35	0.3

Table A.35: Target mechanical and physical level ice properties used in Chapter 6

Test no.	Ice thickness [m]	Flexural strength [MPa]	Ice density [kg/m^3]	Ice-structure friction	Poisson's ratio	E-Module [GPa]	Cohesion [kPa]	Internal angle of friction	Porosity
1 & **2**	1	0.5	900	0.15	0.3	3	8	35	0.3
3 & **4**	1.5	0.5	900	0.15	0.3	3	8	35	0.3

Table A.36: Ice model test campaign

Ice test no.	Velocity [m/s]	Ice thickness [m]
1	0.5	1
2	1	1
3	0.5	1.5
4	1	1.5

Geometry of structures

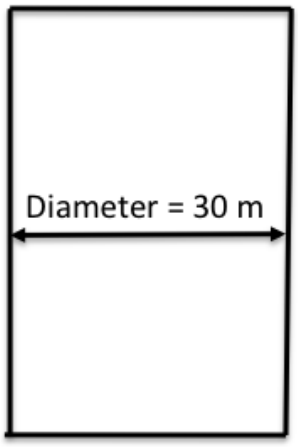

Figure A.42: Vertical structure

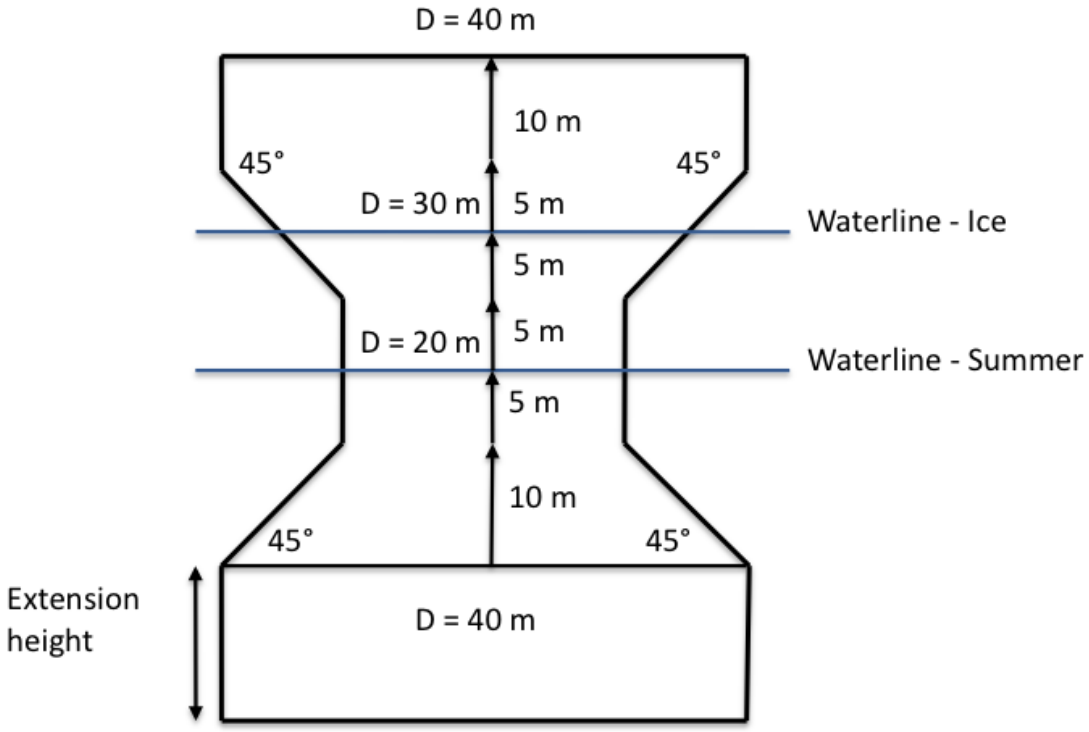

Figure A.43: Downward breaking structure (Model A)

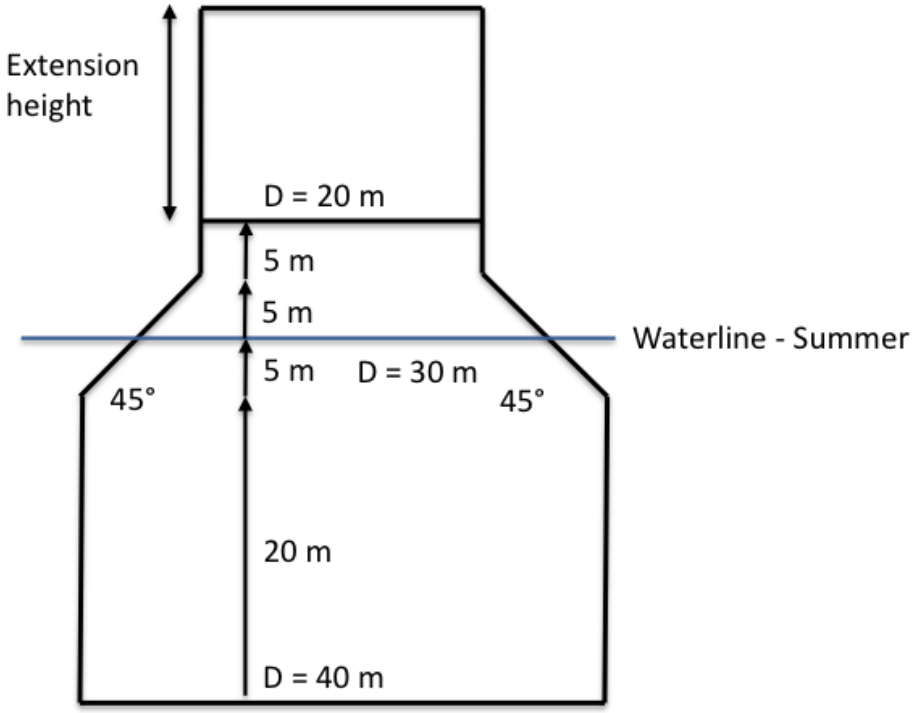

Figure A.44: Upward breaking structure (Model B)

B TIME-DOMAIN ANALYSIS

Actually measured time series

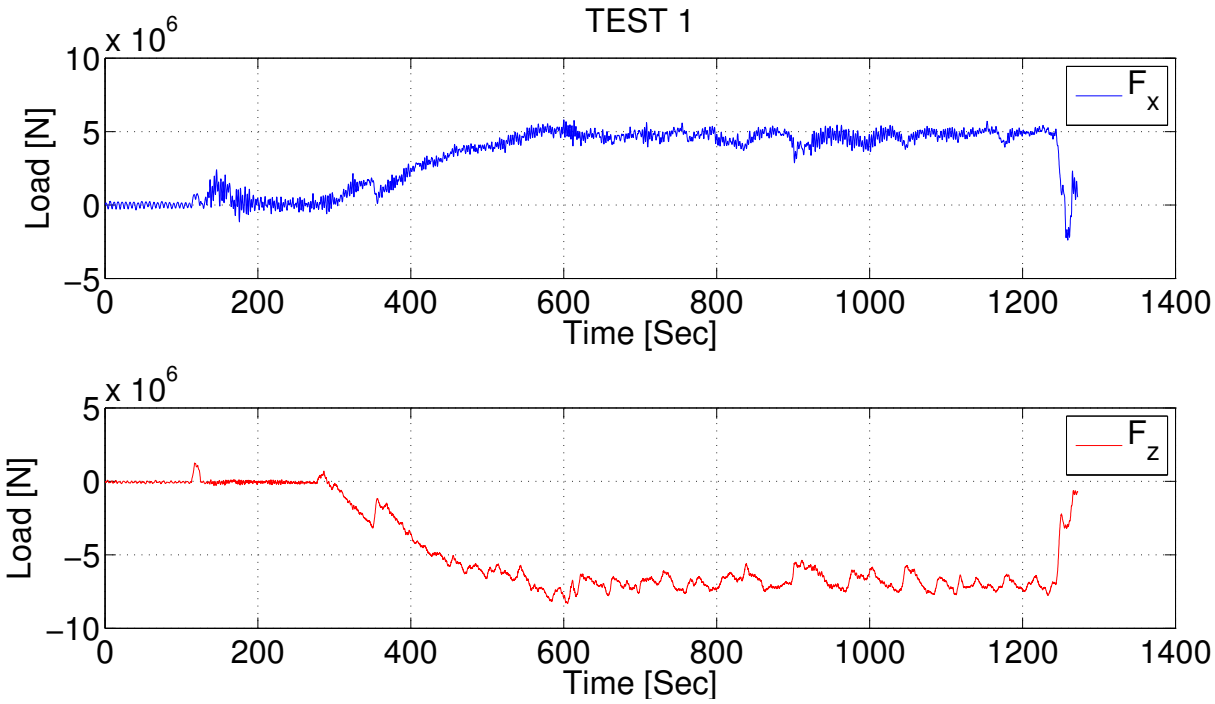

Figure B.45: F_x and F_z vs. time - Ice test no. 1 (Full scale)

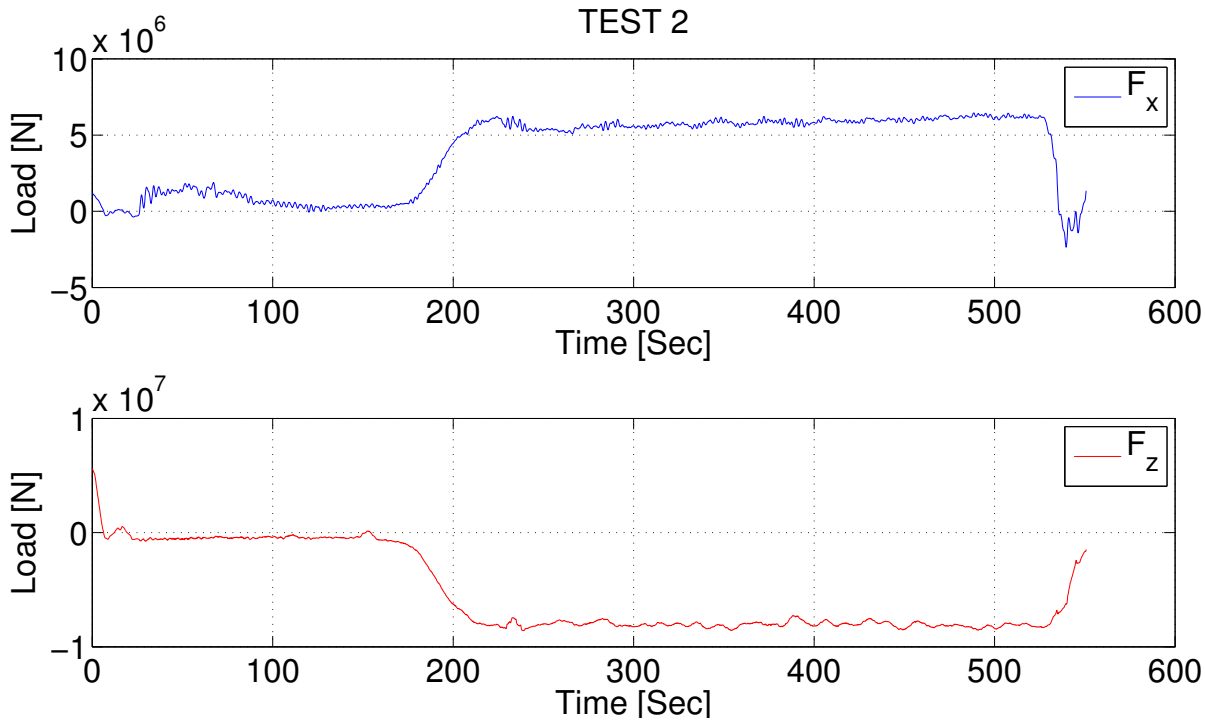

Figure B.46: F_x and F_z vs. time - Ice test no. 2 (Full scale)

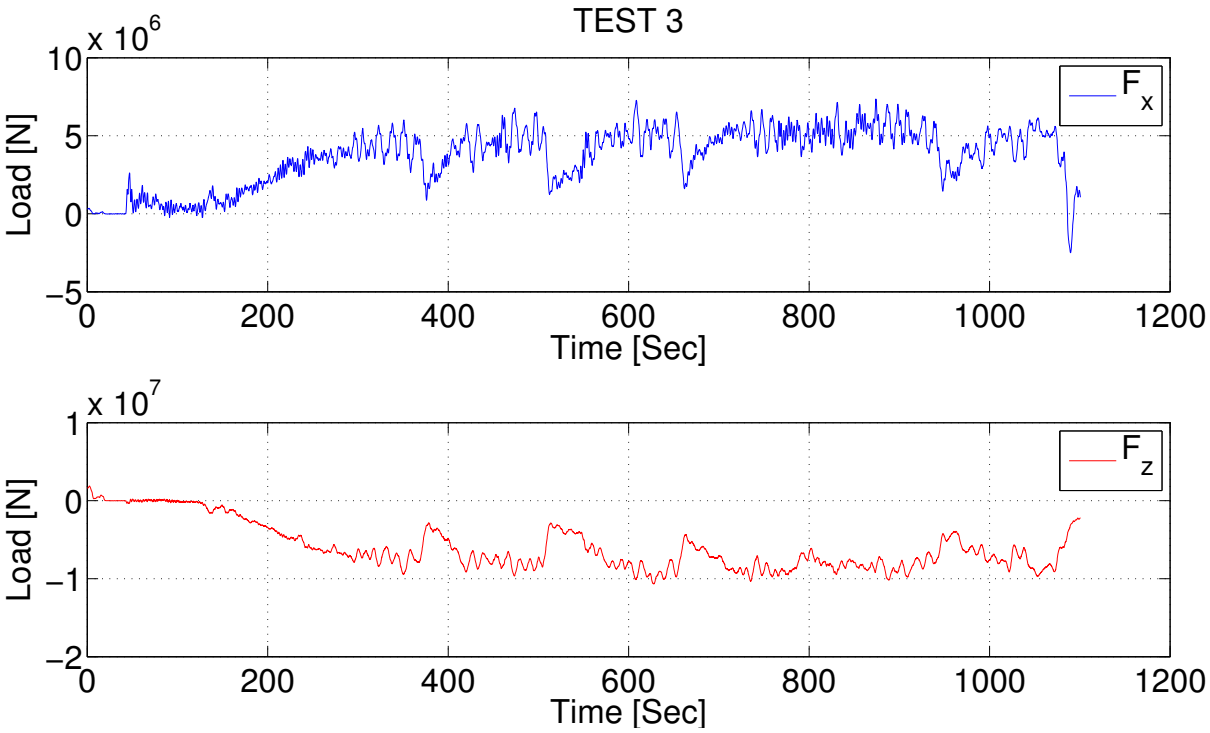

Figure B.47: F_x and F_z vs. time - Ice test no. 3 (Full scale)

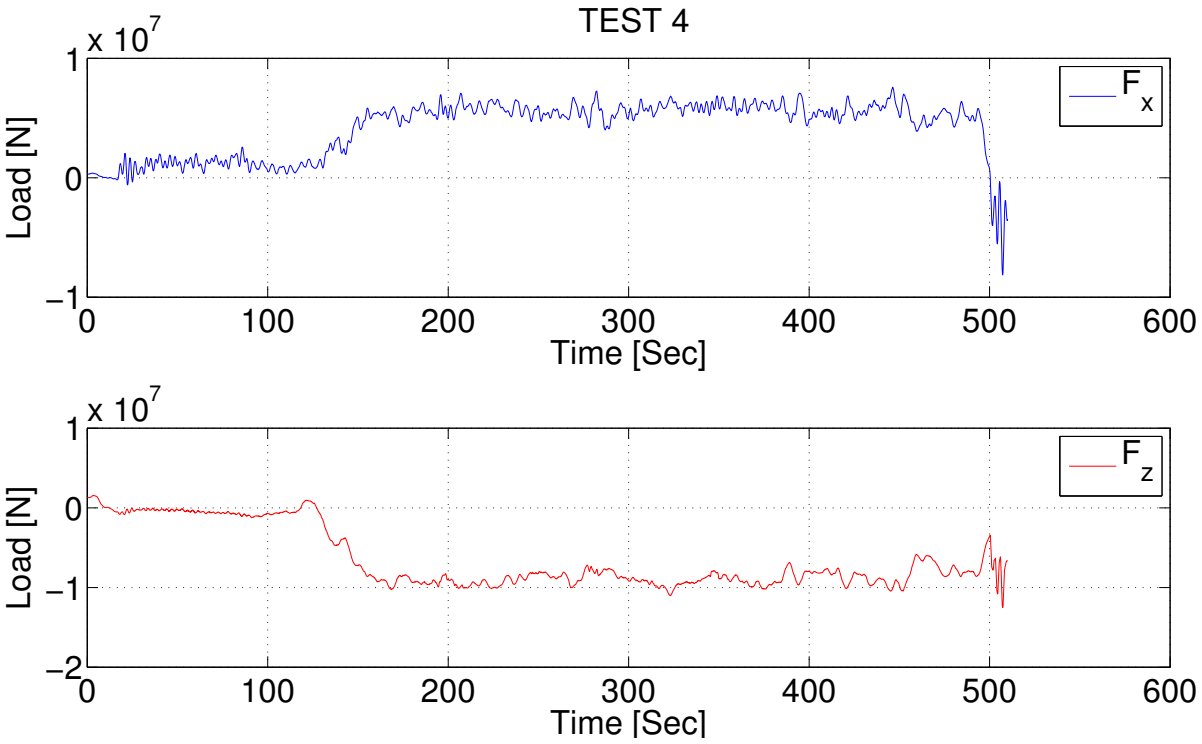

Figure B.48: F_x and F_z vs. time - Ice test no. 4 (Full scale)

Sensitivity tests

Sensitivity test I

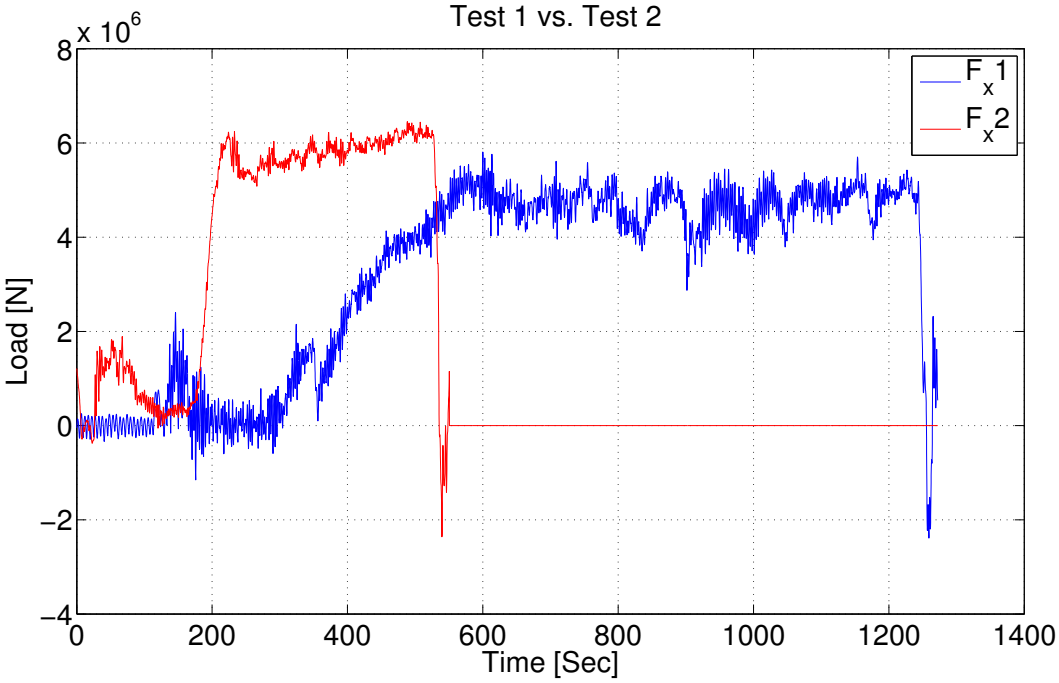

Figure B.49: Ice test no. 1 vs. ice test no. 2 (Constant ice thickness of 1 m) [F_x]

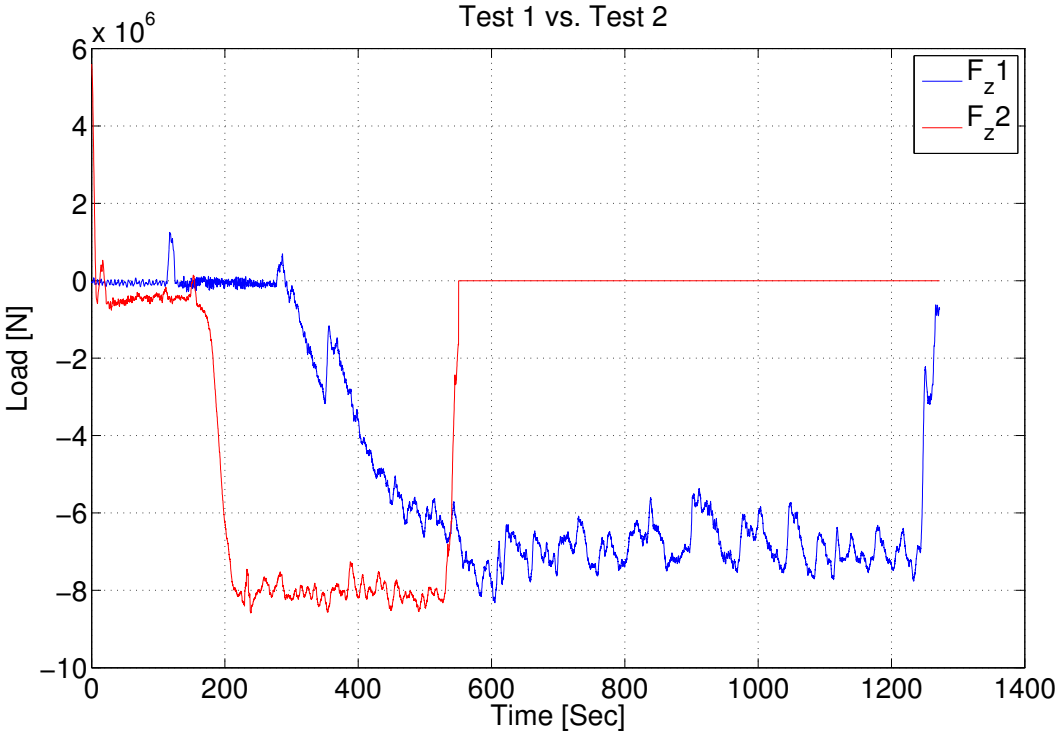

Figure B.50: Ice test no. 1 vs. ice test no. 2 (Constant ice thickness of 1 m) [F_z]

Sensitivity test II

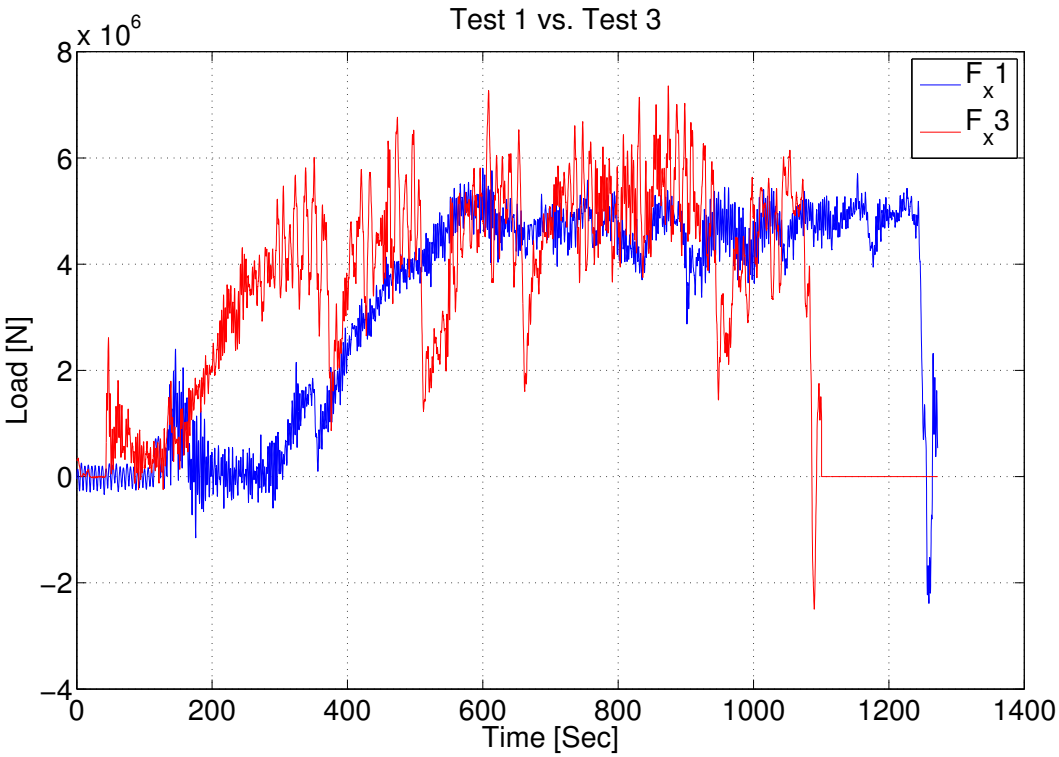

Figure B.51: Ice test no. 1 vs. ice test no. 3 (Constant velocity of 0.5 m/s) [F_x]

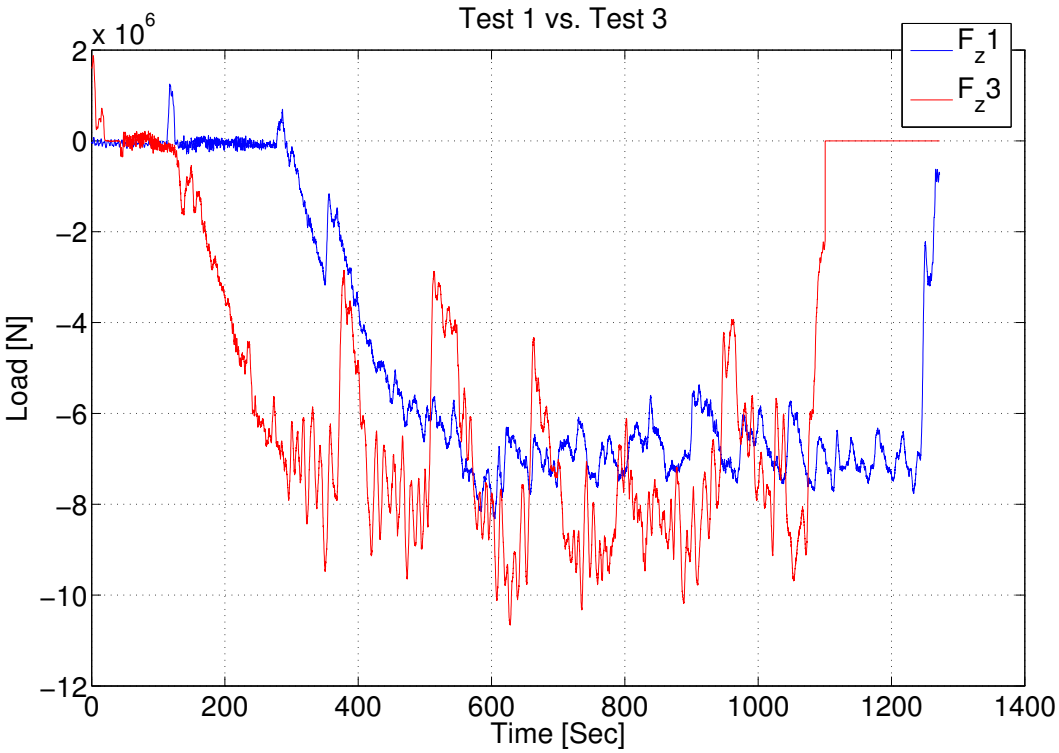

Figure B.52: Ice test no. 1 vs. ice test no. 3 (Constant velocity of 0.5 m/s) [F_z]

Sensitivity test III

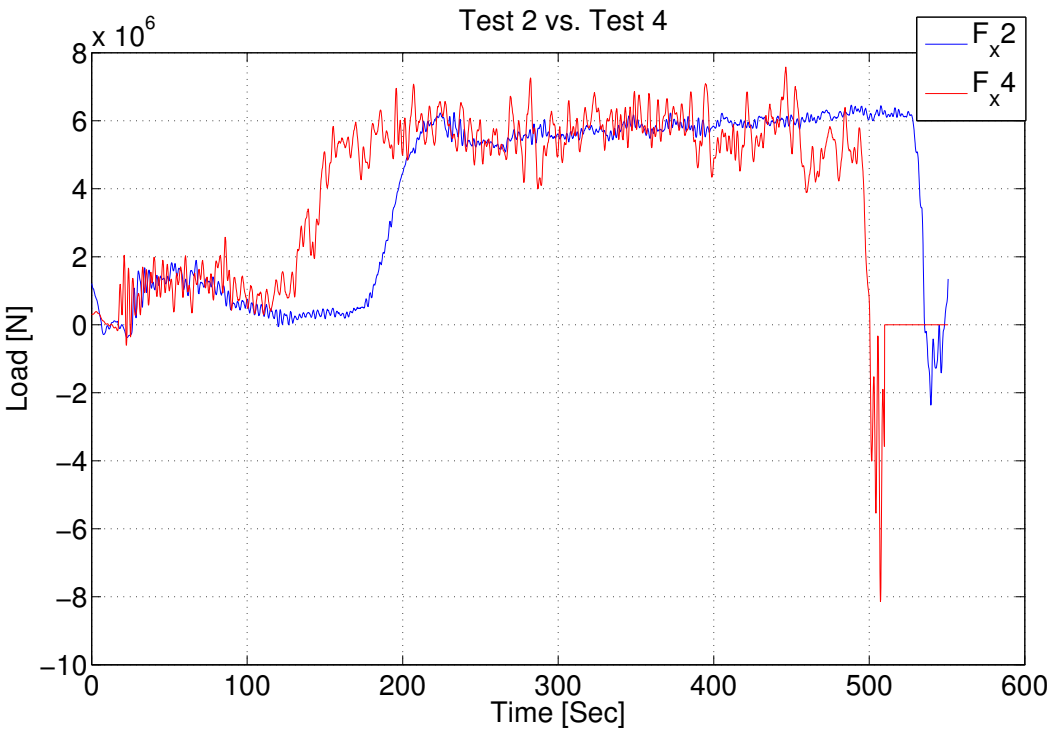

Figure B.53: Ice test no. 2 vs. ice test no. 4 (Constant velocity of 1 m/s) [F_x]

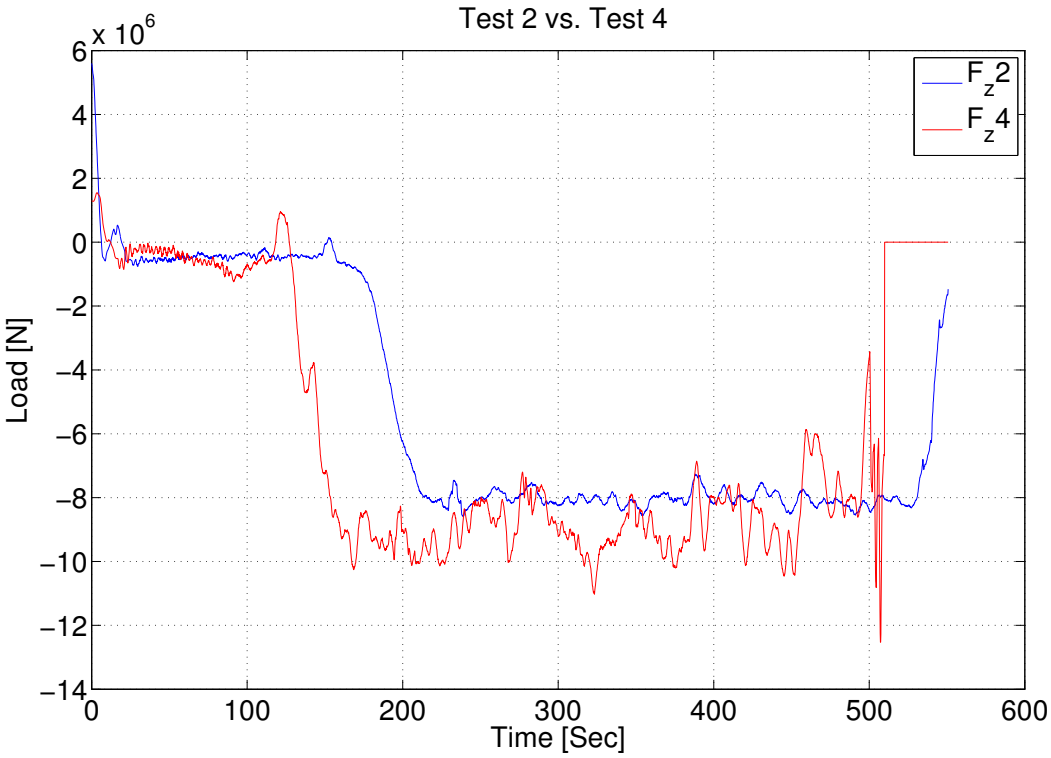

Figure B.54: Ice test no. 2 vs. ice test no. 4 (Constant velocity of 1 m/s) [F_z]

Sensitivity test IV

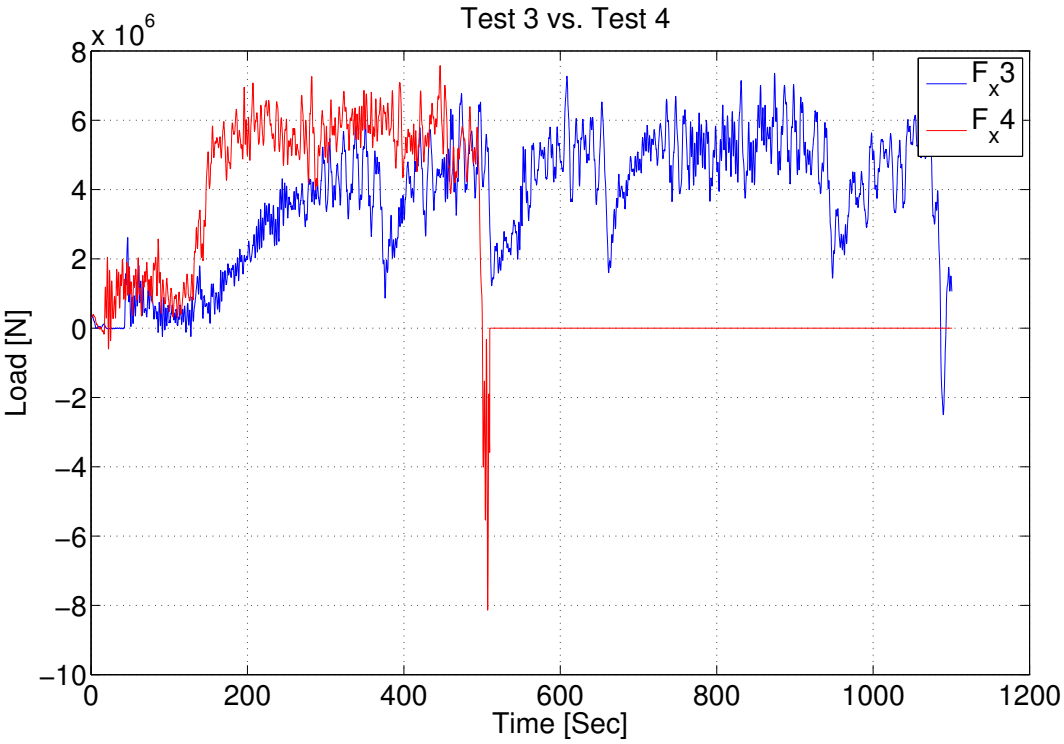

Figure B.55: Ice test no. 3 vs. ice test no. 4 (Constant ice thickness of 1.5 m) [F_x]

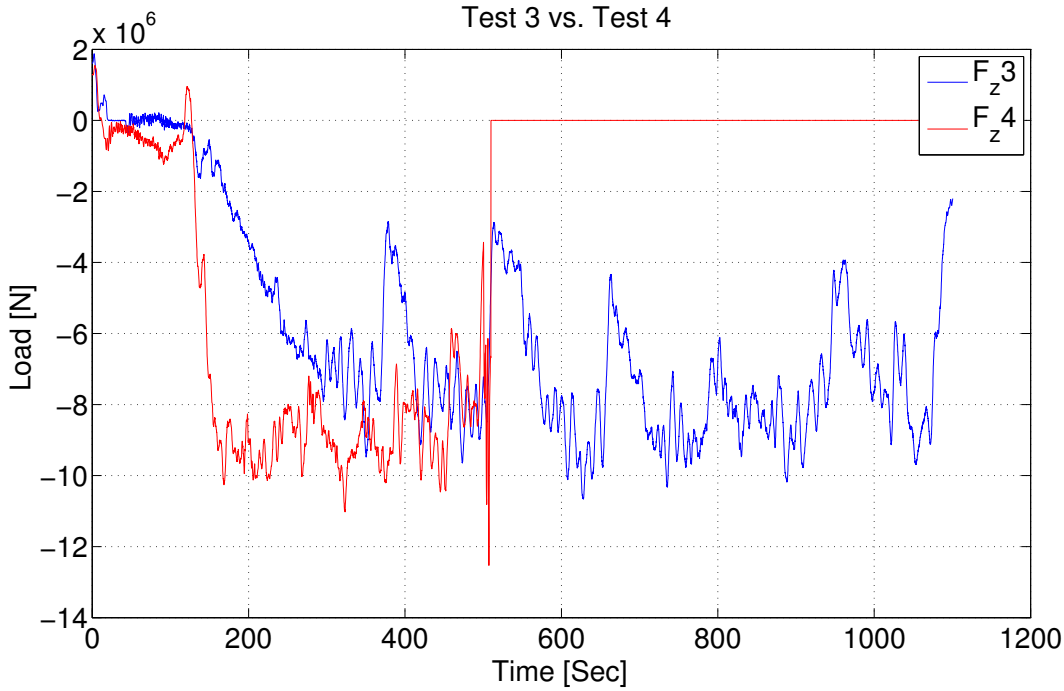

Figure B.56: Ice test no. 3 vs. ice test no. 4 (Constant ice thickness of 1.5 m) [F_z]

C MODEL TESTS

Breaking length and rubble angle

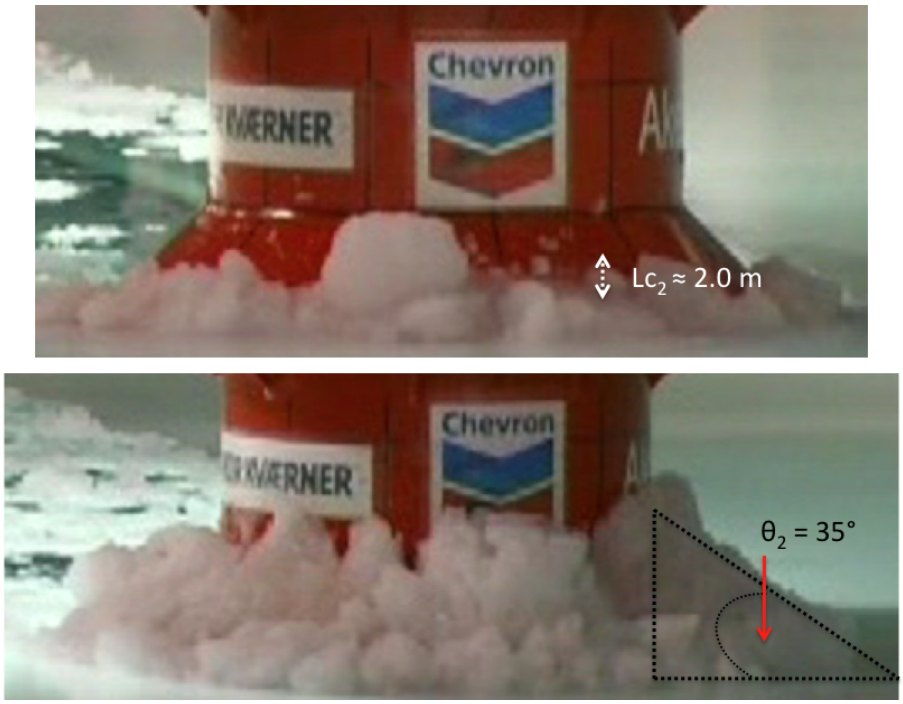

Figure C.57: Rubble geometry and breaking length (ice test no. 2)

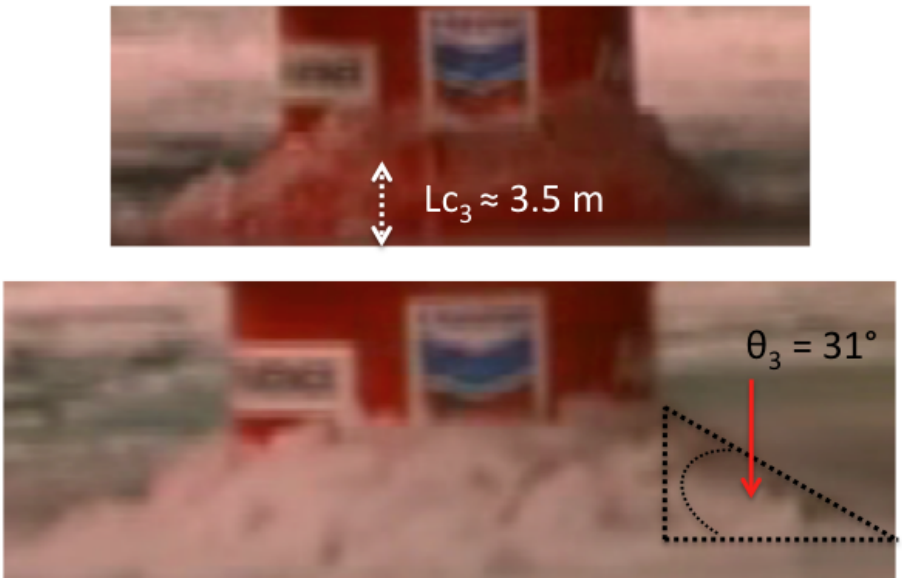

Figure C.58: Rubble geometry and breaking length (ice test no. 3)

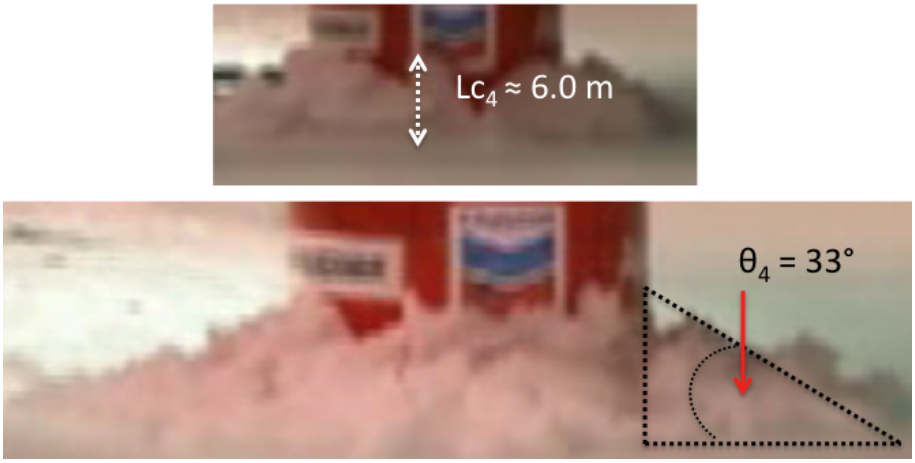

Figure C.59: Rubble geometry and breaking length (ice test no. 4)

Rubble height

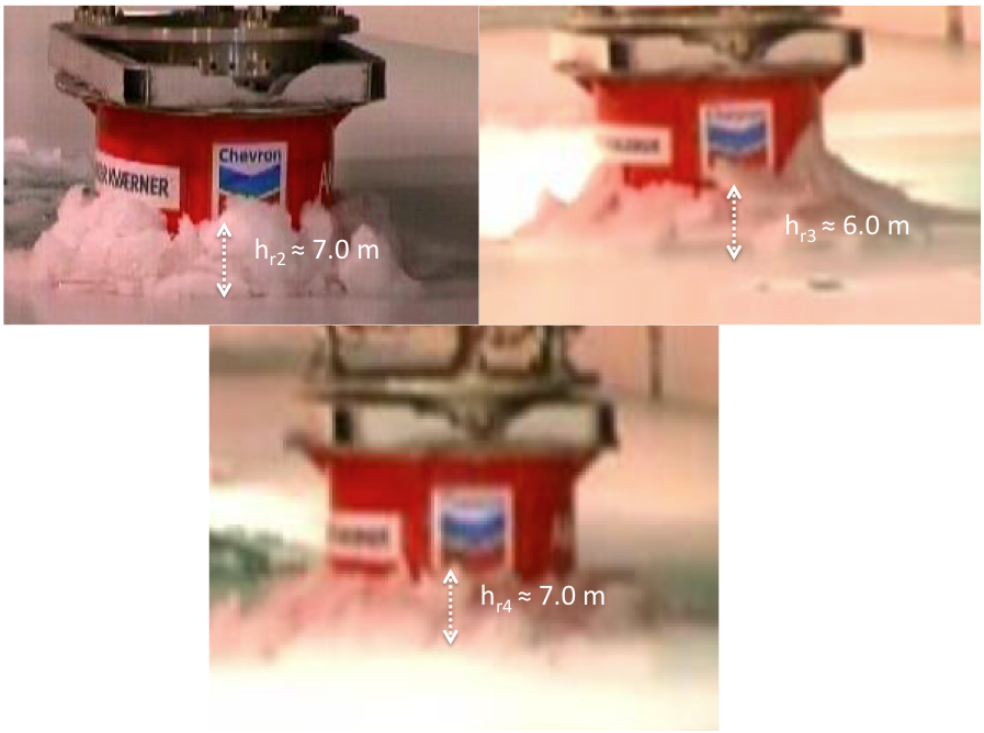

Figure C.60: Rubble height (ice test no. 2, no.3 and no. 4)

D NUMERICAL MODELS

Static analysis

simplebeam.m

simplebeam.m is utilized in the calculations given in Chapter 5.1. The deflection, bending moment and shear force are given by Equation 5.77, Equation 5.78 and Equation 5.79, see "OUTPUT" in script.

justification.m

The comparison study in Chapter 4 is based on the script named justification.m. Three different methods for estimating the ice-structure interaction loads are assessed, namely Ralston's methodology, Croasdale's methodology and a method for calculating forces on a vertical structure. All methods are described in detail in Chapter 3.

Time-domain analysis

Pre-simulation

main.m is the MATLAB-script utilized in Chapter 6 and Chapter 7. The script contains four different cases, see Figure D.61, where the function of each four of them are the following;

- CASE 1: Static analysis of the ice-structure interaction based on Croasdale's methodology
- CASE 2: Static analysis of the ice-structure interaction based on Ralston's methodology
- CASE 3: Time-domain analysis of the ice-structure interaction based on Croasdale's methodology
- CASE 4: Presentation of actually measured ice loads from four ice model tests performed by Aker Solutions

The results presented in Chapter 6 and Chapter 7 are calculated respectively in CASE 3 and CASE 4.

A short explanation of the subscripts in the numerical model is given below.

- parameter.m is the input needed for the calculations.
- Croasdale.m gives the maximum ice-structure interaction loads calculated with Croasdale's methodology (static analysis).
- Ralston.m gives the maximum ice-structure interaction loads calculated with Ralston's methodology (static analysis).
- loadcomp.m calculates the ice-structure interaction loads in the time-domain based on Croasdale's methodology.
- scaling.m introduces the scaling factor between model scale and full scale.
- readinput.m gives four matrices, one for each ice model test. The matrices present the time, velocity, forces and moments measured during the model tests. Notice that the values presented are in model scale.

- statistics.m calculates basic statistics from the four model tests. The statistics are based on the stabilized part of the time series and presented in Chapter 7.2.1.
- results.m is utilized in the sensitivity study of ice thickness and velocity, see Chapter 7.2.3.
- test1.m, test2.m, test3.m, test4.m are the measured time series from the ice model tests.

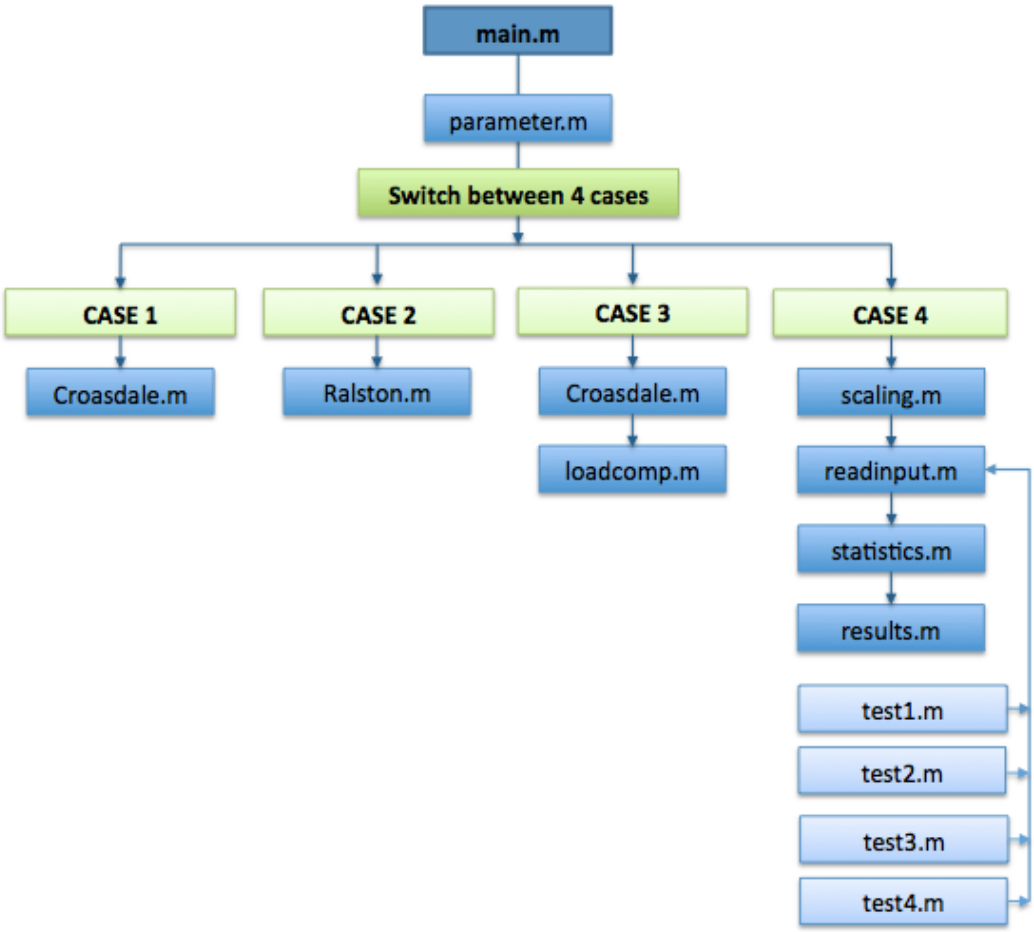

Figure D.61: Numerical model used in Chapter 6 and Chapter 7

CASE study

mainCASESTUDY.m is the numerical model utilized in Chapter 8. Five cases are defined, as shown in Figure D.62. The first four cases are described in Chapter 8 while the fifth case presents the results from the four ice model tests performed by Aker Solutions.

A short explanation of the subscripts in the numerical model is given below.

- input1.m, input2.m, input3.m and input4.m are the input files used in the calculations of the first four cases.
- Croasdale.m gives the maximum ice-structure interaction loads calculated by Croasdale's methodology (static analysis).
- calc1.m, calc2.m, calc3.m and calc4.m give the time-domain analysis of the ice-structure interaction based on Croasdale's methodology for the first four cases.
- out.m, out2.m, out3.m and out4.m give the horizontal, vertical and resultant forces from the stabilized part for the first four case.
- CASE1.txt, CASE2.txt, CASE3.txt and CASE4.txt contain the time, horizontal load, vertical load and the resultant load calculated in CASE 1, CASE 2, CASE 3 and CASE 4.
- read.m gives four matrices, one for each ice model test. The matrices present the time, velocity, forces and moments measured during the model tests. Notice that the values presented are in model scale.
- comp.m plots all four cases vs. the actually measured time series.
- test1.m, test2.m, test3.m, test4.m give the actually measured loads and moments from the four ice model tests.

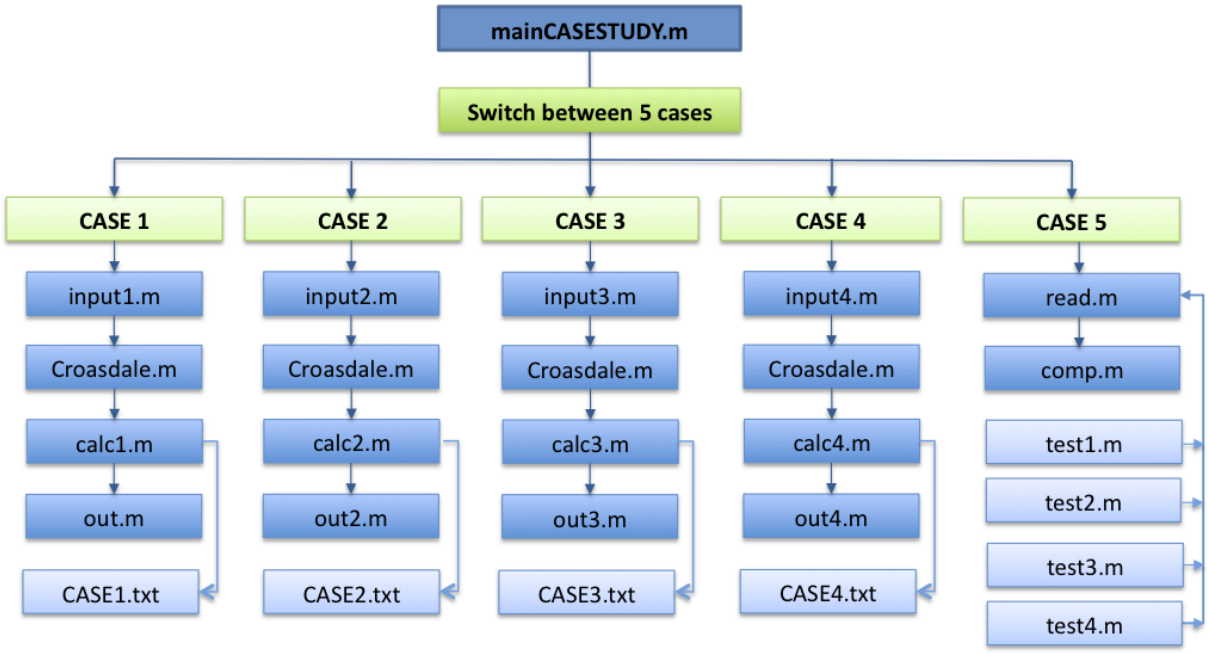

Figure D.62: Numerical model used in Chapter 8

E CD

Contents

- Numerical model
- Report in electronic format
- Confidentiality agreement between Aker Solutions and student